

https://dspace.org/

Cranial asymmetry and inner ear evolution in extant owls and comparative bird species

Twala, Enele

2025-04
University of the Witwatersrand, Johannesburg
https://hdl.handle.net/10539/48370
Twala, Enele. (2025). Cranial asymmetry and inner ear evolution in extant owls and comparative bird species. [Master's dissertation, University of the Witwatersrand, Johannesburg]. WIReDSpace. https://hdl.handle.net/10539/48370

Downloaded from a DSpace repository. https://dspace.org/



Cranial asymmetry and inner ear evolution in extant owls and comparative bird species

by

Enele Twala

(2088547)

ORCiD: 0000-0001-6032-7177

MSc Submission

Submitted in fulfilment of the requirements for the degree:

MSc by Research

in

Palaeontology

in the Faculty of Science, University of the Witwatersrand, Johannesburg, South Africa

Supervisor: Prof. Jonah Choiniere

Co-supervisors: Prof. Roger Benson and Dr Kimberley Chapelle

April 2025

DECLARATION

I declare that this dissertation is my own, unaided work. It is being submitted for the Degree of Master of Science at the University of the Witwatersrand, Johannesburg. It has not been submitted before for any degree or examination at any other University.



_____

(Signature of candidate)

April 2025

at ESI, University of the Witwatersrand

Acknowledgements

I would like to express my deepest gratitude to my supervisors Prof. Jonah Choiniere, Dr Kimberely Chapelle and Prof. Roger Benson. Your unwavering support and constructive feedback have been crucial in shaping this dissertation.

I am also incredibly grateful to the Evolutionary Studies Institute (ESI) for providing the resources necessary for me to complete this research. A special acknowledgement to GENUS and PAST for not only their financial support but the workshops and conferences that they have hosted over the years, which developed many critical skills that have shaped me into the scientist I am today.

To my lab mates, the Stormberg Giants, thank you for all the support, encouragement as and willingness to assist whenever I needed help. A heartfelt thank you the staff and students from the ESI, with a special thank you to Dr Abraham Dabengwa, for all your generosity and guidance. Thank you to my friends for your unwavering belief in me.

A special thank you to my mother, Ntombi Twala, my greatest cheerleader, whose encouragement and love have been my pillar of strength. Thank you to my grandmother, Thembi Twala, for continuously reminding me about the importance of remaining grounded and grateful for everything I have achieved thus far. To my aunt and uncle, Wandile and Brian Gasela, thank you reminding me to spread my wings and dare to do things I never thought I could do. Finally, to my entire family, *Ngiyabonga Ma'Nyamande, Mkhont'oduma njegezulu*! Your unwavering love and support have carried me through this journey.

Table of Contents

Acknowledgements 3

List of Figures 6

List of Tables 6

Abstract 9

Introduction 10

Research Aims 17

Methods and Materials 17

Materials 18

1. CT Scanning and Segmentation 18

Methods 27

1.Natural history observations 27

2. Braincase measurements 30

3. Body mass values 31

4. Hearing performance data 31

5. Landmarking of labyrinths 33

6. Landmarking of skulls 36

7. Landmark analysis 40

8. Statistical tests 44

9. Mapping residuals of the regressions onto the phylogenetic tree 51

Results 52

1. Labyrinth landmark analysis 52

1.1 Cochlear duct and semicircular canal lengths distribution 52

1.2 Semicircular canal size asymmetry 54

1.3 Cochlear duct size asymmetry 56

2. Model outputs 58

3. The relationship between labyrinth lengths, body mass and braincase height.....61
4. The relationship between the length of the cochlear duct and the length of the semicircular canals.....71
5. Hearing performance results.....74
6. Asymmetry results.....78
6.1 Cranial asymmetry.....78
6.2 Labyrinth shape asymmetry.....86
6. Phylogenetic mapping of residuals.....88
Discussion.....97
Conclusion.....108
References.....110
Appendix 1.....120

List of Figures

Figure 1: Anterior and left lateral view of owl skulls.. 24
Figure 2:Anterior view of owl skulls and their associated labyrinths. 25
Figure 3: Anterior view of bird left and right labyrinths showing the variation in cochlear duct length and morphology in birds. 26
Figure 4: Braincase height measurement method shown on *Aegolius acadicus* (AMNH 14467). 30
Figure 5: Illustration of the skeletonized and landmarked left labyrinth of *Macropygia amboinensis* (KU B 93202). 36
Figure 6:Illustration of the cranial landmarks on *Asio otus* (AMNH 3632). 40
Figure 7: A representative tree of birds adapted from Jetz et al (2012) supertree distribution, using the Hackett et al. (2008) phylogeny as a backbone. 51
Figure 8: Box plot depicting the average length of the left and right anterior (ASC), lateral (LSC) and (PSC) semicircular canals for the entire dataset. 53
Figure 9: OLS regression showing the correlation between the logged lengths of the right and left semicircular canals. 55
Figure 10:GLS regression showing the correlation between the logged lengths of the right and left cochlear duct in owl and non-owl birds. 57
Figure 11: PGLS regression illustrating the relationship between log-transformed body mass and log-transformed braincase height in owls and non-owl bird species. 61
Figure 12:PGLS regressions illustrating the relationship between the log-transformed average sum of the semicircular canals against log-transformed braincase height and log-transformed body mass in owls and non-owl bird species.. 63
Figure 13: PGLS regression illustrating the relationship between log-transformed average cochlear duct length and log-transformed braincase height in owls and non-owl bird species. 65
Figure 14: Histogram representing the frequency of the AvCD ~ BCH model residuals for owl and non-owl birds included in the study. 66
Figure 15: PGLS regression showing the relationship between log-transformed average cochlear duct length against log-transformed braincase height and, with distinctions based on hunting styles and bird groups. 67
Figure 16: PGLS regression showing the relationship between log-transformed average cochlear duct length against log-transformed braincase height, with distinctions based on behaviour and bird groups. 68
Figure 17: PGLS regression showing the relationship between log-transformed average cochlear duct length against log-transformed braincase height, with distinctions based on reported asymmetry (Norberg, 2002) and bird groups.. 69
Figure 18: PGLS regression illustrating the relationship between log-transformed average cochlear duct length against log-transformed average sum of the semicircular canal lengths and in owls and non-owl bird species.. 72

Figure 19:PGLS regression showing the residuals of AvSumSCC ~ BCH model against the residuals of the ECD ~ BCH model. 73
Figure 20: PGLS regressions showing the relationship between various hearing performance indicators against the residuals of the AvCD~ BCH model.. 76
Figure 21: Histograms show the frequency of asymmetry in the different part of the cranium across bird taxa. 84
Figure 22:Box plot depicting the levels of shape asymmetry, quantified using Procrustes distance, across various landmark pairs in the cranium. 84
Figure 23: Inferior view of *Asio otus* (AMNH 3632) skull showing the asymmetry of the foramen magnum as indicated by the blue arrow. 85
Figure 24:Box plot depicting the levels of shape asymmetry across various landmark pairs in the labyrinth. 86
Figure 25: Phylogenetic tree of taxon sample set in this study with reported asymmetry from Norberg (2002) and Pecsis et al. (2021) mapped on.. 89
Figure 26: Phylogenetic tree showing the distribution of the cochlear duct and braincase height model residuals. 91
Figure 27: Phylogenetic tree showing the distribution of the braincase height and body mass model residuals. 94
Figure 28: Phylogenetic tree showing the distribution of the sum of the semicircular canal length and cochlear duct length model residuals.. 95

List of Tables

Table 1: Parameters Used for Mesh Creation in VGStudio. 18
Table 2: List of bird specimens and corresponding specimen numbers included in this study. The species numbers were used to indicate specimens in figures. 19
Table 3: The natural history observations and associated classifications used to score all the bird taxa used in study. 27
Table 4: Natural observations gathered from literature, bird watcher websites and bird behaviour videos for each specimen included in the study. The birds were classified using the classifications in Table 3. 28
Table 5: The hearing performance data for some of the bird taxa included in the study. The N/A represents measurements where data was not available. 31
Table 6: List of labyrinth landmarks used to landmark the midline of the semicircular canals and cochlear ducts of the bird labyrinths. Abbreviations: Anterior semicircular canal (ASC); Lateral semicircular canal (LSC); Posterior semicircular canal (PSC); Cochlear duct (ECD) 33
Table 7: List of cranial landmarks used for bird crania. 36
Table 8:Final list of specimens included in cranial asymmetry analysis. 42
Table 9: Table listing all the OLS and PGLS models conducted for this study. With specifications given on which model residuals were mapped onto the phylogenetic tree. Abbreviations: Braincase height (BCH); Body mass (BM); Average sum of the semicircular canal length (AvSumSCC); Average cochlear duct length (AvCD); Left anterior semicircular canal (LASC); Right anterior semi-circular canal (RASC); Left posterior semicircular canal (LPSC); Right anterior semicircular canal (RPSC); Left lateral semicircular canal (LLSC); Right lateral semicircular canal (RLSC); Left cochlear duct (LECD); Right cochlear duct (RECD). 46
Table 10: Summary statistics for the box plot depicting the average length of the left and right semicircular canals in Figure 7. 53
Table 11: Summary of model statistics for the ordinary least squares (OLS) models and the phylogenetic regressions (PGLS) models listed in Table 9. Abbreviations: Braincase height (BCH); Body mass (BM); Average sum of the semicircular canal length (AvSumSCC); Average cochlear duct length (AvCD); Left anterior semicircular canal (LASC); Right anterior semi-circular canal (RASC); Left posterior semicircular canal (LPSC); Right anterior semicircular canal (RPSC); Left lateral semicircular canal (LLSC); Right lateral semicircular canal (RLSC); Left cochlear duct (LECD); Right cochlear duct (RECD); Intercept (b_0); Slope (b_1); Sample size (N) 58
Table 12: Summary statistics for the histogram in Figure 13. 66
Table 13: Summary statistics for the hearing performance models. Abbreviations: Average cochlear duct length (AvCD); Braincase height (BCH); Intercept (b_1); Slope (b_0) 74
Table 14: Measurements of skull asymmetry across various bird species. The highest values across the different skull regions are in bold. 78
Table 15: Summary statistics of cranial shape asymmetry as illustrated by the box plot in Figure 23. 84
Table 16:Summary statistics of labyrinth shape asymmetry as illustrated in Figure 23. Abbreviations: (LSC) Lateral semicircular canal; (ASC) Anterior semicircular canal; (PSC) Posterior semicircular canal 86

Abstract

Hearing is an important sensory function in birds, which is associated with behavioural and ecological adaptations. Among birds, owls have exceptional hearing ability allowing species such as the Barn Owl (*Tyto alba*) to capture prey in complete darkness using only auditory cues. This exceptional hearing ability is attributed to two distinct skeletal adaptations: (1) an elongated cochlear duct of the ear; and (2) cranial asymmetry. These adaptations are conspicuous features of the bird skull, potentially permitting us to infer hearing ability in extinct species along the bird line. However, quantitative datasets suitable for testing their form-function relationships have until now been lacking. This dissertation aims to address this gap by investigating patterns of variation in these skeletal adaptations linked to hearing ability among owls and comparative bird species. I collated digital 3-D reconstructions of bird skulls and their labyrinths and used a geometric morphometric pipeline to assess variation in their shapes and sizes. I identified three independent origins of elongate cochlear ducts, twice among owls and once in the oilbird. Surprisingly, although the superficial bones of the hearing region showed asymmetry, the endosseous labyrinth did not, a finding perhaps attributable to strong developmental constraints on neural architecture. I also found that birds with asymmetry did not have proportionally long cochlear ducts. These results suggest cochlear duct elongation and cranial asymmetry in owls evolved as a distinctive auditory specialisation missing in other birds' perceptions of ambient sound. Finally, I incorporated natural history observations about the bird species studied here, finding that auditory foraging is associated with increased cochlear duct length while other foraging styles are not. This work increases our understanding of the functional and morphological diversity of bird auditory adaptations, provides a framework for understanding the evolution of auditory specialization within the birds, and contributes to the broader discussions on sensory evolution in vertebrates.

Introduction

Hearing is one of the vital components of the vertebrate neurosensory system, evolving early in the evolution of land-dwelling tetrapods (Lombard and Bolt, 1979). The ability to detect airborne sound in tetrapods is accomplished by a complex morphosensory system involving an impedance-matching tympanum (Gray, 1951), middle ear ossicles (minimally including the columella or stapes) (Gray, 1951), and the sensory organ of the inner ear known as the cochlear duct (or lagena) (Gray, 1951), the latter of which contains receptor cells that convert pressure waves into electrical signals (Hudspeth, 1983). Impedance matching is therefore of evolutionary significance for hearing, having evolved in ancestors of living reptiles and birds as key adaptation for detecting ambient sounds (Bronzati et al., 2024).

Sensing of ambient sound plays a crucial role in many aspects of bird ecology. For example, the ability to hear the vocalizations of other birds aids communication with young (Kilner and Johnston, 1997), keeps groups united (Ritchison, 1983), strengthens pair bonds (Swaddle and Page, 2007), attracts mates (Catchpole and Slater, 2008), initiates reproductive behaviours (Kroodsma, 1976), and contributes to competing with same-sex individuals for territory (Catchpole and Slater, 2008). Hearing is also crucial for predator avoidance. For example, the yellow-casqued hornbill (*Ceratogymna elata*) can distinguish between the different predator avoidance alarm calls for eagles and leopards made by Campbell's monkeys (*Cercopithecus campbelli*) and Diana monkeys (*Cercopithecus diana*) (Rainey et al., 2004).

Hearing adaptations in birds

Examples of birds with hearing adaptations abound and are most often associated with specialized navigation or foraging. For instance, pigeons are 50 dB more sensitive to infrasound compared to humans, which has been hypothesized to aid in their navigation (Kreithen and Quine, 1979). Other birds such as swiftlets (*Aerodramus* spp.; *Collocalia troglodytes*) and oilbirds (Steatornithidae, Caprimulgiformes) use their hearing as part of an

echolocation system to navigate in darkness (Brinkløv et al., 2013). Woodpeckers use hearing to find insects such as termites, larvae, beetles, and ants by beak-drumming surfaces then listening for auditory cues of prey (Maclean, 1985). Harriers in the genus *Circus* are diurnal raptors with facial ruff curving around the ear which is thought to allow them to amplify sounds from specific directions, enabling sound location accuracy (Rice, 1980).Among all birds with hearing adaptations, the most striking example is owls. The Barn Owl can capture prey in complete darkness only from sounds produced as the prey moves through the leaf litter (Knudsen, 1981; Payne and Drury, 1985; Marti, 1974). Payne (1971) observed this behaviour in a controlled environment by conducting experiments in a completely dark room, where a mouse was placed onto the leaves on the floor. In addition to studies conducted in controlled environments, research suggests that owls can rely solely on auditory cues to hunt successfully in the wild. Examples include the Great Grey Owl (*Strix nebulosa*),which has been observed capturing prey under complete snow cover (Godfrey, 1967: Hilden and Helo, 1981) and the Short-Eared Owl (*Asio flammeus*) capturing prey under a continuous cover of dead grass (Clark, 1975).

Hearing in birds, like in all tetrapods, is accomplished through organs housed within the inner ear. The bird inner ear is made up of interconnected spaces in the periotic bone called the bony labyrinth (Gray, 1951), comprised of the osseous cochlear and semicircular canals. These canals house a series of interconnected soft tissue ducts and sacs called the membranous labyrinth which aid hearing (cochlear) and balance (semicircular canal) (Gunz et al., 2012). Osseous features of the labyrinth reflect the shape of the membranous ducts contained within them. Therefore, the bony labyrinth can be used as a proxy of the cochlear duct and semicircular canals and can be used to investigate the form and function of the inner ear (e.g. Fleischer, 1976; Geisler & Luo, 1996). Thus, comparisons of relative measurements

of cochlear duct lengths of living and extinct species potentially make it possible to infer hearing ability.

Among the bird species which have been studied thus far, Barn Owls have the proportionally longest cochlear duct. An allometric study of cochlear duct length found that Barn Owl cochlear duct length is three times more than expected from a bird of its body size (Gleich et al., 2005). This finding was corroborated by Choiniere et al. (2021), which used braincase height as an allometric covariate and similarly found high residuals for Barn Owl cochlear length. In birds and mammals, increased length of the cochlear duct and its hearing organs results in greater auditory acuity, defined as the ability to distinguish fine differences in sound intensity and frequency (Lay, 1972). Therefore, the length of the Barn Owl cochlear duct appears to be correlated with greater auditory acuity. The Barn Owl cochlear duct also has other features that make it unique from other owls, including the presence of a dense fibrous mass along the basilar membrane (Gleich et al., 2005). Gleich et al. (2005) suggested that the long cochlear duct, and other specialisations of Barn Owls is consistent with the observation that it has high hearing sensitivity across a wide range of frequencies including high frequencies.

The use of audiograms in assessing the hearing abilities of birds

Hearing acuity among birds is mainly assessed using audiograms. These document hearing sensitivities across the full spectrum of sound frequencies, providing a visual depiction of the birds' auditory capabilities. Audiograms are usually generated by using behavioural tests or physiological measurements that assess how well the bird can detect sounds and varying intensities and frequencies. The x-axis often represents the frequency of the sound in Hertz (Hz), which is the pitch of the sound. The y-axis often represents the hearing threshold, measured in decibels (dB), which indicates the minimum sound intensity required to detect a particular frequency. In many bird species tested, the lowest thresholds occur between two

kHz and four kHz and sensitivity to frequencies above 10 kHz is poor (Dooling, 1992). For sensitive auditory thresholds, birds usually have frequencies below 10 kHz (Van Dijk, 1973; Nieboer and Van der Paardt, 1977). However, the barn owl is very sensitive to sounds of 10 kHz and have an indicated threshold of -6 dB at 10 kHz (Konishi, 1973). This indicates that the barn owl has is much more sensitive to certain sounds compared with other birds.

Cranial asymmetry in owls

An important component of the hearing apparatus of owls is the ability to localise sound effectively, which aids the hunting ability of most owl species. Accurate localisation of sound requires discrimination of its position in the vertical and horizontal planes (Martin, 2010). Directional hearing in owls is aided by asymmetry of the vertical positions of the ear openings and in the shape and asymmetry of the ear flaps and facial disk (Martin, 2010). Asymmetry of the ear takes different forms among owls. Many species show soft tissue asymmetry in the soft tissues surrounding the external acoustic meatus, which is the pathway running from the outer ear to middle ear, whereas other species show asymmetry in the bones of the skull itself (Norberg, 2002). Soft tissue asymmetry in owls occurs when the prenaural flaps are at different vertical levels and are different shapes. This type of asymmetry is mainly observed in the Barn Owl (*Tyto alba),* Oriental Bay Owl (*Phodilus badius*)*,* Mottled Owl *(Strix virgata)* and Eurasian Eagle Owl (*Bubo bubo*; Norberg, 2002). Asymmetry of the skull occurs when the openings of the ear in the skull are not at the same vertical level. This results in bilateral ear and skull asymmetry because of the different orientations and positions of the squamoso-occipital wing. This type of asymmetry has been described in Tengmalm's Owl (*Aegolius funereus*; Norberg, 1977). The extent of these adaptations appears to be variable among owl lineages – for example, up to five separate origins of cranial asymmetry have been hypothesized (Norberg, 1977). However, the variation in asymmetry has yet to be tested in a quantitative morphological framework.

In species such as the Boreal Owl (*Aegolius funereus*), Barn Owl (*Tyto alba*), and Long-eared Owl (*Asio otus*), asymmetry of the vertical positions of the ear openings allows them to create a morphofunctional system whereby sounds reach each ear at slightly different timesdetect the differences in how the sound reaches the ear. These differences differ depending on the position of the sound source relative to the head and allows them to localize sounds more precisely (Norberg, 1968; Payne, 1971; Iljitschew, 1974). Additionally, as the frequency of the sound increases, the differences in how each ear receives the sound becomes more distinct. This assists in precise location of sounds, which is crucial for navigation and hunting (Norberg, 1968; Payne, 1971; Iljitschew, 1974). These studies have led to several theories on how this difference in how sound is received allows for sound localisation (notably in the vertical plane). However, measuring the accuracy with which a bird can locate the sources of sounds, in both the horizontal and vertical plane is difficult. Barn Owls (*Tyto alba*) are the only species for which we have good experimental data on sound localisation. The asymmetry of the soft tissue of Barn Owls' ears allows them to use the difference in frequency to make assessments of elevation more precise. The right ear tends to be more sensitive to sounds coming from an upwards direction while the left ear tends to be more sensitive to sounds coming from a downwards direction (Knudsen, 1981). It has been estimated that Barn Owls (*Tyto alba*) can locate prey in total darkness using sound localisation (Payne, 1971; Knudsen, 1981). Along with its ability to accurately locate prey, Knudsen and Konishi (1979) showed that the Barn Owl had the ability to locate white noise in the horizontal plane and in azimuth, but this was only the case if the sound came from directly ahead of the bird. Therefore, to account for this, barn owls would change the position of their head to make sure that the prey is brought into its frontal plane (Payne, 1971).

Nocturnal foraging adaptations in birds

Morphological features associated with good hearing in owls are generally considered to be adaptations to foraging in low light conditions, yet several owl species are diurnal or crepuscular. Furthermore, other groups of nocturnal birds use senses other than hearing to forage during low light conditions, suggesting that hearing ability may be only loosely correlated with diel activity patterns. For example, olfaction has been correlated as a nocturnal adaptation in the Brown Kiwi (*Apteryx australis*), which has the largest olfactory bulbs among terrestrial birds and a large surface area of its nasal cavity (Bang, 1971). These adaptations have been shown to aid in location of invertebrates including worms and insects in the dark (Reid and Williams, 1975; Wenzel, 1968). Night Parrots *(Pezoporus occidentalis*) have the highest density of taste receptors among birds (Berkhoudt, 1985), and this has been hypothesized to be a sensory nocturnal adaption. Nightjars (*Caprimulgidae*) are one of the few nocturnal birds that forage in a completely open space and have several unique features which have been hypothesized to aid in their nocturnal lifestyle. One of these is the presence of a unique sensory feature on the palate (Cowles, 1967). The palate is thought to be helpful in allowing for a quick reaction to prey when flying (Cramp, 1985). Nightjars also have a tapetum lucidum (Vee et al., 2022). This is a photoreflective structure found posterior to the photoreceptors in their eyes. It works by reflecting light forward to enhance the photosensitivity of the retina during low light conditions. The bill tip organ is a sensory adaptation present in several bird nocturnal species such as kiwis (Cunningham, 2013) and Night Parrots (Gottschaldt, 1985). However, it is also present in birds that mimic nocturnal habits by foraging in dense substrates where vision cannot help with locating prey, such as spoonbills (Threskiornithidae) and other probing birds, which forage by sticking their bills in cloudy water and mud (Cunningham, 2013) to search for prey items.

As of now, we know that hearing is an important aspect of bird ecology, with some birds evolving specialized adaptations. However, a broad framework for quantifying the morphological evolution of hearing adaptations among birds is lacking. Furthermore, although cochlear duct elongation may be an adaptation to nocturnal foraging in owls there is currently no clear evaluation of the link between cochlear duct length and the diel patterns among owls. Therefore, these adaptations remain poorly studied, particularly in the context of modern phylogenetic systematics and imaging methods. However, the purpose of this dissertation is to address this shortcoming.

Research Aim and Objectives

This study seeks to quantify patterns of variation in selected hearing-related skeletal adaptations among owls, , birds closely related to owls, birds that have been documented to use hearing for foraging and birds that have not been documented using hearing as a foraging technique, including ear asymmetry and cochlear duct length. To achieve this goal, I pursued the following aims and objectives:

Objective 1: Assess variation in proportional cochlear duct size among owls and comparative bird species and its relationship to measures of hearing frequency.

Objective 2: Quantitatively evaluate the distribution of external and internal cranial asymmetry in the hearing related structures of owls and comparative bird species.

Objective 3: Examine the pattern of evolution of hearing traits in owls and comparative bird species.

Onjective 4: Determine the relationship between proportional cochlear duct length, cranial asymmetry and ecological traits such as diel activity patterns and foraging style in owls and comparative bird species.

Taken together, this study aims to improve our understanding of how hearing-related traits and their ecological correlates have evolved in living owls and other bird species.

Materials and Methods

Materials

1. CT Scanning and Segmentation

Digital reconstructions and Computed Tomography (CT) scans of bird skulls were either downloaded from Morphosource (www.morphosource.org) or received directly from the American Museum of Natural History (See Appendix 1 for Morphosource media numbers of the digital reconstructions and CT scans). For the CT scans, I used the region-growing tool in VG Studio Max 3.2.2. (Volume Graphics, 2020) to create digital reconstructions of the entire skull and substructures of the bony labyrinth, including: the anterior, posterior and lateral semicircular canals; and the cochlear duct as represented by the endosseous space it occupies. Segmented elements were smoothed, refined and converted into meshes in both .ply and .stl formats. Whole labyrinth models downloaded from Morphosource were segmented into labyrinth substructures using AVIZO 3D 2021.1 (Thermo Fisher Scientific, 2024) and saved in .ply format. Seventy-four bird species were included in the study (Table 2).

Rationale for taxon choice

In assembling the dataset, we aimed to be as inclusive as possible of owl species for which scans were available, ensuring representation across each major lineage and most genera. In addition to owls, we incorporated a broad range of bird species with nocturnal foraging habits, such as the Southern brown kiwi (*Apteryx australis)*. We also included species with known sensory specializations that may not be strictly tied to diel activity patterns, for example, the American woodcock (*Scolopax minor*). To capture broader phylogenetic diversity, we incorporated non-passerine taxa from most major avian lineages, including species like the Red-legged seriema (*Cariama cristata)*, which lack reported sensory

adaptations. Most passerines were excluded due to limited scan availability, the rarity of documented sensory specializations, and their narrow body size range.

Table 1: Parameters Used for Mesh Creation in VGStudio.

Mesh type	**Grid based – precise and watertight**
Definition-used determined surface	Grid-based extraction
Simplification	On
Maximum number of triangles	800000

Table 2: List of bird specimens and corresponding specimen numbers included in this study. The species numbers are used in figures throughout this work.

Species name	Common name	Species number	Specimen number	Justification
Aegotheles cristatus	Australian owlet-nightjar	1	YPM 124258	Nocturnal forager outside of owls
Aegolius acadicus	Northern saw-whet owl	2	AMNH 14467	Owl species
Aegolius funereus	Boreal owl	3	AMNH 17953	Owl species
Alcedo atthis	Common kingfisher	4	NHMUK S/1994.7.1	Subaqueous forager outside of owls
Aptenodytes patagonicus	King penguin	5	UMZC 184D	Subaqueous forager outside of owls
Apteryx australis	Southern brown kiwi	6	FMNH 391011	Nocturnal forager outside of owls
Aramides cajaneus	Grey-cowled wood rail	7	UMZC Vertebrates 300.A	Generalist species outside of owls
Asio otus	Long-eared owl	8	AMNH 3632	Owl species
Athene cunicularia	Burrowing owl	9	AMNH 17584	Owl species
Athene cunicularia troglodytes	Burrowing owl	10	AMNH FLUID 7448	Owl species

Athene noctua	Little owl	11	NHMUK S/1996.11.1	Owl species
Batrachostomus auritus	Large frogmouth	12	NHMUK 1968.74.20	Nocturnal forager outside of owls
Bubo virginianus	Great horned owl	13	OUVC 10220	Owl species
Buteo rufofuscus	Jackal buzzard	14	NHMUK 1862.1.18.1	Generalist species outside of owls
Campethera caroli	Brown-eared woodpecker	15	NHMUK 191.5.31.453	Generalist species outside of owls
Caprimulgus macrurus	Large-tailed nightjar	16	FMNH 392245	Nocturnal forager outside of owls
Cariama cristata	Red-legged seriema	17	UMZC 724	Generalist species outside of owls
Chaetura pelagica	Chimney swift	18	FMNH 4390/1	Generalist species outside of owls
Chloroceryle amazona	Amazon kingfisher	19	UMMZ 20929	Subaqueous forager outside of owls
Chordeiles minor	Common nighthawk	20	UMMZ 233923	Generalist species outside of owls
Strix virgata	Mottled owl	21	AMNH 12654	Owl species
Circus cyaneus	Western marsh harrier	22	AMNH 24085	Diurnal auditory forager outside of owls
Circus aeruginosus	Hen harrier	23	NMSZ 1995.188	Diurnal auditory forager outside of owls
Circus pygargus	Montagu's harrier	24	AMNH 4209	Diurnal auditory forager outside of owls
Colius striatus	Speckled mousebird	25	FMNH 384817	Generalist species outside of owls
Collocalia mearnsi	Philippine swiftlet	26	FMNH 441729	Generalist species outside of owls
Columba livia	Homing pigeon	27	NHMUK pal:001	Generalist species outside of owls
Elanus caeruleus	Black-winged kite	28	NHMUK 1850.8.15.159	Diurnal auditory forager outside of owls

Elanus scriptus	Letter-winged kite	29	NMV B 8617	Diurnal auditory forager outside of owls
Gavia stellata	Red throated loon	30	NHMUK 1891.7.20.132	Subaqueous forager outside of owls
Glaucidium gnoma	Ferruginous pygmy owl	31	AMNH FLUID 2803	Owl species
Glaucidium cuculoides	Asian barred owlet	32	AMNH 28675	Owl species
Glaucidium brasilianum	Mountain pygmy owl	33	AMNH FLUID 7407	Owl species
Haliaeetus leucocephalus	Bald eagle	34	TMMM 7260	Diurnal auditory forager outside of owls
Ketupa ketupu	Buffy fish owl	35	AMNH 1312	Owl species
Macropygia amboinensis	Amboyna cuckoo-dove	36	KU B 93202	Generalist species outside of owls
Megascops kennicottii	Western screech owl	37	AMNH FLUID 9732	Owl species
Melanerpes carolinus	Red-bellied woodpeckers	38	NHMUK S/1988.103.7	Generalist species outside of owls
Melopsittacus undulatus	Budgerigar	39	OUVC 10569	Generalist species outside of owls
Morus bassanus	Northern gannet	40	NHMUK 1896	Subaqueous forager outside of owls
Ninox novaeseelandiae	Morepork	41	AMNH 11495	Owl species
Ninox odiosa	New Britain boobook	42	AMNH 7424	Owl species
Bubo scandiaca	Snowy owl	43	NHMUK S/1998.59.1	Owl species
Nyctibius griseus	Common potoo	44	UMMZ 136371	
Oreotrochilus chimborazo	Ecuadorian hillstar	45	AMNH 6070	Generalist species outside of owls

Otus spilocephalus	Mountain scops owl	46	NHMUK S/1974.25.42	Owl species
Oxyura jamaicensis	Ruddy duck	47	NHMUK 1985.70.4	Subaqueous forager outside of owls
Pandion haliaetus	Osprey	48	FMNH 437336	Subaqueous forager outside of owls
Pelecanoides urinatrix	Common diving petrel	49	NHMUK S/2006.1.14	Subaqueous forager outside of owls
Pelecanus occidentalis	Brown pelican	50	NHMUK S/1973.66.16	Subaqueous forager outside of owls
Pezoporus occidentalis	Night parrot	51	QM O 29055	Nocturnal forager outside of owls
Phalacrocorax carbo	Great cormorant	52	NMS Z 2000	Subaqueous forager outside of owls
Phodilus badius	Oriental bay owl	53	AMNH 7836	Owl species
Picus viridis	European green woodpecker	54	NHMUK S/1982.5.1	Generalist species outside of owls
Podargus strigoides	Tawny frogmouth	55	FMNH 345114	Nocturnal forager outside of owls
Podiceps taczanowskii	Junin grebe	56	UMMZ 156784	Subaqueous forager outside of owls
Podilymbus gigas	Atitlán grebe	57	UMMZ 150794	Subaqueous forager outside of owls
Psittacus erithacus	African grey parrot	58	NMHUK S/1992.41.60	Generalist species outside of owls
Pulsatrix perspicillata	Spectacled owl	59	NHMUK 1871.10,25,6	Owl species
Sagittarius serpentarius	Secretary bird	60	NHMUK 1898.5.7.1	Generalist species outside of owls
Ninox albifacies	Laughing owl	61	UMZC 497d	Owl species
Scolopax minor	American woodcock	62	FMNH 432410	Generalist species outside of owls
Spheniscus demersus	African penguin	63	L JZ 60	Subaqueous forager outside of owls
Steatornis caripensis	Oilbird	64	FMNH 318679	Nocturnal forager outside of owls

Sterna hirundo	Common tern	65	NMUK S/1975.65.4	Subaqueous forager outside of owls
Strigops habroptila	Kakapo	66	NHMUK 1881.1.17.71	Nocturnal forager outside of owls
Strix varia	Tawny owl	67	AMNH 886	Owl species
Strix aluco	Great grey owl	68	NHMUK S/2001.81.1	Owl species
Strix nebulosa	Barred Owl	69	AMNH 32440	Owl species
Surnia ulula	Northern hawk-owl	70	AMNH 27935	Owl species
Turdus olivater	Olive thrush	71	FMNH Birds 319675	Generalist species outside of owls
Turdus olivaceus	Black-hooded thrush	72	L JZ 94	Generalist species outside of owls
Tyto alba	Barn Owl (Lesser Antilles)	73	AMNH FLUID 7473	Owl species
Tyto capensis	African grass owl	74	AMNH 2046	Owl species

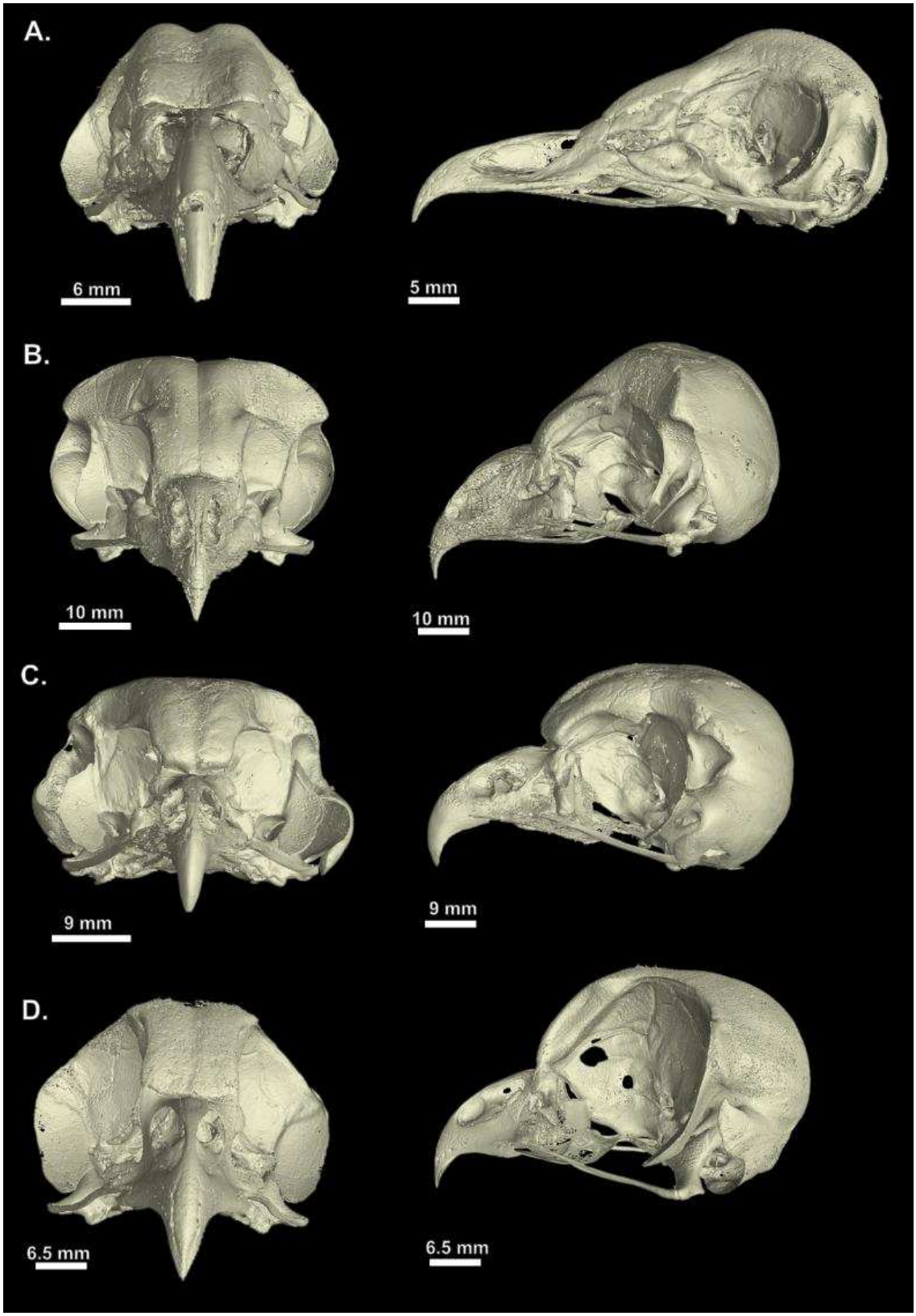


Figure 1: Anterior and left lateral view of owl skulls obtained using the above segmentation technique. A) *Tyto capensis* (AMNH 2046) B) *Asio otus* (AMNH 3632) C) *Aegolius acadicus* (AMNH 14467) (D) *Megascops kennicottii* (AMNH FLUID 9732). These owl taxa represent the diversity in the morphology of the owl braincase.

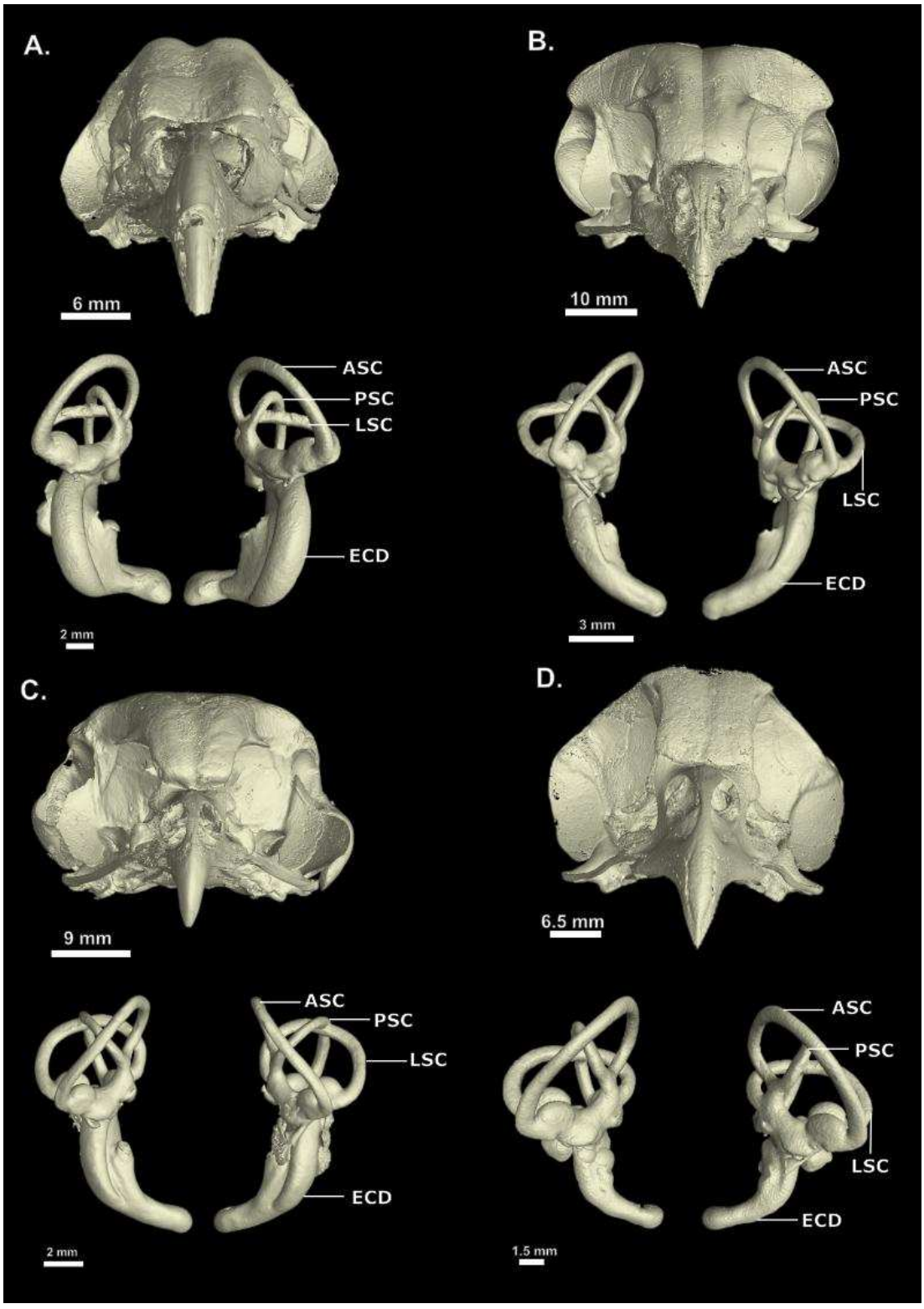


Figure 2:Anterior view of owl skulls and their associated labyrinths segmented using the above described technique. A) ***Tyto capensis*** **(AMNH 2046) B)** ***Asio otus*** **(AMNH 3632) C)** ***Aegolius acadicus*** **(AMNH 14467) D)** ***Megascops kennicotti*** **(AMNH FLUID 9732)**

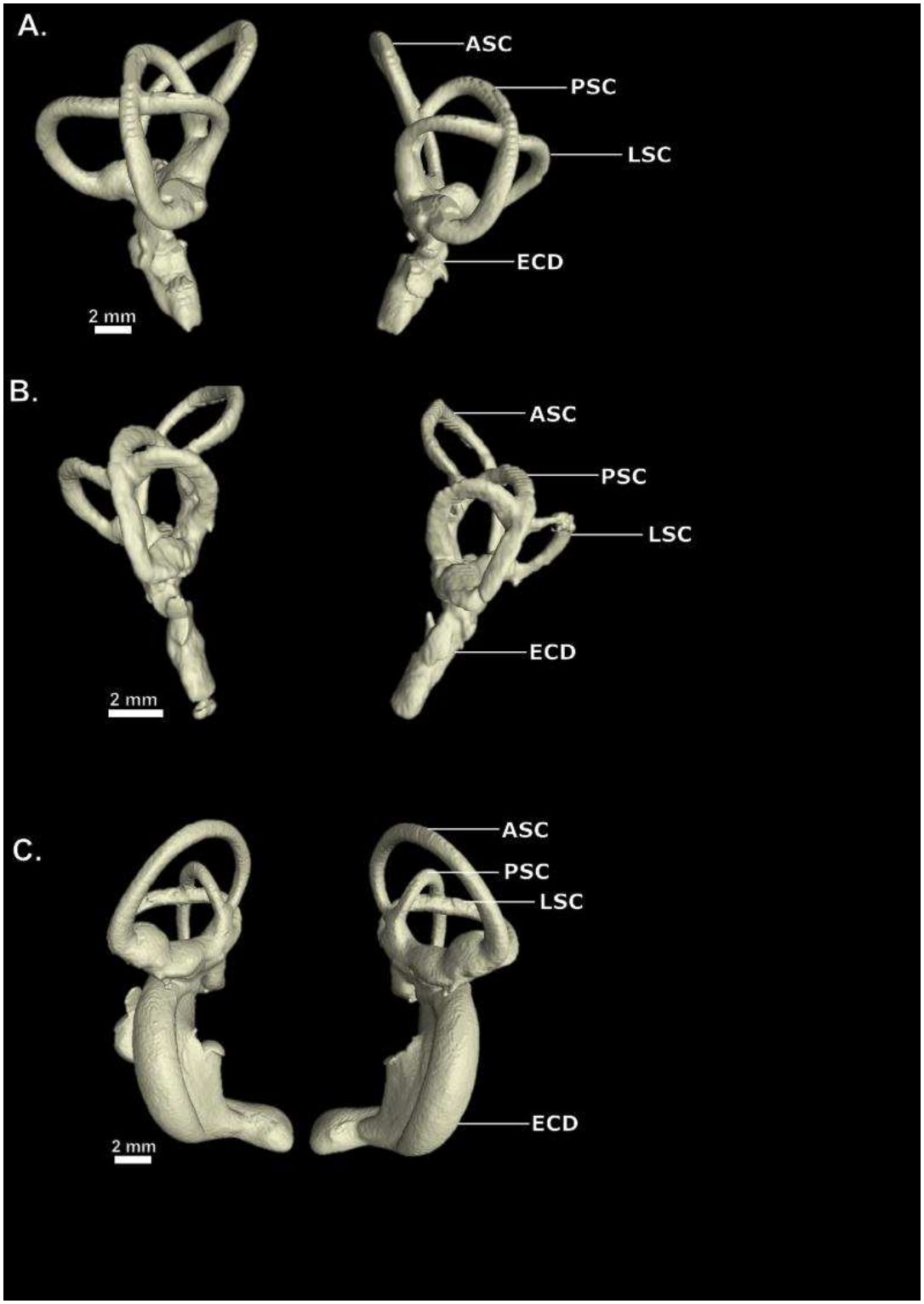


Figure 3: Anterior view of bird left and right labyrinths segmented using the above described technique showing the variation in cochlear duct length and morphology in birds. A) *Haliaeetus leucocephalus* (TMMM 7260) B) *Pandion haliaetus* (FMNH 437336) C) *Tyto capensis* (*AMNH 2046)*. Abbreviations: Cochlear duct (ECD); Anterior semicircular canal (ASC); Lateral semicircular canal (LSC); Posterior semicircular canal (PSC)

Methods

1. Natural history observations

Categorical variables were created for natural history observations such as diet, hunting techniques and diel activity patterns. Information used to score the birds based on the natural history observations categories was obtained from the already existing academic literature, bird watcher websites (www.birdsoftheworld.org) and bird behaviour videos (www.youtube.com). The categories and respective classifications can be found in Table 3. The subaqueous hunting category refers to birds such as penguins and loons and not osprey. For diet, the classifications were made using what the birds' diet consistently mostly of throughout the year. Hunting techniques were based on the dominant foraging strategy. When multiple foraging strategies were described by literature (e.g., visual and auditory), both strategies were indicated for that bird. For the diel activity patterns, whenever a bird was described as falling under multiple classifications, e.g. diurnal and crepuscular or nocturnal and crepuscular, the birds were classified as only diurnal or nocturnal. However, if a bird was described as nocturnal, diurnal and crepuscular, I classified them as unknown. The final table showing the natural history observations can be found in Table 4. All the classifications were binary variables

Table 3: The natural history observations and associated classifications used to score all the bird taxa used in study.

Category	Classification
Diet	1. Mainly mammals 2. Mainly arthropods 3. Mainly fish 4. Mainly plant material 5. Opportunistic
Hunting technique	1. Auditory 2. Vision 3. Subaqueous 4. Olfaction

Diel activity pattern	1. Nocturnal 2. Diurnal 3. Crepuscular 4. Unknown

Table 4: Natural observations gathered from literature, bird watcher websites and bird behaviour videos for each specimen included in the study. The birds were classified using the classifications in Table 3.

Species name	Hunting technique	Diel activity pattern	Diet
Aegotheles cristatus	Vision	Nocturnal	Arthropods
Aegolius acadicus	Auditory	Nocturnal	Mammals
Aegolius funereus	Auditory	Nocturnal	Mammals
Alcedo atthis	Subaqueous	Diurnal	Fish
Aptenodytes patagonicus	Subaqueous	Diurnal	Fish
Apteryx australis	Olfaction	Nocturnal	Arthropods
Aramides cajaneus	Vision	Nocturnal	Arthropods
Asio otus	Auditory and Vision	Nocturnal	Mammals
Athene cunicularia	Vision	Nocturnal	Mammals
Athene cunicularia troglodytes	Vision	Nocturnal	Mammals
Athene noctua	Vision	Nocturnal	Mammals
Batrachostomus auritus	Vision	Nocturnal	Arthropods
Bubo virginianus	Auditory and Vision	Nocturnal	Mammals
Buteo rufofuscus	Vision	Diurnal	Mammals
Campethera caroli	Vision	Diurnal	Arthropods
Caprimulgus macrurus	Vision	Nocturnal	Arthropods
Cariama cristata	Vision	Diurnal	Arthropods
Chaetura pelagica	Vision	Diurnal	Arthropods
Chloroceryle amazona	Subaqueous	Diurnal	Arthropods
Chordeiles minor	Vision	Nocturnal	Arthropods
Strix virgata	Auditory	Nocturnal	Mammals
Circus cyaneus	Auditory	Crepuscular	Mammals
Circus aeruginosus	Auditory	Diurnal	Mammals
Circus pygargus	Vision	Diurnal	Arthropods
Colius striatus	Vision	Diurnal	Plants
Collocalia mearnsi	Vision	Diurnal	Arthropods
Columba livia	Vision	Diurnal	Plants

Elanus caeruleus	Vision	Diurnal	Mammals
Elanus scriptus	Vision	Nocturnal	Mammals
Gavia stellata	Subaqueous	Diurnal	Fish
Glaucidium gnoma	Vision	Diurnal	Mammals
Glaucidium cuculoides	Vision	Diurnal	Arthropods
Glaucidium brasilianum	Vision	Diurnal	Mammals
Haliaeetus leucocephalus	Vision	Diurnal	Fish
Ketupa ketupu	Vision	Nocturnal	Fish
Macropygia amboinensis	Vision	Diurnal	Plants
Megascops kennicottii	Auditory	Nocturnal	Mammals
Melanerpes carolinus	Vision	Diurnal	Generalist
Melopsittacus undulatus	Vision	Diurnal	Plants
Morus bassanus	Subaqueous	Diurnal	Fish
Ninox novaeseelandiae	Vision	Nocturnal	Arthropods
Ninox odiosa	Vision	Nocturnal	Arthropods
Bubo scandiaca	Auditory	Diurnal	Mammals
Nyctibius griseus	Unknown	Nocturnal	Arthropods
Oreotrochilus chimborazo	Olfaction	Diurnal	Plants
Otus spilocephalus	Auditory	Nocturnal	Arthropods
Oxyura jamaicensis	Subaqueous	Diurnal	Arthropods
Pandion haliaetus	Subaqueous	Diurnal	Fish
Pelecanoides urinatrix	Subaqueous	Diurnal	Arthropods
Pelecanus occidentalis	Subaqueous	Diurnal	Fish
Pezoporus occidentalis	Unknown	Nocturnal	Plants
Phalacrocorax carbo	Subaqueous	Diurnal	Fish
Phodilus badius	Auditory	Nocturnal	Mammals
Picus viridis	Vision	Diurnal	Arthropods
Podargus strigoides	Vision	Nocturnal	Arthropods
Podiceps taczanowskii	Subaqueous	Diurnal	Fish
Podilymbus gigas	Subaqueous	Diurnal	Fish
Psittacus erithacus	Vision	Diurnal	Plants
Pulsatrix perspicillata	Auditory	Nocturnal	Arthropods
Sagittarius serpentarius	Vision	Diurnal	Arthropods
Ninox albifacies	Unknown	Nocturnal	Arthropods
Scolopax minor	Vision	Diurnal	Arthropods
Spheniscus demersus	Subaqueous	Diurnal	Fish
Steatornis caripensis	Olfaction	Nocturnal	Plants
Sterna hirundo	Subaqueous	Diurnal	Fish
Strigops habroptila	Olfaction	Nocturnal	Plants
Strix varia	Unknown	Nocturnal	Mammals
Strix aluco	Auditory and Vision	Unknown	Mammals

Strix nebulosa	Auditory and Vision	Nocturnal	Opportunistic
Surnia ulula	Vision	Diurnal	Mammals
Turdus olivater	Vision	Diurnal	Plants
Turdus olivaceus	Vision	Diurnal	Arthropods
Tyto alba	Auditory	Nocturnal	Mammals
Tyto capensis	Auditory	Nocturnal	Mammals

2. Braincase measurements

Choiniere et al. (2021) used braincase height as a scalar for understanding the allometric relationships between inner ear measurements and body size, based on use of statistical model comparison to evaluate which measurement is most suitable for normalising cochlear duct length in birds. I collected braincase height measurements for my dataset by using the complete segmented skull meshes and taking the measurement from the basicranial floor to the top of the skull roof using the 3D length function in Amira 5.4.5 (Choiniere et al., 2021). Figure 3 shows an example of a braincase height measurement.



Figure 4: Braincase height measurement method shown on *Aegolius acadicus* (AMNH 14467).

3. Body mass values

Bird species body mass values were collected to enable the testing of this allometric covariate against braincase height to assess which variable better explains size variation in cranial features. These body mass values were obtained from the EltonTraits Database (Wilman et al., 2014), where measurements are derived from the natural history literature. No average or midpoint values had to be calculated as none of the body mass values provided were ranges. Sexual dimorphism could not be considered in this thesis, as the relevant data are generally not available for scans or for species-specific body mass in the available literature. However, given that the measurements were derived from the same set of specimens and given that I was looking for broad trends across the tree, I do not envision that sample variance due to sexual dimorphism is a complicating factor. 4. Hearing performance data

Variables derived from audiograms available in ornithology literature were used to assess the relationships of cochlear duct length to hearing performance. Data on the hearing frequency range (kHz) including the high and low frequency limit, the best frequency (kHz) and best sensitivity (dB SPL) from audiograms published in the ornithological literature was collected. The frequency range provides the range of frequencies the birds can perceive. The cut-off sound levels chosen were 60- and 35-dB SPL. Sixty dB is the typical sound level from a human perspective and has traditionally been used in similar studies of mammals (Heffner et al. 2004; Heffner et al 2007). However, a cut-off of 35 dB was also used to maximize available data available on birds. Experimental techniques used in the literature were not used as a restriction in obtaining the audiogram data. The final table with the hearing performance data can be found in Table 5.

Table 5: The hearing performance data for some of the bird taxa included in the study. The N/A represents measurements where data was not available.

Species	Audiogram reference	High frequency limit (kHz) (6odb cut off)	Low frequency limit (kHz) (60dB cut off)	High frequency limit (kHz) (35db cut off)	Low frequency limit (kHz) (35dB cut off)	Best sensitivity (dB SPL	Best frequency (kHz)
Aeogolius acadicus	Beatini et al., 2017	10	N/A	8.45	0.55	4	4
Asio otus	Van Dijk, 1972	N/A	N/A	9.5	N/A	-21	6
Columba livia	Heffner et al 2013	6.463	0.0404	4.976	0.186	15	1
Gavia stellata	Crowel et al., 2016	0,51	N/A	4.8	0.51	61	2
Haliaeetus leucocephalus	McGee et al., 2019	7.98	N/A	4.8	0.39	2	2
Melanerpes carolinus	Lohr et al., 2013	5.6	0.5	N/A	N/A	40	2.86
Melopsittacus undulatus	Heffner et al., 2016	7.621	0.086	6.462	0.218	1	3.2
Ninox novaeseelandie	Calford, 1988	7.3	N/A	5.9	2.1	28	3
Oxyura jamaicensis	Crowel et al., 2015	N/A	3.44	N/A	N/A	38	2.9
Phalacrocorax carbo sinensis	Maxwell et al., 2017	N/A	N/A	3.9	1.1	19	2
Spheniscus demersus	Wever et al., 1969	N/A	N/A	N/A	N/A	-58	1.26

Strix aluco	Van Dijk, 1973	N/A	N/A	N/A	N/A	-15	6
Tyto alba	Dyson et al., 1998	N/A	N/A	12.067	N/A	-20	13.1

5. Landmarking of labyrinths

A combination of curve landmarks and point landmarks were used to measure the lengths of the different components of the labyrinth and for shape analysis. A single point landmark determines the start or end of the semicircular canal or cochlear duct. The list of landmarks can be found in Table 6. For the semicircular canals, these included a combination of point landmarks, located on the ampullae, and curve landmarks along the curve of the semicircular canals. For the cochlear duct, these included point landmarks placed at the beginning and end of the cochlear duct and curve landmarks that were placed along the length of the cochlear duct. The landmarks were placed on the models using the auto skeleton function in Avizo 3D 2021.1 to obtain the midline of the semicircular canals and the cochlear duct. Landmarks were manually adjusted in some instances where the skeletonization process led to inaccurate midline visualizations.

Table 6: List of labyrinth landmarks used to landmark the midline of the semicircular canals and cochlear ducts of the bird labyrinths. Abbreviations: Anterior semicircular canal (ASC); Lateral semicircular canal (LSC); Posterior semicircular canal (PSC); Cochlear duct (ECD)

Landmark name	**Landmark type**
Labyrinth ASC Ampulla	Point landmark
Labyrinth ASC	Curve landmarks
Labyrinth ASC Vestibule	Point landmark
Labyrinth LSC Ampulla	Point landmark

Labyrinth LSC	Curve landmarks
Labyrinth LSC Vestibule	Point landmark
Labyrinth PSC Ampulla	Point landmark
Labyrinth PSC	Curve landmarks
Labyrinth PSC Vestibule	Point landmark
Labyrinth ECD length start points	Point landmark
Labyrinth ECD length	Curve landmarks
Labyrinth ECD length end point	Point landmark

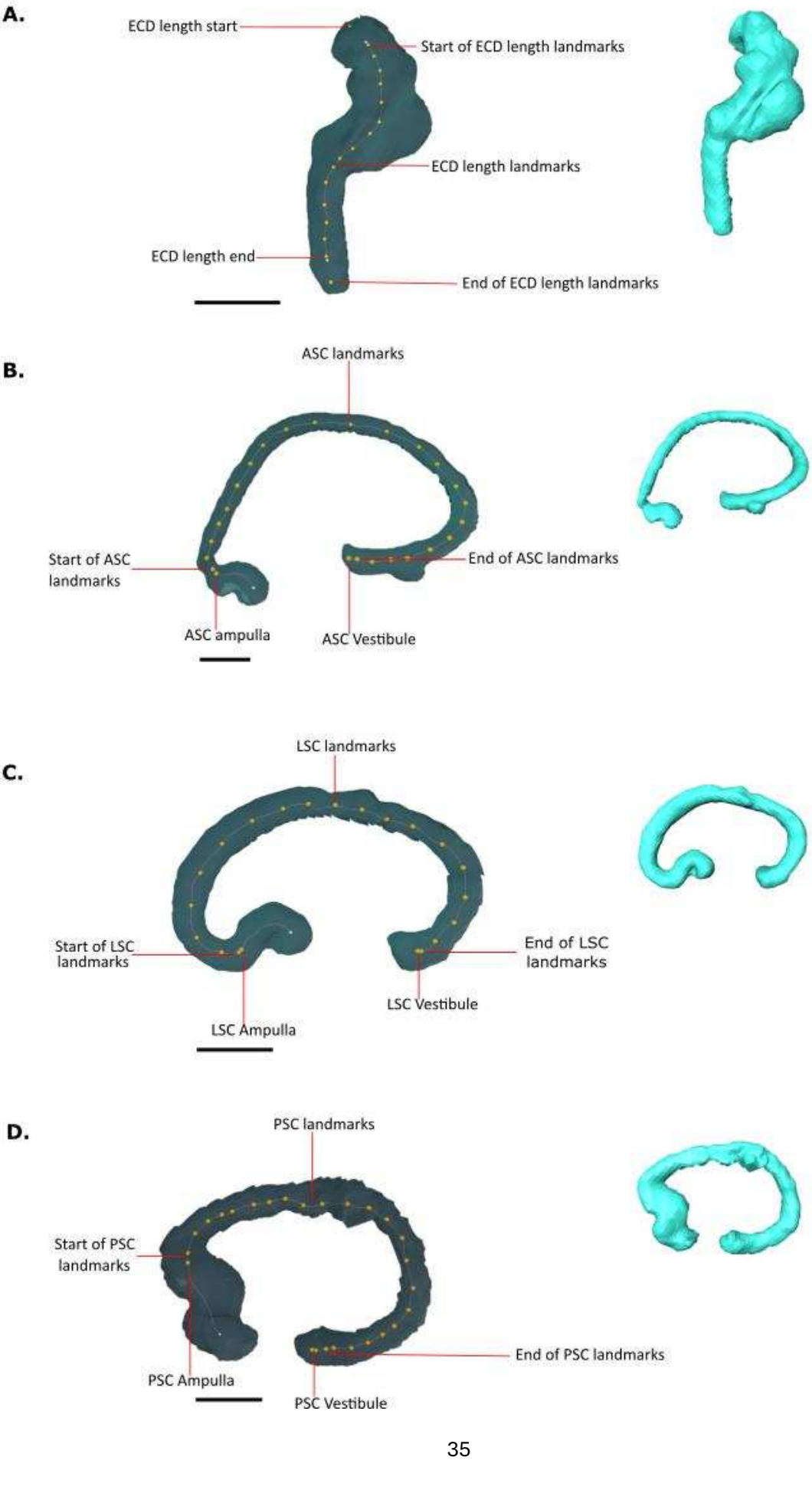

A.
ECD length start
Start of ECD length landmarks
ECD length landmarks
ECD length end
End of ECD length landmarks
B.
ASC landmarks
Start of ASC landmarks
End of ASC landmarks
ASC ampulla
ASC Vestibule
C.
LSC landmarks
Start of LSC landmarks
End of LSC landmarks
LSC Vestibule
LSC Ampulla
D.
PSC landmarks
Start of PSC landmarks
End of PSC landmarks
PSC Ampulla
PSC Vestibule

Figure 5: Illustration of the skeletonized and landmarked left labyrinth of *Macropygia amboinensis* (KU B 93202). A) Semi-transparent cochlear duct model showing placed landmarks. B) Semi-transparent anterior semicircular canal model showing placed landmarks. C) Semi-transparent lateral canal model showing placed landmarks. D) Semi-transparent posterior semicircular canal model showing placed landmarks. Scale for the semi-transparent model=1mm

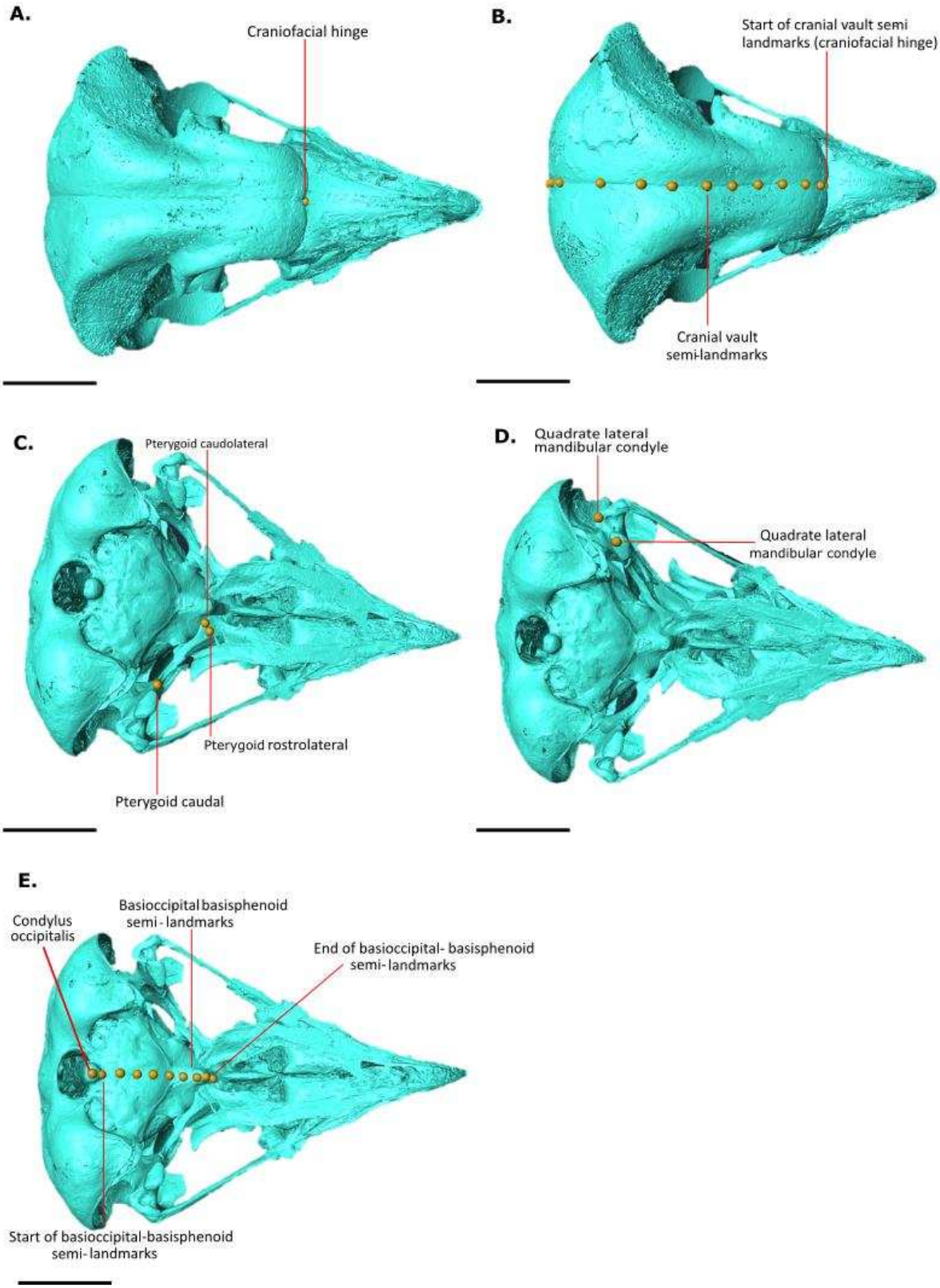
6. Landmarking of skulls

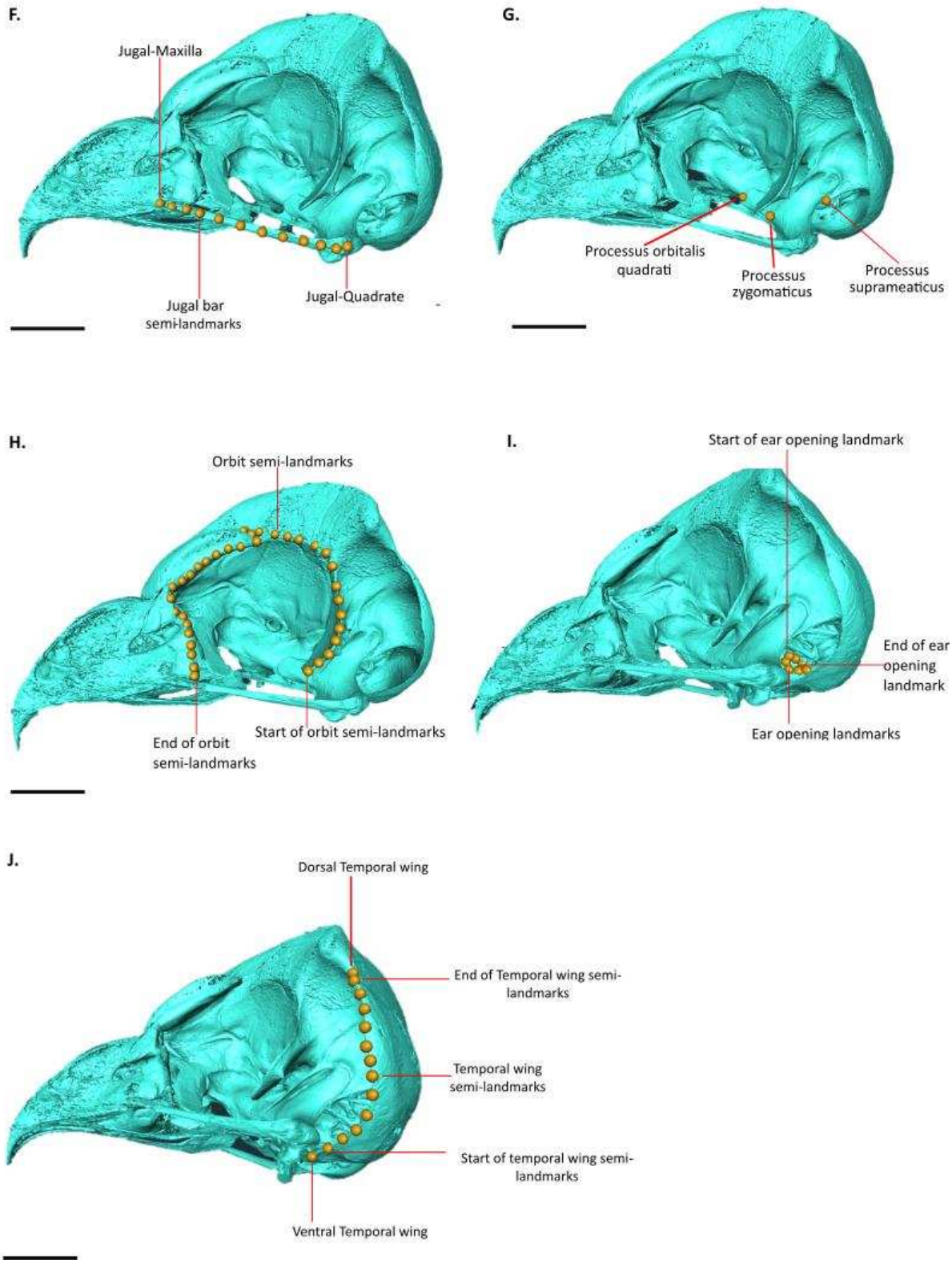
Skull shapes of birds were characterised with a combination of curve landmarks and point landmarks. The aim of these landmarks was to capture the variation in the posterior part of the skull, particularly the temporal wing as this was the region shown to be asymmetrical in some owls (Norberg, 2002). Most of the landmarks were the same as those used by Bjarnason & Benson (2021). These included orbit, jugal, basioccipital, basisphenoid, cranial vault, beak, quadrate, pterygoid, condylus occipitalis and foramen magnum landmarks. I adjusted this landmark list by removing the beak landmarks as they are unrelated to testing my core hypotheses. I added landmarks for the temporal wing and the opening of the ear as these regions could potentially exhibit asymmetry. A list of the final fixed and semi-landmarks used to landmark the skulls can be found in and is illustrated by Figure 2. All the landmarks and sliding landmarks were manually placed using Avizo 2D 2021.1.

Table 7: List of cranial landmarks used for bird crania.

Landmark name	**Landmark type**	**Side**
Skull Cranial Facial Hinge	Point landmark	Midline
Skull Jugal maxilla articulation	Point Landmark	Left/Right
Skull Jugal quadrate articulation	Point Landmark	Left/Right
Skull Jugal	Semi-landmark series	Left/Right
Skull Processus Zygomaticus	Point Landmark	Left/Right

Skull Processus Suprameatica	Point Landmark	Left/Right
Skull Quadrate Optical Process	Point Landmark	Left/Right
Skull Quadrate Medial Mandibular Condyle	Point Landmark	Left/Right
Skull Quadrate Lateral Mandibular Condyle	Point Landmark	Left/Right
Skull Pterygoid Posterior	Point Landmark	Left/Right
Skull Pterygoid Anterior Medial	Point Landmark	Left/Right
Skull Pterygoid Anterior Lateral	Point Landmark	Left/Right
Skull Condylus Occipitalis	Point Landmark	Midline
Skull Orbit	Curve landmarks	Left/Right
Skull Cranial Vault	Curve landmarks	Midline
Skull Foramen Magnum	Curve landmarks	Left/Right
Skull Basioccipital Basisphenoid	Curve landmarks	Midline
Skull Dorsal Temporal Wing	Point Landmark	Left/Right
Skull Ventral Temporal Wing	Point Landmark	Left/Right
Skull Temporal Wing Edge	Curve landmarks	Left/Right
Skull Ear Opening	Curve landmarks	Left/Right


A.
Craniofacial hinge
B.
Start of cranial vault semi landmarks (craniofacial hinge)
Cranial vault semi-landmarks
C.
Pterygoid caudolateral
Pterygoid rostrolateral
Pterygoid caudal
D.
Quadrate lateral mandibular condyle
Quadrate lateral mandibular condyle
E.
Condylus occipitalis
Basioccipital basisphenoid semi-landmarks
End of basioccipital- basisphenoid semi-landmarks
Start of basioccipital-basisphenoid semi-landmarks


F.
Jugal-Maxilla
Jugal bar semi-landmarks
Jugal-Quadrate
G.
Processus orbitalis quadrati
Processus zygomaticus
Processus suprameaticus
H.
Orbit semi-landmarks
End of orbit semi-landmarks
Start of orbit semi-landmarks
I.
Start of ear opening landmark
End of ear opening landmark
Ear opening landmarks
J.
Dorsal Temporal wing
End of Temporal wing semi-landmarks
Temporal wing semi-landmarks
Start of temporal wing semi-landmarks
Ventral Temporal wing

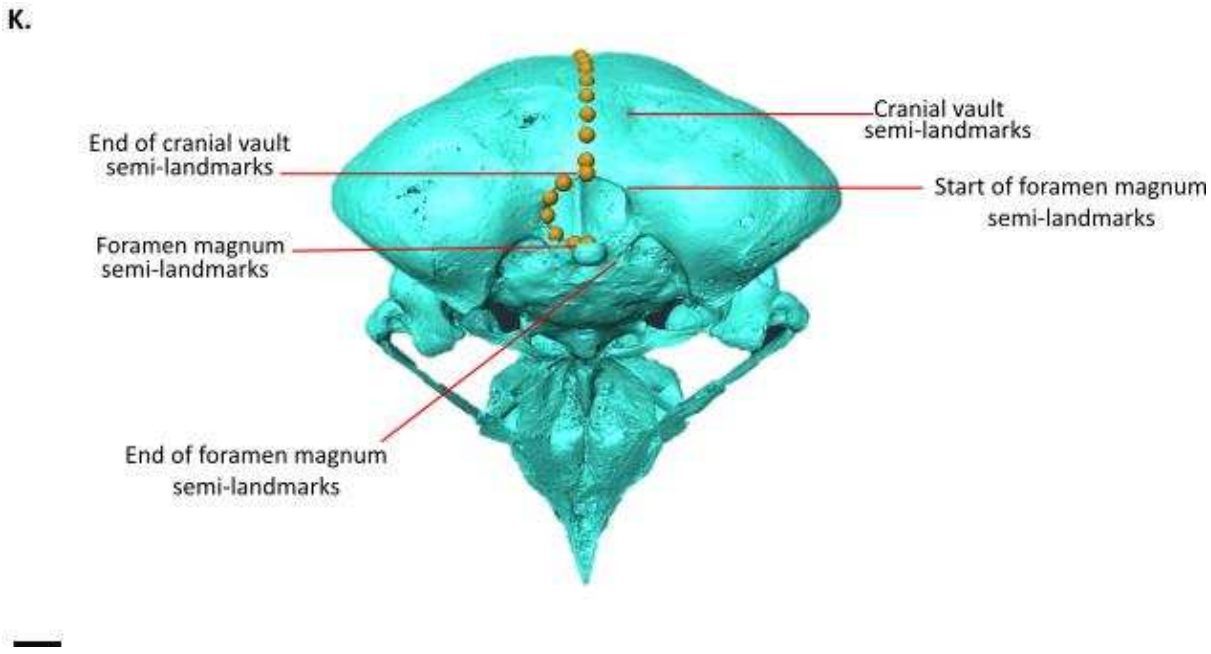


Figure 6:Illustration of the cranial landmarks on *Asio otus* (AMNH 3632). A) Craniofacial hinge landmark. B) Cranial vault landmarks. C) Pterygoid landmarks. D) Quadrate landmarks. E) Condylus occipitalis and basioccipital basisphenoid landmarks. F) Jugal landmarks. G) Processus landmarks. H) Orbit landmarks. I) Landmarks along the opening of the ear. J) Temporal wing landmarks. K) Cranial vault landmarks and foreman magnum landmarks. Scale=10mm

7. Landmark analysis

7.1 Labyrinth length calculations

All analysis of labyrinth landmarks took place in RStudio 2024.04.1 (R Core Team, 2023) using RStudio IDE (RStudio Team, 2023) using functions from the packages geomorph version 4.0.7 (Baken et al., 2021; Adams et al., 2024) and phytools version 2.3.0 (Revell, 2024). In R Studio, the landmarks were compiled and organized into anterior, lateral, posterior semicircular canals and cochlear duct rows.

Using the landmark array, and the row numbers for the different semicircular canals and cochlear ducts, the Euclidean distances between the curve landmark points, and the end landmark points were measured. The distances were calculated in series to represent the total length of each structure. Finally, the distances were then summed to get the total length along

the structure. This was done for each semicircular canal and each cochlear duct for the species in Table 2.

7.2 Asymmetry calculations

7.2.1 Calculating cranial asymmetry values

Due to damage, some of the skulls were missing portions of the anatomy, and so did not have complete cranial landmark sets. Therefore, a decision had to be made on whether to analyse more sets of landmarks, in fewer specimens, or fewer sets of landmarks, in more specimens. When making this decision, the landmarks on structure that have well-documented asymmetry in some species, such as the temporal wing, were prioritized to maximise the number of bird skulls that can be used in this analysis. The final list of specimens included in cranial asymmetry analysis can be found in Table 8.

In R Studio, cranial landmarks were compiled into left and right arrays (e.g. *Asio otus* left landmarks and *Asio otus* right landmarks). I reflected the left landmarks so that their points were transposed to the anatomical space defined by the right landmarks. I then aligned these reflected landmarks to their contralateral sides using Procrustes alignment. The Procrustes (Euclidean) distances between each of the landmark pairs was calculated for each specimen. The resulting summed distance reflects the total geometric offset in three dimensions between individual landmark points for each anatomical area. The Procrustes distances were calculated for the orbit, jugal, temporal wing and basioccipital-basisphenoid landmarks using R studio package geomorph version 4.0.7 (Baken et al., 2021; Adams et al., 2024).

Table 8:Final list of specimens included in cranial asymmetry analysis.

Species name	Common name	Species number	Specimen number
Aegolius acadicus	Northern saw-whet owl	2	AMNH 14467
Aegolius funereus	Boreal owl	3	AMNH 17953
Apteryx australis	Southern brown kiwi	6	FMNH 391011
Aramides cajaneus	Grey-cowled wood rail	7	UMZC Vertebrates 300.A
Asio otus	Long-eared owl	8	AMNH 3632
Athene cunicularia	Burrowing owl	9	AMNH 17584
Athene cunicularia troglodytes	Burrowing owl	10	AMNH FLUID 7448
Athene noctua	Little owl	11	NHMUK S/1996.11.1
Bubo virginianus	Great horned owl	13	OUVC 10220
Buteo rufofuscus	Jackal buzzard	14	NHMUK 1862.18.1
Caprimulgus macrurus	Large-tailed nightjar	16	FMNH 392245
Chloroceryle amazona	Amazon kingfisher	19	UMMZ 20929
Strix virgata	Mottled owl	21	AMNH 12654
Circus aeruginosus	Hen harrier	23	NMSZ 1995.188
Colius striatus	Scpeckled mousebird	25	FMNH 384817
Columba livia	Homing pigeon	27	NHMUK pal:001
Gavia stellata	Red throated loon	30	NHMUK 1891.7.20.132
Glaucidium cuculoides	Asian barred owlet	32	AMNH 28675
Haliaeetus leucocephalus	Bald eagle	34	TMMM 7260
Ketupa ketupu	Buffy fish owl	35	AMNH 1312
Macropygia amboinensis	Amboyna cuckoo-dove	36	KU B 93202
Megascops kennicottii	Western screech owl	37	AMNH FLUID 9732

Melanerpes carolinus	Red-bellied woodpeckers	38	NHMUK S/1988.103.7
Morus bassanus	Northern gannet	40	NHMUK 1896
Ninox novaeseelandiae	Morepork	41	AMNH 11495
Ninox odiosa	New Britain boobook	42	AMNH 7424
Oreotrochilus chimborazo	Ecuadorian hillstar	45	AMNH 6070
Otus spilocephalus	Mountain scops owl	46	NHMUK S/1974.25.42
Oxyura jamaicensis	Ruddy duck	47	NHMUK 1985.70.4
Pelecanoides urinatrix	Common diving petrel	49	NHMUK S/2006.1.14
Pelecanus occidentalis	Brown pelican	50	NHMUK S/1973.66.16
Picus viridis	European green woodpecker	54	NHMUK S/1982.5.1
Podargus strigoides	Tawny frogmouth	55	FMNH 345114
Podiceps taczanowskii	Junin grebe	56	UMMZ 156784
Podilymbus gigas	Atitlán grebe	57	UMMZ 150794
Psittacus erithacus	African grey parrot	58	NMHUK S/1992.41.60
Pulsatrix perspicillata	Spectacled owl	59	NHMUK 1871.10,25,6
Sagittarius serpentarius	Secretary bird	60	NHMUK 1898.5.7.1
Ninox albifacies	Laughing owl	61	UMZC 497d
Scolopax minor	American woodcock	62	FMNH 432410
Strigops habroptila	Kakapo	66	NHMUK 1881.1.17.71
Strix aluco	Great grey owl	68	NHMUK S/2001.81.1

Strix nebulosa	Barred owl	69	AMNH 32440
Surnia ulula	Northern hawk-owl	70	AMNH 27935
Turdus olivater	Olive thrush	71	FMNH Birds 319675
Tyto alba insularis	Barn owl (Lesser Antilles)	73	AMNH FLUID 7473
Tyto capensis	African grass owl	74	AMNH 2046

7.2.2 Calculating semicircular canal asymmetry values

The semicircular canal asymmetry values were calculated using the same process outlined for the cranial asymmetry. In R studio, the semicircular canal landmarks were compiled into left and right arrays. Left semi-circular canals were then reflected so that their points entered anatomical space defined by the right semi-circular canals. The reflected landmarks were aligned to their contralateral sides using Procrustes alignment. The Procrustes (Euclidean) distances between the left and right landmark sets were then calculated for each specimen. The resulting summed distance reflects the total geometric offset in three dimensions between individual landmark points for each anatomical area. The Procrustes distances were calculated for the anterior, posterior and lateral semicircular canal landmarks. R studio package geomorph version 4.0.7 (Baken et al., 2021; Adams et al., 2024) was used to do this.

8. Statistical tests

Ordinary least squares regressions and phylogenetic regressions

Ordinary least squares regressions and phylogenetic least squares PGLS regressions were used to test the relationships between semicircular canal lengths, cochlear duct lengths and other size metrics. To obtain the average cochlear duct lengths, the sums of the left and right cochlear duct lengths were calculated and divided by two. In cases where a species only had

one cochlear duct, only that cochlear duct measurement was used. The average sum of the semicircular canal lengths was calculated by getting the sum of the average of the left and right semicircular canals. The average values were used to account for uncertainties in landmark positions. All measurements were $\log_{10}$-transformed prior to analysis.

Two types of regressions were employed: Generalized Least Squares (OLS) and Phylogenetic Generalized Least Squares (PGLS). OLS models assume equal (or zero) covariances between the traits of different species, ignoring the expected differences in covariation due to shared phylogenetic history (Felsenstein 1985). This model is appropriate when assessing correlations where phylogenetic covariance is not expected to be a complicating factor – for example when assessing measured lengths of the left and right sides of the same bird. Phylogenetic regressions (Grafen, 1989) are a form of generalised least squares regression that addresses the problem of high type II (i.e. false positive) error rates when analysing comparative data using ordinary least squares regression (e.g. Felsenstein 1985). Modelling the phylogenetic covariances, ensures that resulting covariances do not result only from differences in duration of shared evolutionary history and is useful for evaluating ecomorphological relationships. The final list of OLS and PGLS models which were run can be found in Table 8.

The tree used for the phylogenetic regressions was downloaded from the phylogeny subsets in Vertlife.org website. It is a representative tree of birds adapted from the Jetz et al (2012) supertree distribution, using the Hackett et al. (2008) phylogeny as a backbone. I did the analysis by choosing a single phylogeny from among the 100 total trees that most closely resemble current consensus on bird phylogeny (see final phylogeny in Figure 6). Future work will enable me to check my findings on multiple trees to assess their robustness. However, the phylogenetic structure of owls appears to have little variation in the various competing phylogenetic hypotheses. As this phylogeny has only extant taxa and has no subspecies,

extinct taxa such as *Ninox albifacies*, *Podilymbus gigas* and the subspecies *Athene cunicularia troglodytes* were not included in the PGLS.

OLS regressions were implemented using the functions glm() from the stats package (R Core Team, 2023). PGLS regressions were implemented using the functions gls() from the ape package version 5.8 (Paradis and Schliep, 2019). I used a method that calculates the coefficient of determination, implemented in the performance package version 0.12.4 (Lüdecke et al., 2021) to calculate the R^2 values. Models were visualized using ggplot2 version 3.5.1 (Wickham, 2016) and phytools version 2.3.0 (Revell, 2024).

Table 9: Table listing all the OLS and PGLS models conducted for this study. With specifications given on which model residuals were mapped onto the phylogenetic tree. Abbreviations: Braincase height (BCH); Body mass (BM); Average sum of the semicircular canal length (AvSumSCC); Average cochlear duct length (AvCD); Left anterior semicircular canal (LASC); Right anterior semi-circular canal (RASC); Left posterior semicircular canal (LPSC); Right anterior semicircular canal (RPSC); Left lateral semicircular canal (LLSC); Right lateral semicircular canal (RLSC); Left cochlear duct (LECD); Right cochlear duct (RECD).

Statistical model	OLS	PGLS	Reason	Residuals mapped onto phylogeny
LASC length ~RASC length	Yes	No	To quantify size asymmetry between the left and right anterior semicircular canal	No
LPSC length ~RPSC length	Yes	No	To quantify size asymmetry between the left and right posterior semicircular canal	No
LLSC length ~RLSC length	Yes	No	To quantify size asymmetry	No

			between the left and right lateral semicircular canal	
LECD length ~ RECD length	Yes	Yes	To quantify size asymmetry between the left and right cochlear duct	No
AvCD length~ BCH	Yes	Yes	To quantify the relationship between braincase height and cochlear duct length in birds and to generate residuals that index relative size of the cochlear duct for the braincase height.	Yes
AvCD length ~ BM	Yes	Yes	To quantify the relationship between body mass and cochlear duct length in birds and to generate residuals that index relative size of the cochlear duct for the body mass.	Yes
BCH ~ BM	Yes	Yes	To quantify the relationship between body mass and braincase height in birds and to generate residuals that	Yes

			index relative size of the braincase height for the body mass.	
AvSumSCC ~ BCH	Yes	Yes	To quantify the relationship between braincase height and the sum of the semicircular canals in birds and to generate residuals that index relative size of the average sum of the semicircular canals for the braincase height.	No
AvSumSCC ~ BM	Yes	Yes	To quantify the relationship between body mass and the sum of the semicircular canals in birds and to generate residuals that index relative size of the average sum of the semicircular canals for the body mass.	No
AvSumSCC ~ AvCD	Yes	Yes	To quantify the relationship between cochlear duct length and the sum of the length of the semicircular canals and to	Yes

			generate residuals that index relative size of the average sum of the semicircular canals for the cochlear duct length.	
BCH residuals ~ AvCD residuals	Yes	No	To quantify the relationship between relative semicircular canal lengths and relative cochlear duct length.	
AvCD ~ BCH + diel activity patterns	No	Yes	To quantify the effects of diel activity patterns on the relative length of the cochlear duct after controlling for variation in braincase height.	No
AvCD ~ BCH + Hunting style	No	Yes	To quantify the effects different hunting techniques on the average length of the cochlear duct after controlling for variation in braincase height.	

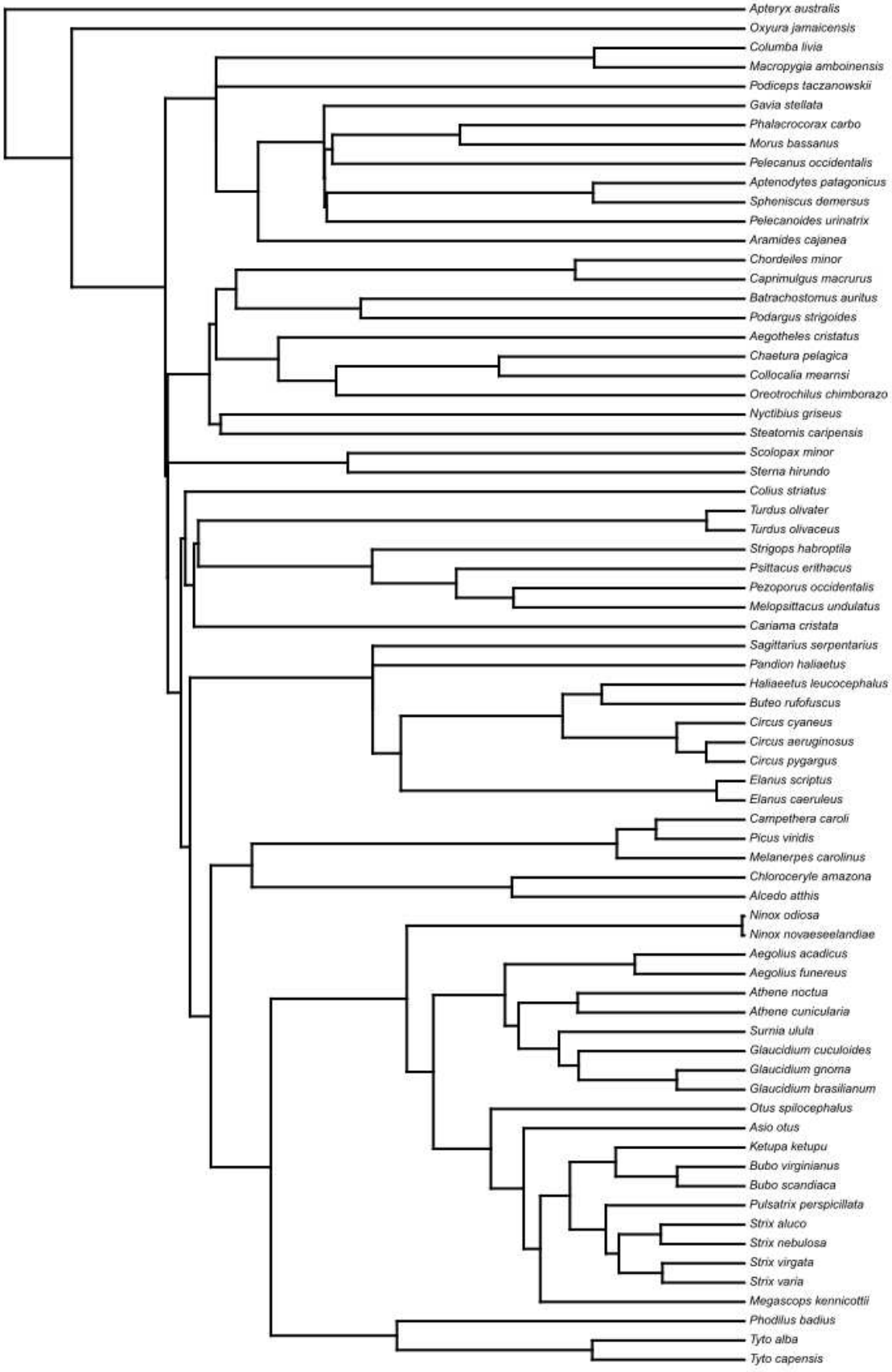

Apteryx australis
Oxyura jamaicensis
Columba livia
Macropygia amboinensis
Podiceps taczanowskii
Gavia stellata
Phalacrocorax carbo
Morus bassanus
Pelecanus occidentalis
Aptenodytes patagonicus
Spheniscus demersus
Pelecanoides urinatrix
Aramides cajanea
Chordeiles minor
Caprimulgus macrurus
Batrachostomus auritus
Podargus strigoides
Aegotheles cristatus
Chaetura pelagica
Collocalia mearnsi
Oreotrochilus chimborazo
Nyctibius griseus
Steatornis caripensis
Scolopax minor
Sterna hirundo
Colius striatus
Turdus olivater
Turdus olivaceus
Strigops habroptila
Psittacus erithacus
Pezoporus occidentalis
Melopsittacus undulatus
Cariama cristata
Sagittarius serpentarius
Pandion haliaetus
Haliaeetus leucocephalus
Buteo rufofuscus
Circus cyaneus
Circus aeruginosus
Circus pygargus
Elanus scriptus
Elanus caeruleus
Campethera caroli
Picus viridis
Melanerpes carolinus
Chloroceryle amazona
Alcedo atthis
Ninox odiosa
Ninox novaeseelandiae
Aegolius acadicus
Aegolius funereus
Athene noctua
Athene cunicularia
Surnia ulula
Glaucidium cuculoides
Glaucidium gnoma
Glaucidium brasilianum
Otus spilocephalus
Asio otus
Ketupa ketupu
Bubo virginianus
Bubo scandiaca
Pulsatrix perspicillata
Strix aluco
Strix nebulosa
Strix virgata
Strix varia
Megascops kennicottii
Phodilus badius
Tyto alba
Tyto capensis

Figure 7: A representative tree of birds adapted from Jetz et al (2012) supertree distribution, using the Hackett et al. (2008) phylogeny as a backbone.

9. Mapping residuals of the regressions onto the phylogenetic tree

To visualize patterns of trait evolution and distributions, particularly for cranial asymmetry and proportional cochlear duct length, I mapped residuals from some of the phylogenetic regressions on the phylogenetic tree in Figure 6. The list of models that had their regressions mapped on the phylogeny can be found in Table 9. Residuals were mapped onto this tree using the ape version 5.8 (Paradis and Schliep, 2019), geiger version 2.0.11 (Pennell et al., 2024) and ggplot2 version 3.5.1 (Wickham, 2016) packages in R Studio.

Results

1. Labyrinth landmark analysis

1.1 Cochlear duct and semicircular canal lengths distribution

The anterior semicircular canals are the longest, and the posterior canals are the shortest, on average (see Fig. 8). There is very little overall variation among the lengths of the comparable semicircular canals as indicated by the small standard deviation values for all the semicircular canals (see Table 10). The lateral semicircular canals have the most outliers, however certain taxa are recuring outliers. *Haliaeetus leucocephalus* is a positive outlier for both LSC and PSC lengths and *Oreotrochilus chimborazo* is a negative outlier for both ASC and LSC lengths.

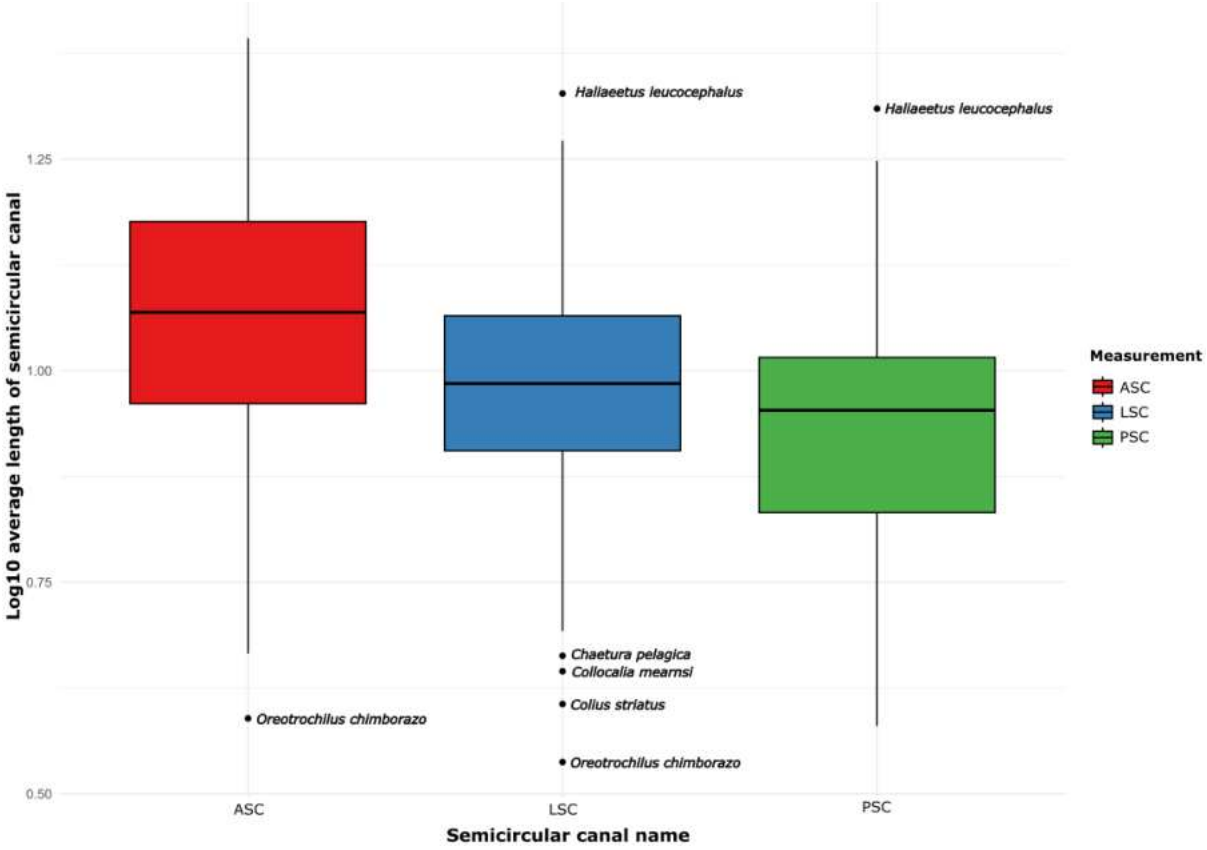


Figure 8: Box plot depicting the average length of the left and right anterior (ASC), lateral (LSC) and (PSC) semicircular canals for the entire dataset. The boxplot illustrates the distribution of average left and right semicircular canal lengths across the birds in the dataset. The central line of each box plots represents the median, while the lower and upper boundaries of the boxes correspond to the first (Q1) and third quartiles (Q3) respectively. This indicates the interquartile range (IQR) and these values can be found in Table 11. Outliers are represented by individual points.

Table 10: Summary statistics for the box plot depicting the average length of the left and right semicircular canals in Figure 7.

Measurement	Min	Q1	Median	Mean	Q3	Max	SD
ASC	0.5891	0.9611	1.0691	1.0672	1.1764	1.3931	0.1788
LSC	0.5376	0.9056	0.985	0.9691	1.065	1.3277	0.1659
PSC	0.5801	0.8324	0.9533	0.9385	1.0157	1.3099	0.1571

1.2 Semicircular canal size asymmetry

Regressions of left vs right semicircular canal log-lengths reveal tight positive correlations in all cases (Fig 8). R-squared values are strong (~0.9; see Table 12) in all such regressions indicating that the contralateral semicircular canals have generally similar lengths. Residuals from this relationship are generally low and symmetrically distributed, with little bias between owls and non-owls.

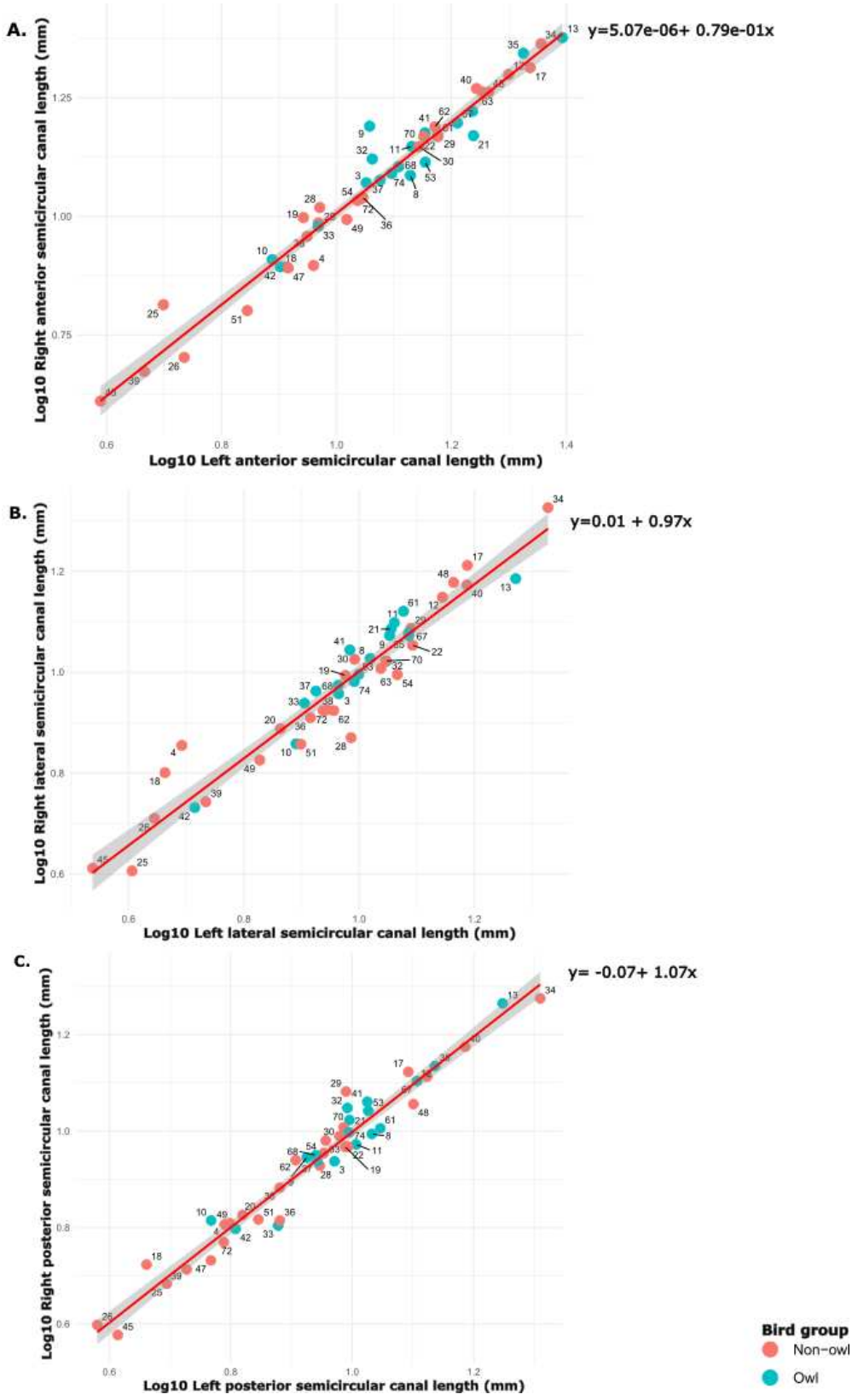


Figure 9: OLS regression showing the correlation between the logged lengths of the right and left semicircular canals. A) Anterior semicircular canals. B) Lateral semicircular canals. C) Posterior semicircular canals. Relevant model parameters can be found in Table 12. The regression illustrates the relationship between the length of

the left semicircular canals and the size of the right semicircular canals for the analysed bird species. Individual species are represented by singular points numbered according to the numbers in Table 2. The blue points represent the owls while the non-owl birds are represented by the pink points. The x-axis corresponds to the logged left semicircular canal length (mm) and the y-axis corresponds to the logged right semi-circular canal length (mm). The red line indicates the line of best fit and the shaded region around the line indicates the 95% confidence interval.

1.3 Cochlear duct size asymmetry

Regressions of left vs right cochlear duct log-lengths reveal a strong positive correlation (Fig 9). The correlation coefficient is strong (~0.801; see Table 12) indicating that the contralateral cochlear ducts have generally similar lengths. This relationship has higher residuals than the semicircular canals, however the residuals are symmetrically distributed, with little bias between owls and non-owls. The larger number of residuals in the cochlear duct measurements than the semicircular measurements is because the measurement error is larger for cochlear duct length. This is a result of the larger amount of variation in calculation of the midline skeletons of the cochlear ducts using the autoskeleton function, due to their wider diameters.

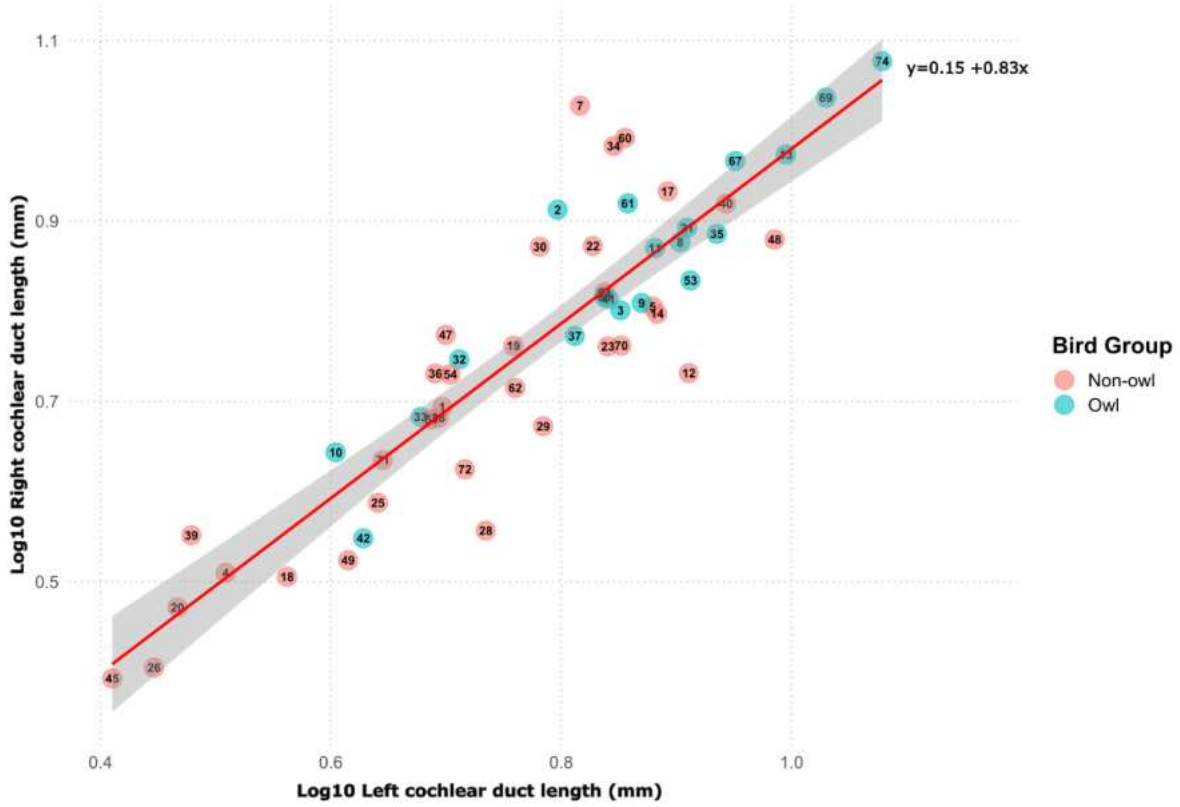


Figure 10:GLS regression showing the correlation between the logged lengths of the right and left cochlear duct in owl and non-owl birds. The scatterplot in shows the relationship between the logged left cochlear duct length and the logged length of the right cochlear duct length across the bird taxa included in the study. The x-axis represents the logged length of the left cochlear duct length (mm), while the y-axis denotes the logged length of the right cochlear duct (mm). A single species is represented by each point, with numbers indicating the species according to Table 12. Owls are represented by the blue points while birds which are not owls are represented by the pink points. The red line indicates the line of best fit and the shaded region around the line indicates the 95% confidence interval.

2. Model outputs

Table 11: Summary of model statistics for the ordinary least squares (OLS) models and the phylogenetic regressions (PGLS) models listed in Table 9. Abbreviations: Braincase height (BCH); Body mass (BM); Average sum of the semicircular canal length (AvSumSCC); Average cochlear duct length (AvCD); Left anterior semicircular canal (LASC); Right anterior semi-circular canal (RASC); Left posterior semicircular canal (LPSC); Right anterior semicircular canal (RPSC); Left lateral semicircular canal (LLSC); Right lateral semicircular canal (RLSC); Left cochlear duct (LECD); Right cochlear duct (RECD); Intercept (b_0); Slope (b_1); Sample size (N)

Model name	Term	P-value (PGLS)	P-value (OLS)	b_0	b_1	R^2 (OLS)	AIC (OLS)	AIC (PGLS)	N
LASC ~ RASC	$\log_{10}$ RASC length	N/A	<2e-16 ***	5.07e-06	9.96e-01	0.959	-163.27	N/A	45
LPSC ~ RPSC	$\log_{10}$ RPSC length	N/A	<2e-16 ***	0.01	0.97	0.957	-174.45	N/A	45
LLSC ~ RLSC	$\log_{10}$ RLSC length	N/A	<2e-16 ***	-0.07	1.07	0.924	-138.26	N/A	45
LECD ~ RECD	$\log_{10}$ RECD length	N/A	<2e-16 ***	0.15	0.83	0.801	-132.37	N/A	54
AvCD ~ BCH	$\log_{10}$ AvCD length	$<1.0 \times 10^{-4}$ ***	<2e-16 ***	0.65	2.36	0.690	-140.33	-148.66	73
AvCD ~ BM	$\log_{10}$ BM	$<1.0 \times 10^{-4}$ ***	6.32e-08 ***	0.42	0.14	0.340	-88.47	-107.14	73
BCH ~ BM	$\log_{10}$ BM	$<1.0 \times 10^{-4}$ ***	<2e-16 ***	0.82	0.21	0.675	-139.3	-140.88	74
AvSumSCC ~ BCH	$\log_{10}$ BCH	$<1.0 \times 10^{-4}$ ***	< 2e-16 ***	0.34	0.86	0.817	-128.93	-137.97	54
AvSumSCC ~ BM	$\log_{10}$ BM	$<1.0 \times 10^{-4}$ ***	8.36e-15 ***	0.97	0.21	0.689	-100.27	-90.45	54
AvCD ~ AvSumSCC	$\log_{10}$ AvSumSCC	$<1.0 \times 10^{-4}$ ***	5.79e-13 ***	-0.42	0.81	0.635	-89.406	-93.41	54

(Residuals of AvSumSCC ~ BCH) ~ (Residuals of AvCD ~ BCH)	Residuals of AvSumSCC ~ BCH	N/A	0.1211	-0.0001	0.05	0.034	-168.70	N/A	54
AvCD ~ BCH+ Hunting style	log_{10} Braincase	<1.0 × 10^{-4} ***	N/A			N/A	N/A	-153.66	
	Intercept	<1.0 × 10^{-4} ***							
	Vision	0.8947							
	Auditory	0.0274 *							
	Olfaction	0.4555							
	Subaqueous	0.9358							
AvCD ~ BCH + Diel activity patterns	log_{10} Braincase	<1.0 × 10^{-4} ***						-149.29	
	Intercept	<1.0 × 10^{-4} ***							
	Diurnal	0.5714							
	Nocturnal	0.5283							
	Crepuscular	0.1908							

*** Indicates highly significant values ($p < 0.001$); * Indicates significant values ($p < 0.05$)

The labyrinth lengths models have very high R^2 values ranging from 0.801 in the LECD~RECD model to 0.959 in the LASC ~ RASC model. This indicates very little

difference in the lengths of the left and right semicircular canal lengths and cochlear duct lengths. The AvCD ~ BCH and AvSumSCC ~ BCH models have R^2 values that are higher than AvCD ~ BM and AvSumSCC ~ BM models, indicating that braincase height is a better proxy for labyrinth lengths. The (Residuals of AvSumSCC ~ BCH) ~ (Residuals of AvCD ~ BCH) has the lowest R-squared value from the models in Table 12 despite having a significant p-value. This result indicates that variation in the relative length of the cochlear duct does not place constraint on the relative size of the semicircular canals. Overall, the AIC values for PGLS models are lower than that of the OLS models, except for the AvSumSCC ~ BM model, indicating better model fits when using phylogenetic regressions. All the hunting styles, apart from vision, have no significant effect on cochlear duct length in birds as indicated by the non-significant p-vales for the AvCD ~ BCH+ Hunting style model in Table 12. Furthermore, all the p-values for the AvCD ~ BCH + Diel activity patterns model are non-significant, indicating that diel activity patterns do not affect the cochlear duct length of birds.

3. The relationship between labyrinth lengths, body mass and braincase height

The PGLS regression between $\log_{10}$ braincase height and $\log_{10}$ body mass has a strong positive correlation but has significant residual structure where positive residuals reflect birds with larger braincase heights relative to body mass, and negative residuals reflect birds with smaller braincase heights relative to body mass. Residuals are symmetrically distributed with owls making up majority of the positive residuals. This residual pattern indicates that many owls have a head size larger than what is expected for their body mass, with only a few exceptions having smaller head sizes.

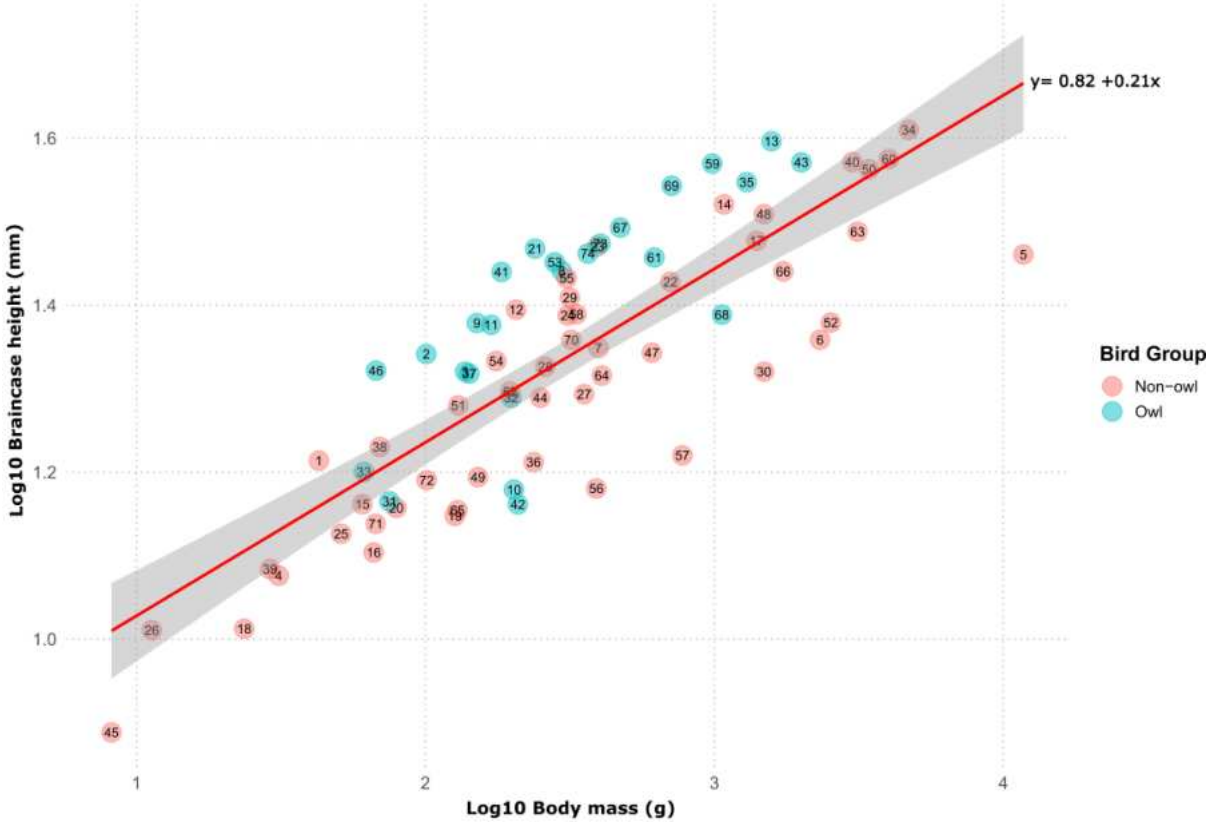


Figure 11: PGLS regression illustrating the relationship between log-transformed body mass and log-transformed braincase height in owls and non-owl bird species. The scatterplot shows the relationship between logged body mass and the logged braincase height across the bird taxa included in the study. The x-axis represents the logged body mass (g) values, while the y-axis denotes the logged braincase height (mm) values. A single species is represented by each point, with numbers indicating the species according to Table 2. Owls are represented by the blue points while birds which are not

owls are represented by the pink points. The red line indicates the line of best fit and the shaded region around the line indicates the 95% confidence interval.

The average sum of the semicircular canal lengths is positively correlated with both body mass and braincase height, even when phylogenetic covariance structure is accounted for Table 12. More variation in the average semicircular canal is explained by braincase height than body mass, therefore I consider braincase height to be more appropriate as a normalization factor for average sum of the semicircular canal lengths in all my subsequent analyses.

PGLS regressions between $\log_{10}$ semicircular canal length and $\log_{10}$ braincase height are strong but have significant residual structure where positive residuals reflect birds with longer semicircular canals than expected and negative residuals reflect birds with shorter semicircular canals than expected. The residuals have little pattern and owls do not contribute significantly to the lowest or highest values. Owls, however, in general have low residuals, falling close to the regression line, indicating they have close to average relative semicircular canal lengths when indexed on braincase height. Larger positive residuals include birds such as *Chloroceryle amazona, Batrachostomus auritus* and *Buteo rufofuscus.* These taxa have proportional semicircular size that is approximately 1.4 times more than what is expected for their braincase height. Larger negative residuals include *Oxyura jamaicensis, Pelecanus occidentalis* and *Tyto capensis.* These taxa have proportional semicircular size that is approximately 1.4 times less than what is expected for their braincase height.

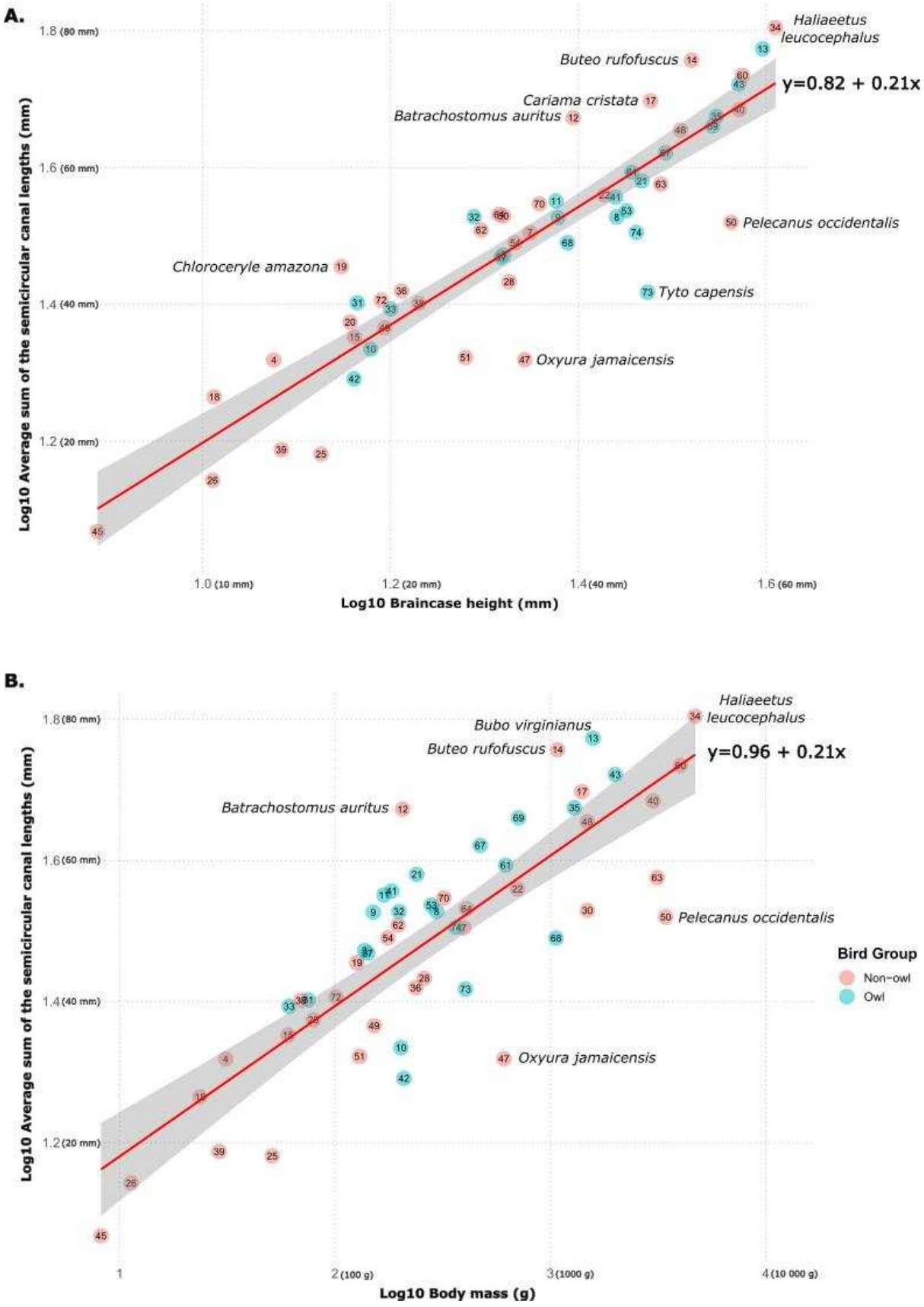


Figure 12:PGLS regressions illustrating the relationship between the log-transformed average sum of the semicircular canals against log-transformed braincase height and

log-transformed body mass in owls and non-owl bird species. Figure 12(A) shows the relationship between braincase height and the logged average sum of the semicircular canals across the bird taxa included in the study. The x-axis represents the logged braincase height (mm) values, while the y-axis denotes the logged average sum of the semicircular canals length (mm) values. A single species is represented by each point, with numbers indicating the species according to Table 2. Owls are represented by the blue points while birds which are not owls are represented by the pink points. The red line indicates the line of best fit and the shaded region around the line indicates the 95% confidence interval. Figure 11(B) shows the relationship between logged body mass and the logged average sum of the semicircular canal length in the bird taxa included in the study. The x-axis represents the logged body mass (g) values, while the y-axis denotes the logged average sum of the semicircular canal length (mm) values. A single species is represented by each point, with numbers indicating the species according to Table 2 Owls are represented by the blue points while birds which are not owls are represented by the pink points. The red line indicates the line of best fit and the shaded region around the line indicates the 95% confidence interval.

The PGLS regression between $\log_{10}$ average cochlear duct length and $\log_{10}$ braincase height (Fig.12) has a moderate positive correlation with significant residual structure where positive residuals reflect birds with a longer cochlear duct relative to braincase height and negative residuals reflect birds with a shorter cochlear duct relative to braincase height. Both the distributions between owls and non-owls are relatively symmetrical, however owls have a slight right skew as the mean is greater than the median (Table 12; Fig. 14). Furthermore, the residuals are roughly symmetrically distributed, although owls are skewed towards proportionally longer cochlear ducts (Fig. 13). All owls have cochlear ducts either proportionally average or proportionally greater than predicted from their braincase heights, with most of their positive residuals lying above the 95% confidence intervals (Fig. 12). Furthermore, non-owl birds show more variability while owls have more tightly clustered residuals (Table 12). The owls with the highest positive distributions include *Tyto capensis* and *Bubo scandiaca,* however high positive residuals are also present in non-owl birds such as *Steatornis caripensis.* These birds have cochlear ducts that are ~1.86 times the predicted length for their braincase heights. Other owls with positive distributions (e.g., *Aegolius acadicus, Aegolius funereus, Athene noctua, Phodilus badius, Strix varia, Strix nebulosa*) have cochlear ducts that are ~1.31-1.15 times their predicted lengths for birds of similar head

sizes. A smaller number of non-owl birds enter this space of positive residuals (e.g., *Chloroceryle amazona*, *Podiceps taczanowskii*, *Nyctibius griseus*, *Pandion haliaetus*). Birds with the lowest negative distributions have cochlear ducts that are proportionally ~ 1.78 times smaller than predicted for birds of similar head sizes. This includes *Strigops habroptila*, *Phalacrocorax carbo* and *Haliaeetus leucocephalus.* A larger number of non-owl birds enter this space of negative residuals (e.g., *Chordeiles minor*, *Podilymbus gigas*, *Elanus caeruleus*, *Apteryx australis*, *Pelecanus occidentalis*) with their cochlear ducts being ~ 1.51 – 1.1 times smaller than the predicted length for birds of similar head sizes.

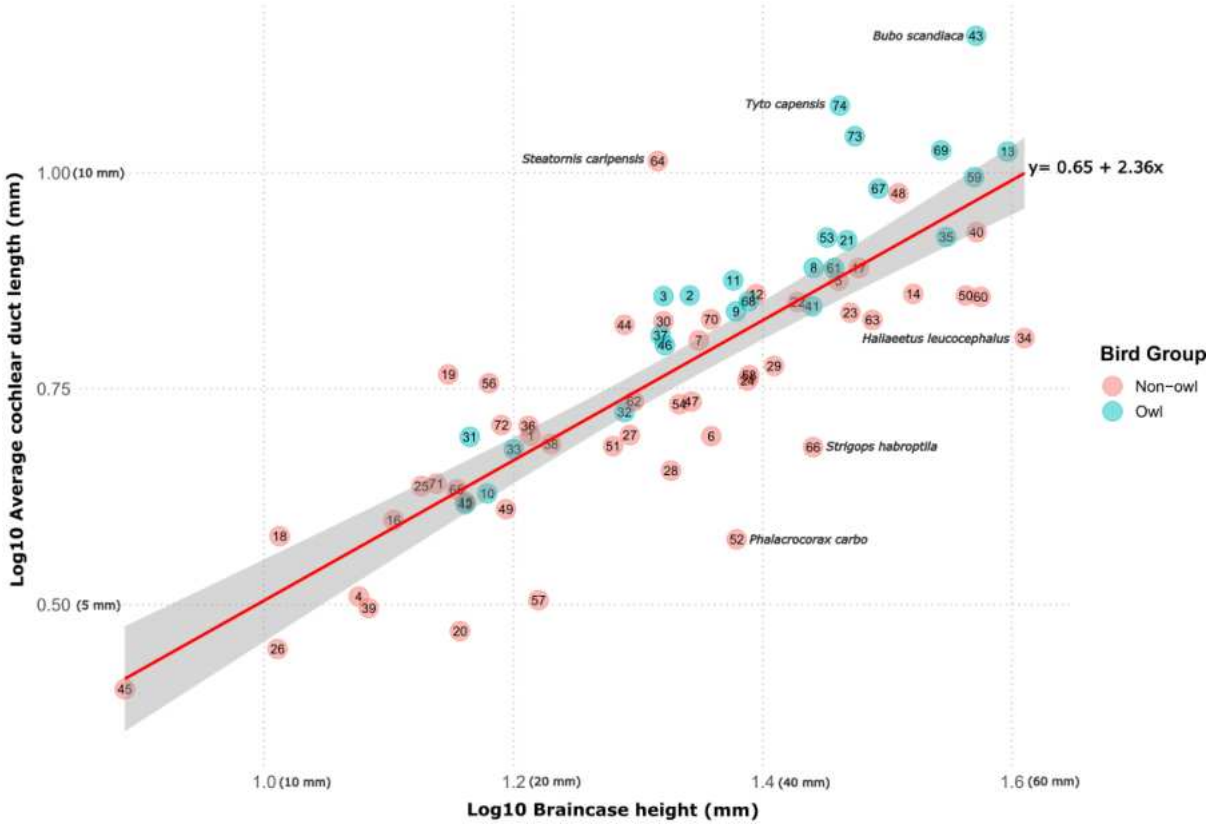


Figure 13: PGLS regression illustrating the relationship between log-transformed average cochlear duct length and log-transformed braincase height in owls and non-owl bird species. The x-axis represents the logged braincase height (mm) values, while the y-axis denotes the logged average cochlear duct length (mm) values. A single species is

represented by each point, with numbers indicating the species according to Table 2. Owls are represented by the blue points while birds which are not owls are represented by the pink points. The red line indicates the line of best fit and the shaded region around the line indicates the 95% confidence interval

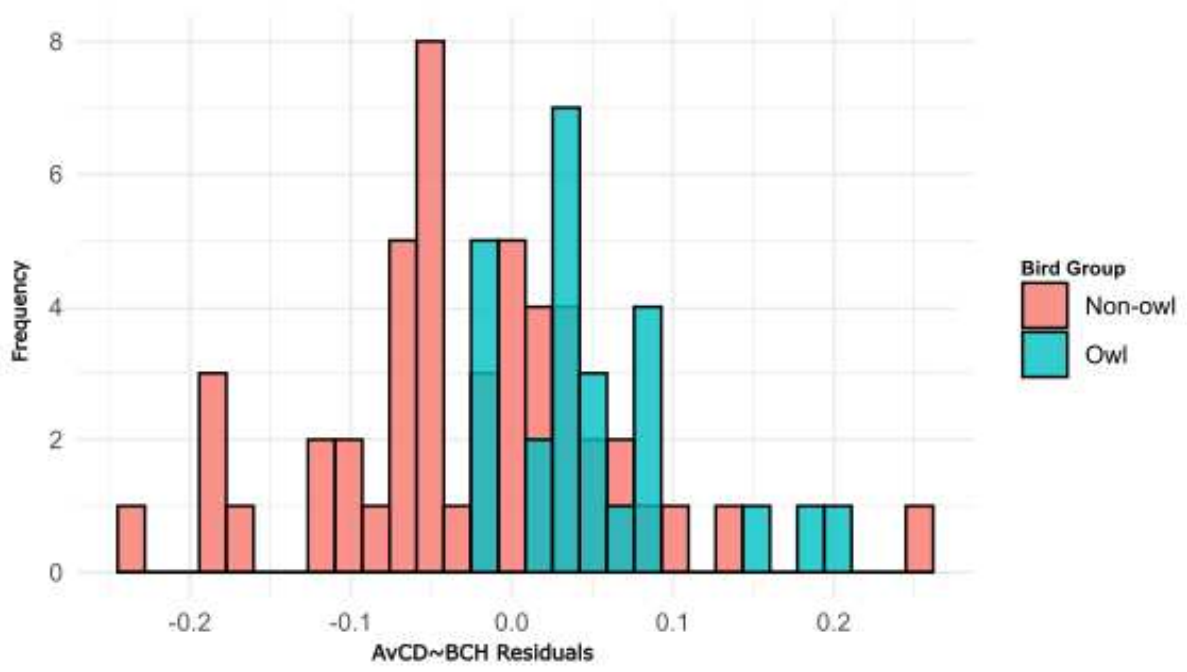


Figure 14: Histogram representing the frequency of the AvCD ~ BCH model residuals for owl and non-owl birds included in the study. The y-axis represents the frequency and the x-axis represents the AvCD ~ BCH model residuals. Higher residual values represent the proportionally longer cochlear ducts. Lower residual values represent the proportionally shorter cochlear ducts. The pink bars represent non-owl birds and owls are represented by the blue bars.

Table 12: Summary statistics for the histogram in Figure 13.

Bird group	Mean	Median	SD	Min	Max	Q1	Q3	Count
Non-owl	-0.026	-0.027	0.089	-0.237	0.253	-0.066	0.025	49
Owl	0.05	0.036	0.06	-0.023	0.199	0.014	0.076	25

The distribution of the points shows no clear clustering patterns for any of the hunting style categories except for the auditory category. Many birds, both owl and non-owl, that were categorized as being auditory hunters, lie either within the 95% confidence interval or are positive residuals. This indicates that birds which are auditory hunters, have cochlear ducts that are either the predicted size or longer than the predicted size for their braincase height. These observations are supported by the p-values for the different hunting categories in Table 12.

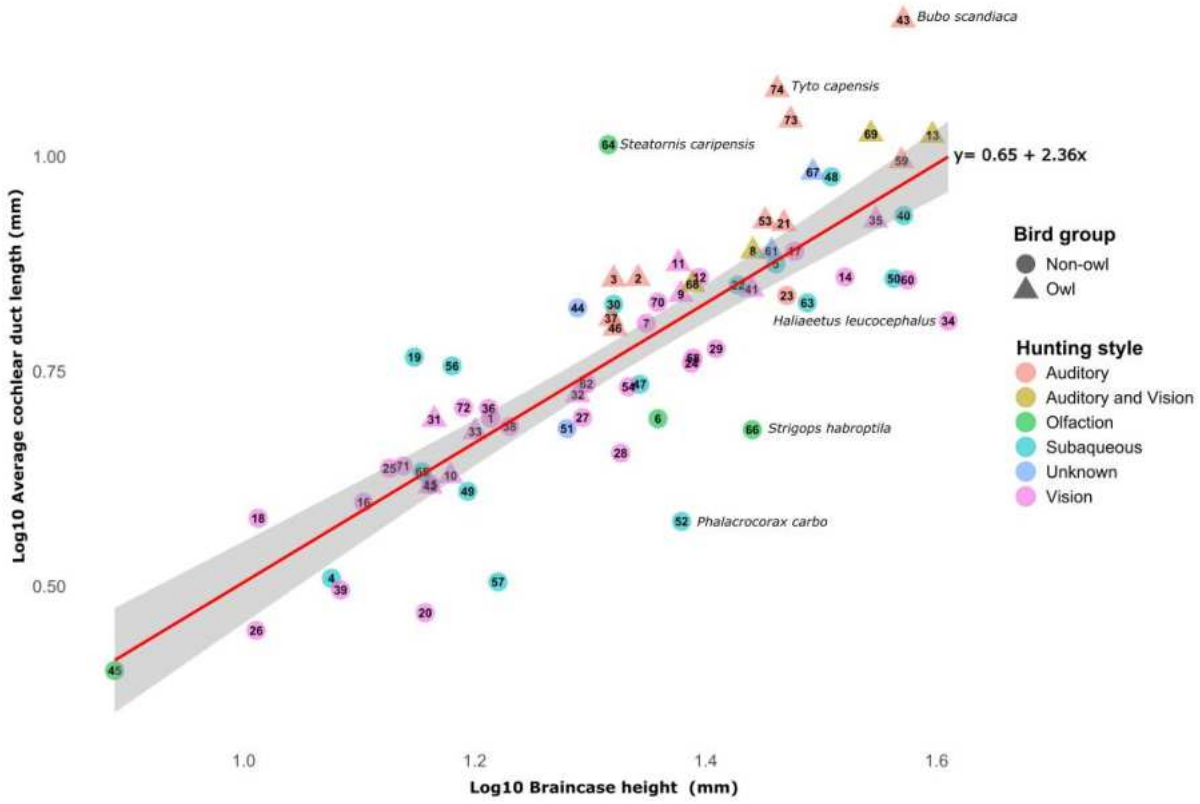


Figure 15: PGLS regression showing the relationship between log-transformed average cochlear duct length against log-transformed braincase height and, with distinctions based on hunting styles and bird groups. The x-axis represents the logged braincase height (mm) values, while the y-axis denotes the logged average cochlear duct length (mm) values. A single species is represented by each point, with numbers indicating the species according to Table 2. Owls are represented by the triangles while birds which are not owls are represented by the circle. The different hunting styles are distinguished by different colours. The pink points represent an auditory hunting style. The gold points represent an auditory and visual hunting style. The green points represent a subaqueous diving style. The aqua blue points represent olfaction. The purple points represent a visual hunting style and unknown hunting styles are represented by the

darker blue points. The red line indicates the line of best fit and the shaded region around the line indicates the 95% confidence interval.

All the nocturnal owls either fall within the 95% confidence interval or are positive outliers. However, this is not the case for nocturnal birds in general, as there are several non-owl nocturnal birds with negative residuals. Therefore, amongst nocturnal birds, there is no clear difference in distribution between owl and non-owl birds. Diurnal birds, particularly non-owl diurnal birds, form a majority of the negative residuals, but also include some positive residuals. Therefore, the regression indicates that diel activity patterns may not have a significant effect on average cochlear duct length is birds as there is no clear distribution pattern between the different diel activity patterns amongst birds. This observation is supported by the p-values in Table 12.

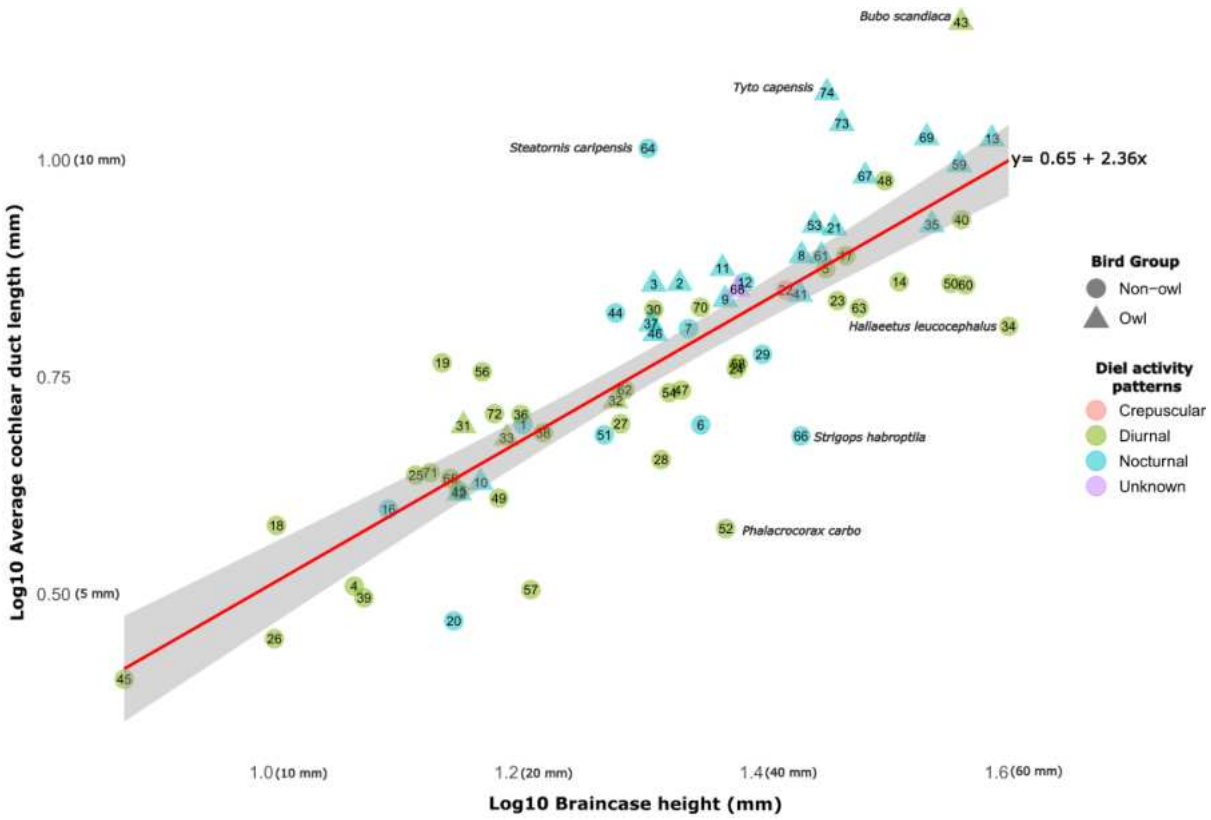


Figure 16: PGLS regression showing the relationship between log-transformed average cochlear duct length against log-transformed braincase height, with distinctions based on behaviour and bird groups. The x-axis represents the logged braincase height (mm)

values, while the y-axis denotes the logged average cochlear duct length (mm) values. A single species is represented by each point, with numbers indicating the species according to Table 2. Owls are represented by the triangles while birds which are not owls are represented by the circle. The different diel activity patterns are represented by different colours. Crepuscular birds are represented by the pink points. Diurnal birds are represented by the green points. Nocturnal birds are represented by the blue points and the birds with no clear diel activity pattern are represented by purple points. The red line indicates the line of best fit and the shaded region around the line indicates the 95% confidence interval.

All birds with reported symmetry (based on Norberg, 2002), whether head skeleton or soft anatomy, have positively distributed residuals. Their distribution indicates that all owls with reported asymmetry have proportionally long cochlear duct lengths. However, all the non-owl birds with a proportionally longer cochlear duct length, have no reported asymmetry.

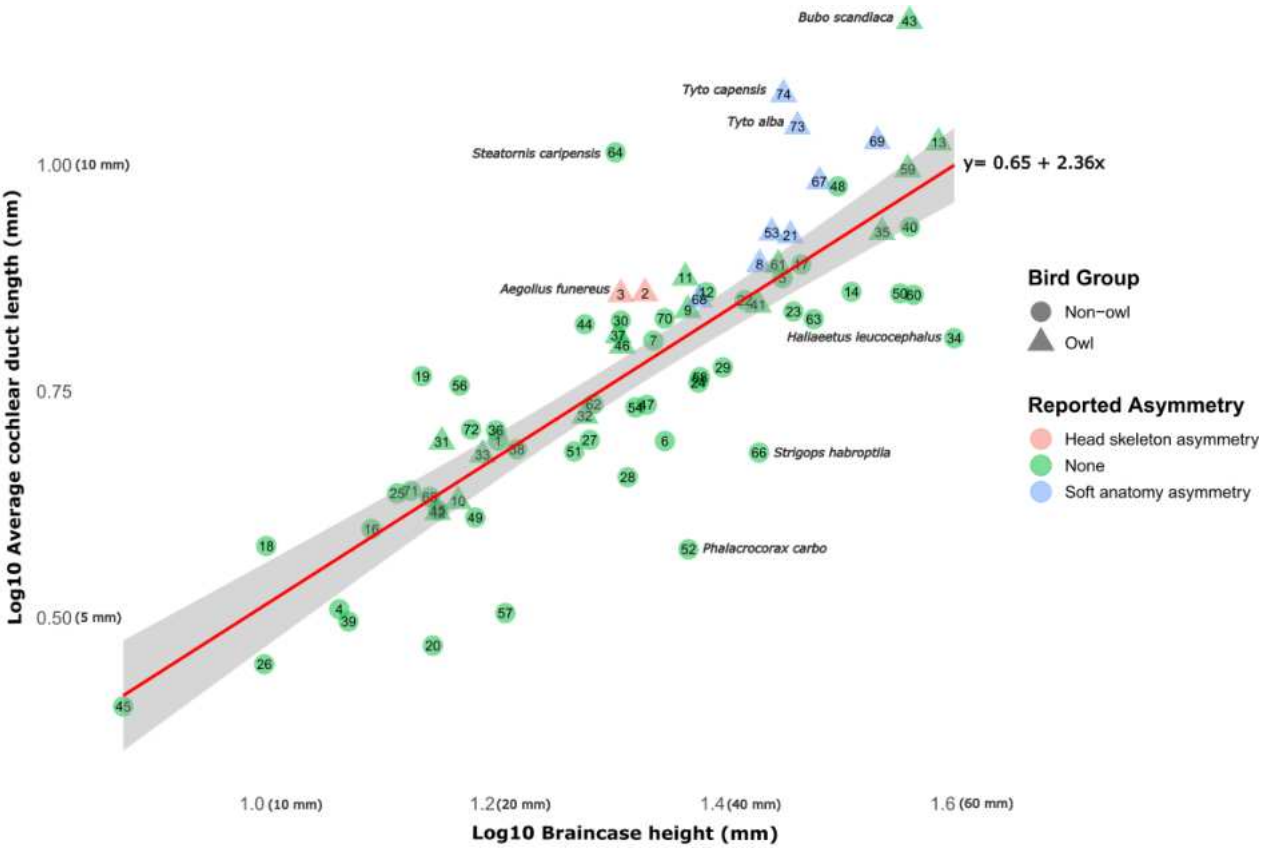


Figure 17: PGLS regression showing the relationship between log-transformed average cochlear duct length against log-transformed braincase height, with distinctions based on reported asymmetry (Norberg, 2002) and bird groups. The x-axis represents the

logged braincase height (mm) values, while the y-axis denotes the logged average cochlear duct length (mm) values. A single species is represented by each point, with numbers indicating the species according to Table 2. Owls are represented by the triangles while birds which are not owls are represented by the circle. The reported asymmetry categories were determined from Norberg (2002) who reported on asymmetry in various owl lineages and are represented by different colours. Head skeleton asymmetry is indicated by the pink points. Soft anatomy asymmetry is indicated by the blue points and no cranial asymmetry is indicated by green points. The red line indicates the line of best fit and the shaded region around the line indicates the 95% confidence interval.

4. The relationship between the length of the cochlear duct and the length of the semicircular canals

The PGLS regression between $\log_{10}$ average cochlear duct length and $\log_{10}$ average sum of the semicircular canal lengths has a strong positive correlation with significant residual structure where positive residuals reflect birds with a longer cochlear duct length than expected and negative residuals reflect birds with a shorter cochlear duct length than expected relative to their semicircular canal lengths. Residuals are symmetrically distributed with most of the owls distributed either within the 95% confidence interval or are positive residuals. The birds with the highest residuals are mostly owls (e.g., *Tyto alba, Tyto capensis, Bubo scandiaca*) but also include non-owl birds such as *Steatornis caripensis.* Their propotional cochlear duct lengths are ~ 1.5-1.66 times the predicted length for the length of their semicircular canals. Other birds that are distributed in the positive residuals space (e.g., *Colius striatus*, *Oxyura jamaicensis*, *Aegolius funereus*, *Phodilus badius*, *Strix varia*, *Strix nebulosa*) have proportional cochlear duct lengths that are ~1-1.25 times longer the predicted length for the size of their semicircular canals. Example of birds with the proportionally shortest cochlear ducts are *Chordeilies minor* and *Haliaeetus leucocephalus*. Their cochlear ducts are ~ 1.78 times shorter than predicted length for the size of their semicircular canals. Other birds that are distributed within the negative residual space (e.g., *Alcedo atthis*, *Sagittarius serpentarius*, *Buteo rufofuscus*, *Bubo virginianus*) have proportional cochlear duct lengths that are ~1.070-1.51 times shorter than the predicted length for the size of their semicircular canals.

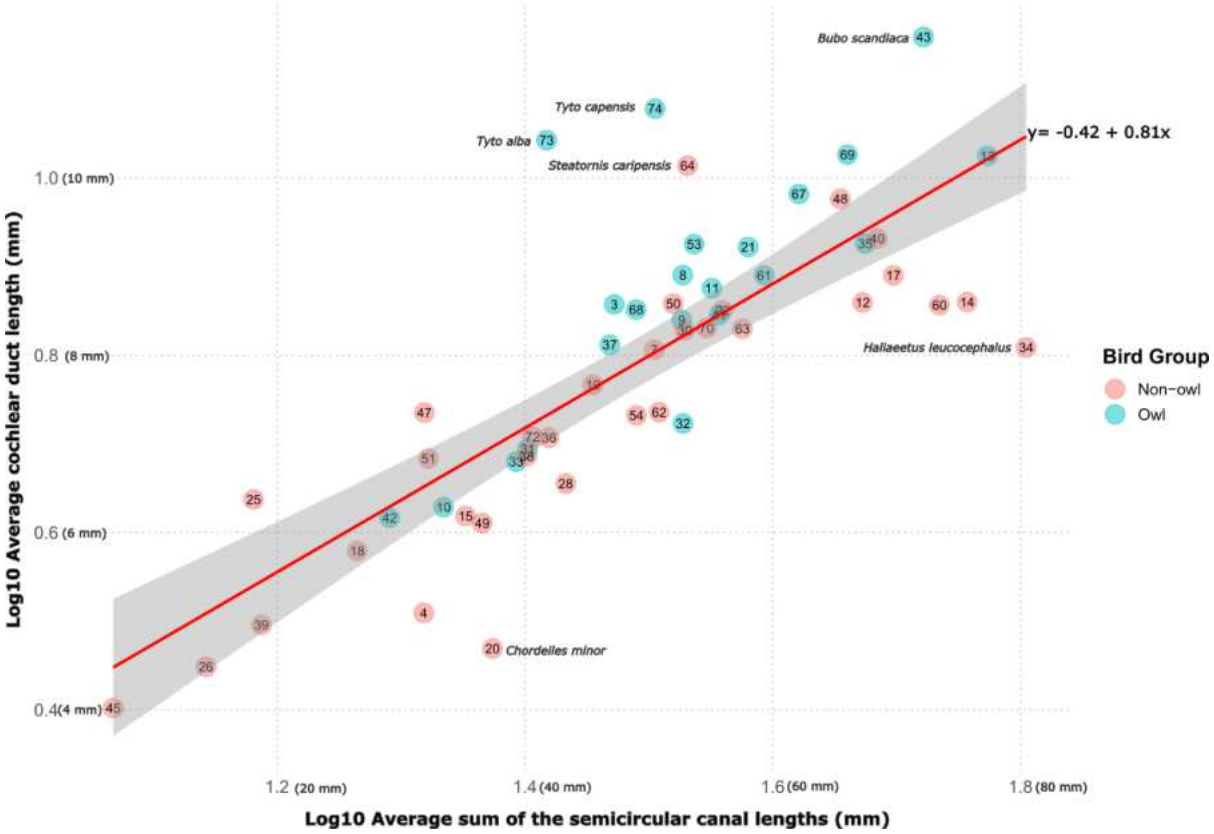


Figure 18: PGLS regression illustrating the relationship between log-transformed average cochlear duct length against log-transformed average sum of the semicircular canal lengths and in owls and non-owl bird species. The x-axis represents the logged average sum of the semicircular canals length (mm) values, while the y-axis denotes the logged average cochlear duct length values (mm). A single species is represented by each point, with numbers indicating the species according to Table 2. Owls are represented by the blue points while birds which are not owls are represented by the pink points. The red line indicates the line of best fit and the shaded region around the line indicates the 95% confidence interval.

The PGLS regression between the residuals of AvSumSCC ~ BCH model and the residuals of the ECD ~ BCH model indicate a very weak positive correlation between the two sets of residuals with significant residual structure as many of the data points distributed outside the 95% confidence interval. The model is non-significant ($p = 0.1211$) with a very weak R^2 value ($R^2 = 0.007$). The weak relationship indicates that relative cochlear duct length has no effect on the relative size of the semicircular canals in birds.

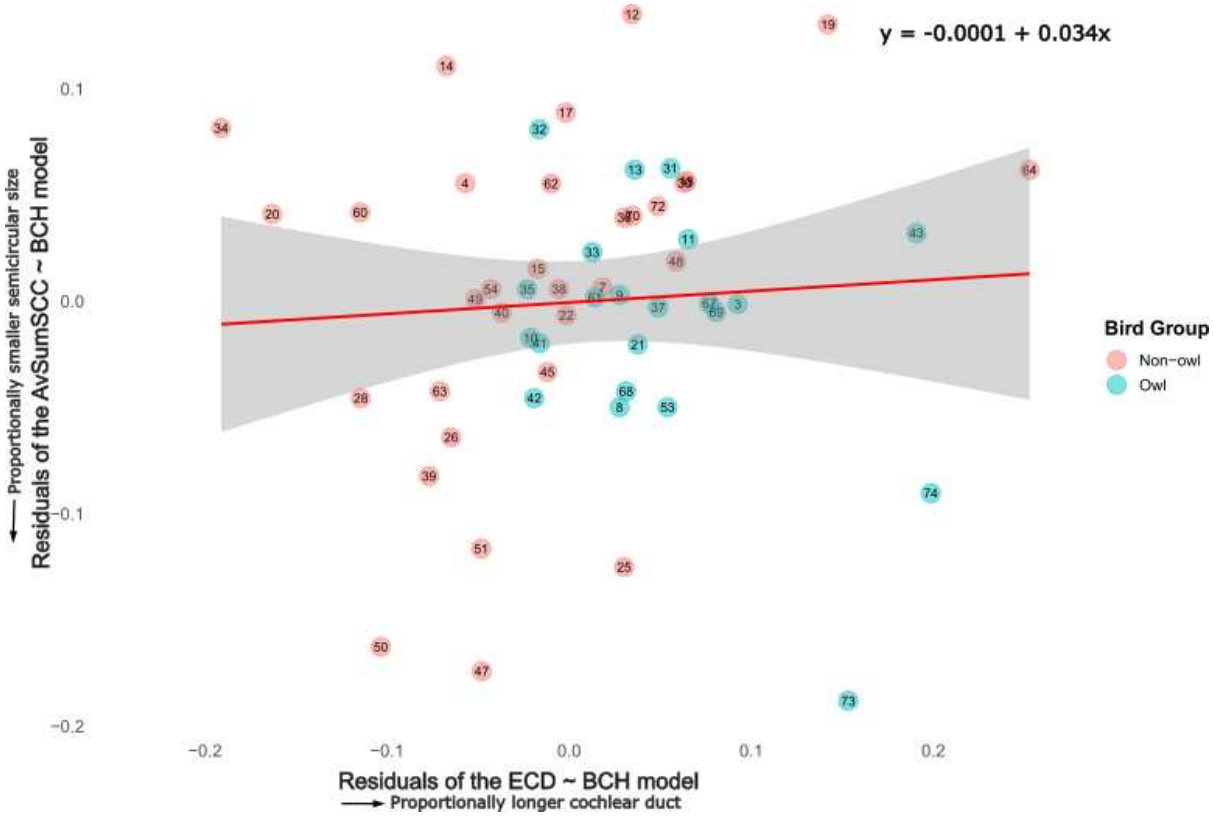


Figure 19:PGLS regression showing the residuals of AvSumSCC ~ BCH model against the residuals of the ECD ~ BCH model. The x-axis represents the ECD~ BCH model residuals and the y-axis represents the AvSummScc ~ BCH residuals. A single species is represented by each point, with numbers indicating the species according to Table 2. Owls are represented by the blue points while birds which are not owls are represented by the pink points. The red line indicates the line of best fit and the shaded region around the line indicates the 95% confidence interval.

5. Hearing performance results

Table 13: Summary statistics for the hearing performance models. Abbreviations: Average cochlear duct length (AvCD); Braincase height (BCH); Intercept (b_1); Slope (b_0)

Model name	Term	P-value	R^2	b_1	b_0	AIC values	Sample size
Best frequency (kHz) ~ (Residuals of AvCD ~ BCH)	Residuals of AvCD ~ BCH	0.13562	0.230	4.06	-2.3	59.832	11
High frequency limit (kHz) 35 dB cutoff ~ (Residuals of AvCD ~ BCH)	Residuals of AvCD ~ BCH	0.0242 *	0.539	7.1	-2.65	41.393	9
Low frequency limit (kHz) 35 dB cutoff ~ (Residuals of AvCD ~ BCH)	Residuals of AvCD ~ BCH	0.8269	0.011	0.75	-0.09	19.296	6
Best sensitivity dB SPL ~ (Residuals of AvCD ~ BCH)	Residuals of AvCD ~ BCH	0.394	0.082	14.12	10.43	106.41	9
High frequency limit (kHz) 60 dB cutoff ~ (Residuals of AvCD ~ BCH)	Residuals of AvCD ~ BCH	0.706	0.031	7.4	-0.38	29.2	4
Low frequency limit (kHz) 60 dB cutoff ~ (Residuals of AvCD ~ BCH)	Residuals of AvCD ~ BCH	0.382	0.382	1.09	2.4	18.177	6

* Indicates significant p-values ($p < 0.05$)

Majority of the models are non-significant as indicated by their p-values except for the high frequency limit (kHz) 35 dB cutoff ~ (Residuals of AvCD ~ BCH) model. Furthermore, most of the models are weakly correlated as indicated by the extremely low R-squared values which range from 0.011 to 0.382. The High frequency limit (kHz) 35 dB cutoff ~ (Residuals of AvCD ~ BCH) model is moderately correlated with a R-squared value of 0.539.

Relationships between measures of hearing performance, including Figures 18A, 18C, 18D 18E and 18F, have weak correlations with non-significant p-values (Table 14, Figure 18). Only the relationship between high frequency limit (kHz) 35 dB cutoff and the residuals of AvCD ~ BCH is significant (Table 14, Figure 18D). The PGLS regression in Fig. 18D, has a negative moderate correlation with significant residual structure. As the residuals of AvCD ~ BCH increase, the high frequency limit (kHz) 35 dB decreases. This indicates that as the proportional length of the cochlear duct decreases, the high frequency limit decreases as well. Therefore, birds with a proportionally longer cochlear duct have a higher high frequency limit (kHz) at a 35dB cut off. However, for many of the investigated measures of hearing performance, the sample sizes are very small (Table 14), therefore the results of the models are tentative.

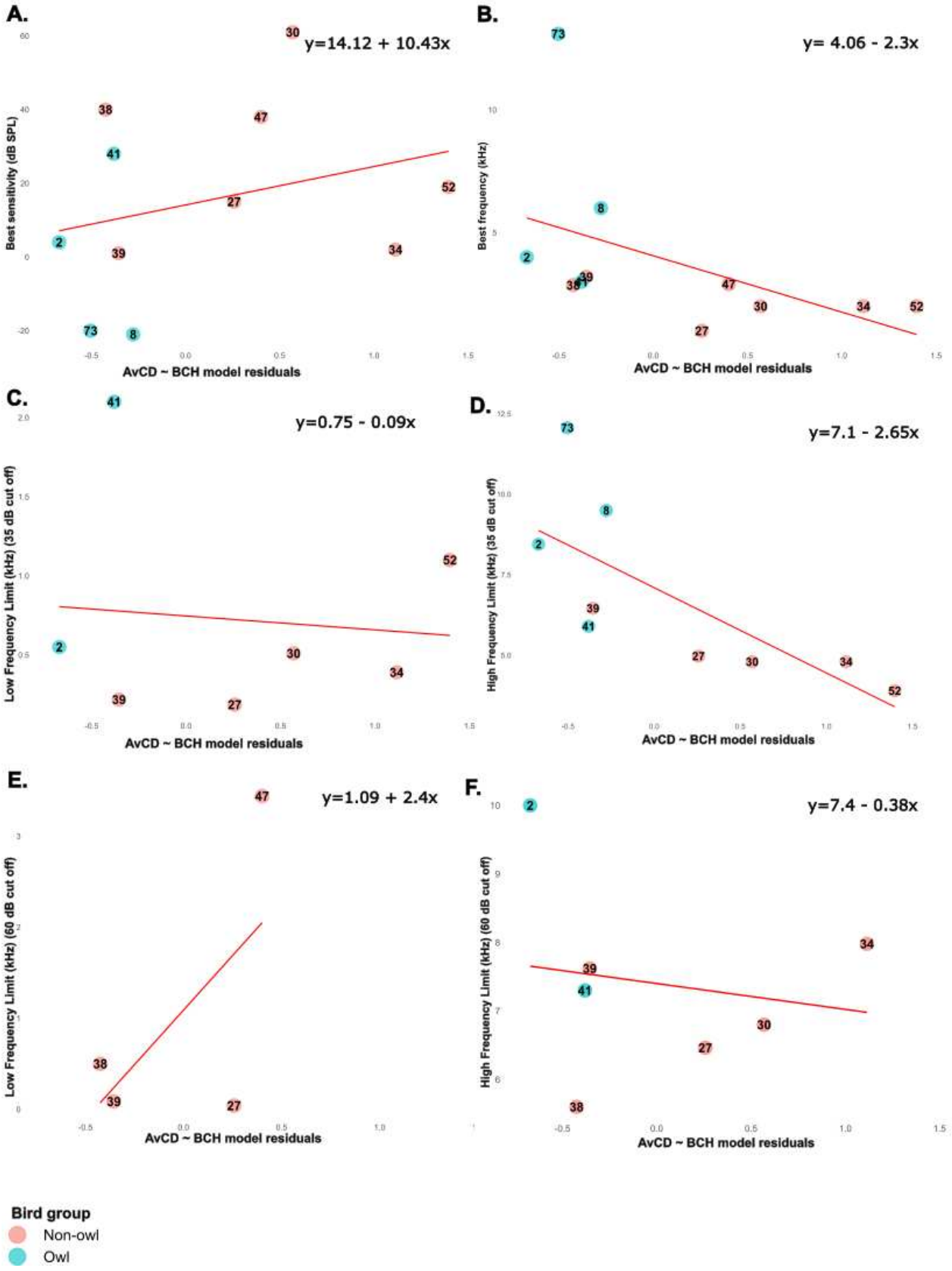


Figure 20: PGLS regressions showing the relationship between various hearing performance indicators against the residuals of the AvCD~ BCH model. The x-axis represents the AvCD ~ BCH model residuals and negative values on the axis represent proportionally longer cochlear duct length. The y-axis represents the measurements of

hearing performance. A single species is represented by each point, with numbers indicating the species according to Table 2. Owls are represented by the blue points while birds which are not owls are represented by the pink points. The red line indicates the line of best fit. A) PGLS regression showing the relationship between best sensitivity (dB SPL) against the residuals of the AvCD~ BCH model. B) PGLS regression showing the relationship between best frequency (kHz) against the residuals of the AvCD~ BCH model. C) PGLS regression showing the relationship between low frequency limit (kHz) (35 dB cut off) against the residuals of the AvCD~ BCH model. D) PGLS regression showing the relationship between high frequency limit (kHz) (35 dB cut off) against the residuals of the AvCD~ BCH model. E) PGLS regression showing the relationship between low frequency limit (kHz) (60 dB cut off) against the residuals of the AvCD~ BCH model. F) PGLS regression showing the relationship between low frequency limit (kHz) (60 dB cut off) against the residuals of the AvCD~ BCH model.

6. Asymmetry results

6.1 Cranial asymmetry

Table 14: Measurements of skull asymmetry across various bird species. The highest values across the different skull regions are in bold.

Common name	Species name	Temporal wing	Foramen Magnum	Basioccipital-Basisphenoid
Australian owlet-nightjar	*Aegotheles cristatus*	NA	NA	NA
Boreal owl	*Aegolius funereus*	**0.1126**	0.0186	0.0126
Northern saw-whet owl	*Aegolius acadicus*	0.1010	0.0255	0.0127
Common kingfisher	*Alcedo atthis*	NA	NA	NA
King penguin	*Aptenodytes patagonicus*	0.0219	0.0103	0.0063
Southern Brown Kiwi	*Apteryx australis*	0.0189	0.0143	0.0099
Grey-cowled wood rail	*Aramides cajanea*	0.0208	0.0166	0.0028
Long-eared owl	*Asio otus*	0.0212	**0.0934**	0.0143
Little owl	*Athene noctua*	0.0178	0.0126	0.0059
Burrowing owl	*Athene cunicularia*	0.0168	0.0170	0.0037
Burrowing owl	*Athene cunicularia troglodytes*	0.0514	0.0245	0.0096
Large frogmouth	*Batrachostomus auritus*	0.0305	0.0061	0.0052
Great horned owl	*Bubo virginianus*	0.0757	0.0195	**0.0202**
Jackal buzzard	*Buteo rufofuscus*	0.0124	0.0138	0.0076
Brown-eared woodpecker	*Campethera caroli*	NA	NA	NA
Nightjar	*Caprimulgus macrurus*	0.0196	0.0189	0.0079

Red-legged seriema	*Cariama cristata*	0.0519	0.03025	0.0158
Chimney swift	*Chaetura pelagica*	NA	NA	NA
Amazon kingfisher	*Chloroceryle amazona*	NA	0.0089	0.0079
Common nighthawk	*Chordeiles minor*	NA	NA	NA
Mottled owl	*Strix virgata*	0.0188	0.0079	0.0049
Western Marsh Harrier	*Circus cyaneus*	0.0133	0.0699	0.0071
Hen Harrier	*Circus aeruginosus*	NA	NA	NA
Montagu's harrier	*Circus pygargus*	NA	NA	NA
Speckled mousebird	*Colius striatus*	0.0315	0.0104	0.0043
Philippine swiftlet	*Collocalia mearnsi*	NA	NA	NA
Homing pigeon	*Columba livia*	NA	0.00986	0.0043
Black-winged kite	*Elanus caeruleus*	NA	NA	NA
Letter-winged kite	*Elanus scriptus*	NA	NA	NA
Red throated loon	*Gavia stellata*	0.0300	0.0067	0.0085
Asian barred owlet	*Glaucidium cuculoides*	0.0260	0.0122	0.0181
Ferruginous pygmy owl	*Glaucidium gnoma*	0.017	0.0094	0.0042
Mountain pygmy owl	*Glaucidium brasilianum*	NA	NA	NA
Bald eagle	*Haliaeetus leucocephalus*	0.0232	0.0104	0.0061
Buffy fish owl	*Ketupa ketupu*	0.0135	0.0101	0.0084
Amboyna cuckoo-dove	*Macropygia amboinensis*	0.0179	0.0116	0.0063
Western screech owl	*Megascops kennicottii*	0.0188	0.0102	0.0040

Red-bellied woodpeckers	*Melanerpes carolinus*	0.0366	0.007	0.008
Budgerigar	*Melopsittacus undulatus*	NA	0.0109	0.0061
Northern gannet	*Morus bassanus*	0.02601	0.0064	0.0054
Morepork	*Ninox novaeseelandiae*	0.0294	0.0109	0.007
New Britain Boobook	*Ninox odiosa*	0.0321	0.0207	0.0125
Snowy owl	*Bubo scandiaca*	0.0092	0.0059	0.0038
Common potoo	*Nyctibius griseus*	0.0176	0.0055	0.0061
Ecuadorian hillstar	*Oreotrochilus chimborazo*	0.0267	0.0110	0.0047
Mountain scops owl	*Otus spilocephalus*	0.0251	0.0067	0.0047
Ruddy duck	*Oxyura jamaicensis*	0.0102	0.0138	0.0091
Osprey	*Pandion haliaetus*	NA	NA	NA
Common diving petrel	*Pelecanoides urinatrix*	0.0218	0.0088	0.0083
Brown pelican	*Pelecanus occidentalis*	0.0215	0.0141	0.0128
Night parrot	*Pezoporus occidentalis*	NA	NA	NA
Great cormorant	*Phalacrocorax carbo*	0.0149	0.0043	0.0034
Oriental bay owl	*Phodilus badius*	NA	NA	NA
European green woodpecker	*Picus viridis*	0.0783	0.0103	0.0148
Tawny frogmouth	*Podargus strigoides*	0.0112	0.0077	0.0066
Junin grebe	*Podiceps taczanowskii*	0.0591	0.0187	0.0153
Atitlán grebe	*Podilymbus gigas*	0.0210	0.0082	0.0064
African grey parrot	*Psittacus erithacus*	0.0221	0.0081	0.0051

Spectacled owl	*Pulsatrix perspicillata*	0.0391	0.0119	0.0102
Secretary bird	*Sagittarius serpentarius*	0.0321	0.0107	0.0111
Laughing owl	*Ninox albifacies*	0.0232	0.0058	0.0048
American woodcock	*Scolopax minor*	0.0183	0.0102	0.0097
African penguin	*Spheniscus demersus*	NA	NA	NA
Oilbird	*Steatornis caripensis*	NA	NA	NA
Common tern	*Sterna hirundo*	NA	NA	NA
Kakapo	*Strigops habroptila*	0.0117	0.0104	0.0031
Great grey owl	*Strix aluco*	0.0691	0.0178	0.0144
Tawny owl	*Strix varia*	NA	0.0065	0.006
Barred Owl	*Strix nebulosa*	NA	NA	NA
Northern hawk-owl	*Surnia ulula*	0.0338	0.0108	0.0064
Black-hooded thrush	*Turdus olivaceus*	0.0056	0.0042	0.0059
Olive thrush	*Turdus olivater*	NA	NA	NA
Barn Owl (Lesser Antilles)	*Tyto alba*	0.018	0.0133	0.0036
African grass owl	*Tyto capensis*	0.0322	0.0147	0.0054

Table 15 presents the asymmetry values for various parts of the crania of bird species analysed. It includes asymmetry values for the temporal wing, foramen magnum and basioccipital-basiophenoid. The highest values for each category are in bold. The taxa with the highest asymmetry value for the temporal wing, foremen magnum and basioccipital-basisphenoid landmarks are *Aegolius funereus, Asio otus and Bubo virginianus* respectively.

All the histograms in Fig.21 are positively skewed indicating minimal shape asymmetry across bird taxa. However, all the histograms have outlier values, with the highest outliers consisting mainly of owl taxa. This indicates that these owl taxa exhibit asymmetry in the specific regions of the cranium.

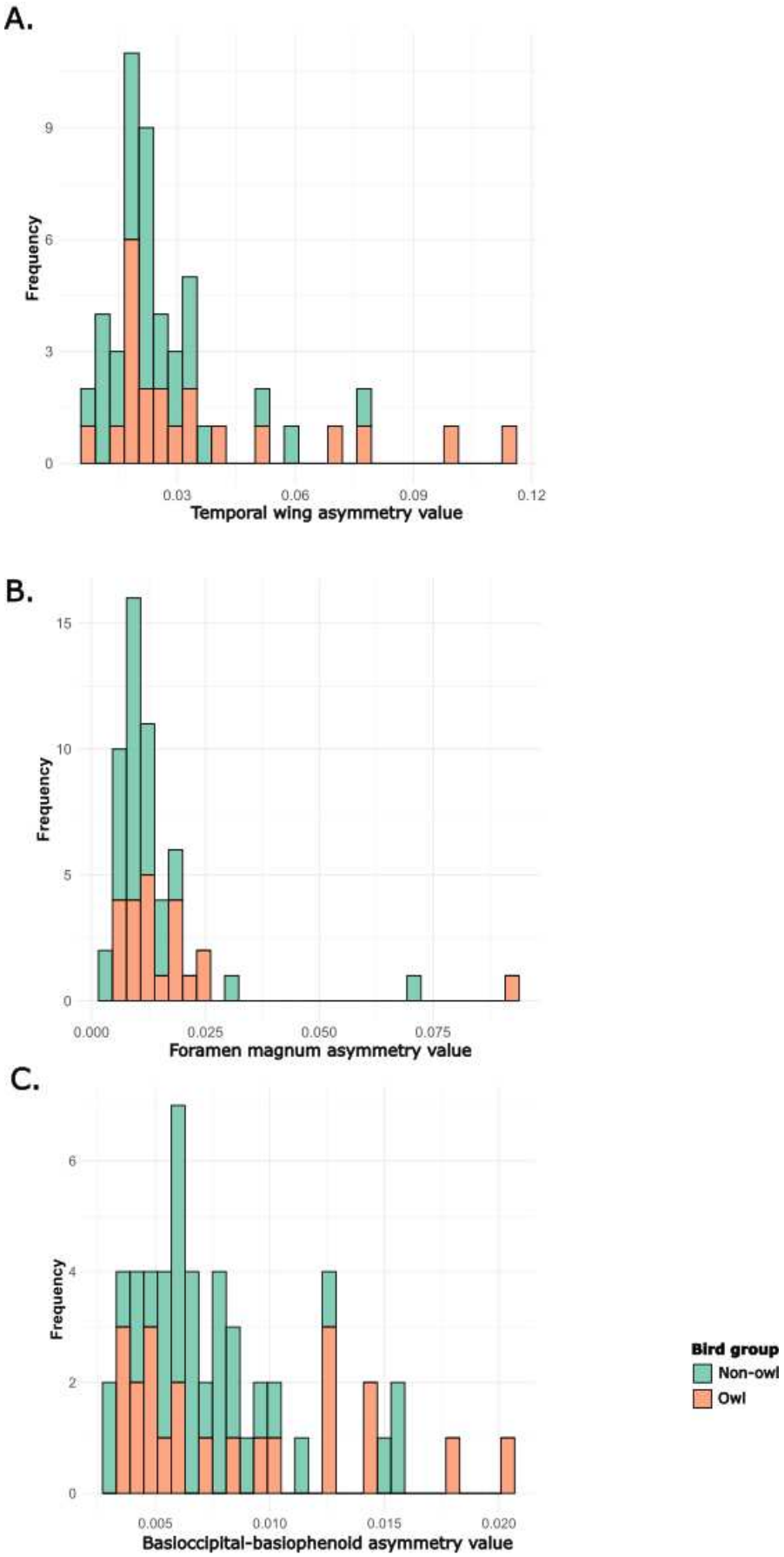

A.
Frequency
0
3
6
9
0.03
0.06
0.09
0.12
Temporal wing asymmetry value
B.
Frequency
0
5
10
15
0.000
0.025
0.050
0.075
Foramen magnum asymmetry value
C.
Frequency
0
2
4
6
0.005
0.010
0.015
0.020
Basioccipital-basiophenoid asymmetry value
Bird group
Non-owl
Owl

Figure 21: Histograms show the frequency of asymmetry in the different part of the cranium across bird taxa. The x-axis represents the asymmetry values, and the y-axis represents the frequency. A) Histogram of temporal asymmetry values. B) Histogram of foramen magnum asymmetry values. C) Histogram of basioccipital-basiophenoid asymmetry values.

.

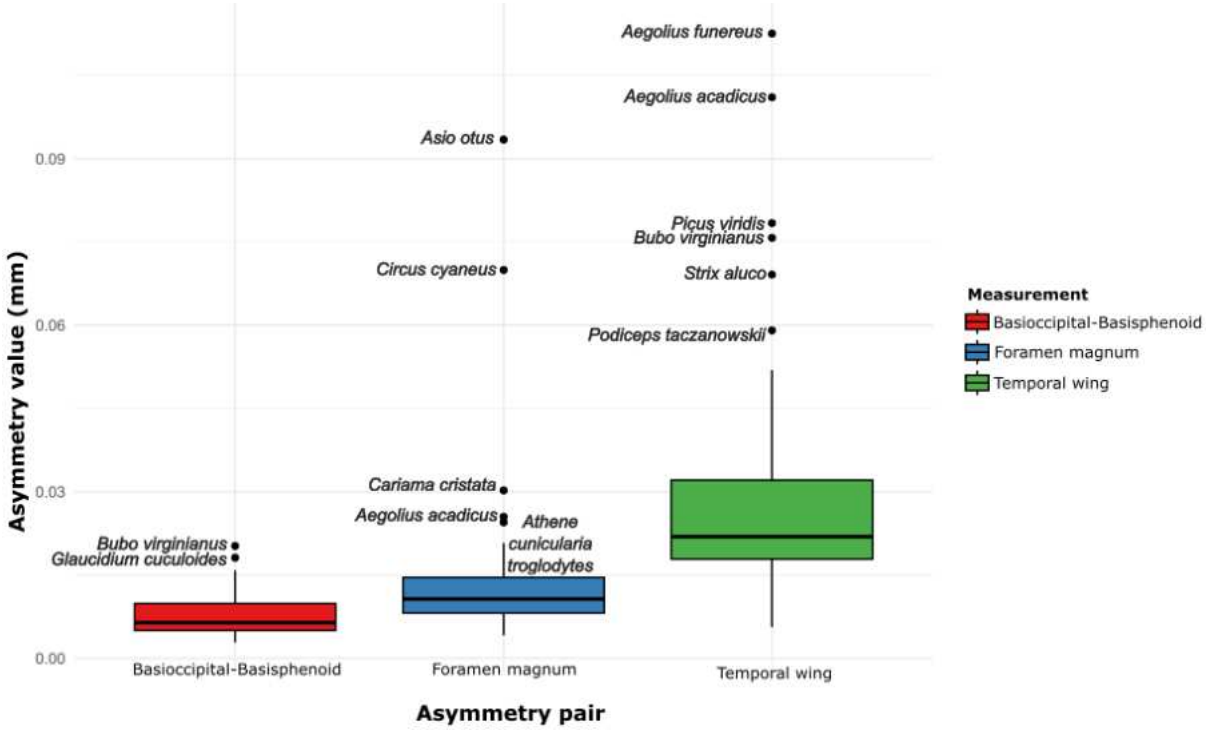


Figure 22:Box plot depicting the levels of shape asymmetry, quantified using Procrustes distance, across various landmark pairs in the cranium. The distribution of asymmetry measurements is represented for each landmark pair, highlighting differences in positional variation among them. The x-axis represents the different landmark pairs while the y-axis represents the asymmetry values (mm). The individual points indicate outliers.

Table 15: Summary statistics of cranial shape asymmetry as illustrated by the box plot in Figure 22.

Measurement	Min	Q1	Median	Mean	Q3	Max	SD
Basioccipital-Basisphenoid	0.0029	0.0051	0.0064	0.008	0.0099	0.0202	0.0041
Foramen magnum	0.0042	0.0082	0.0106	0.0144	0.0145	0.0935	0.0144
Temporal wing	0.0056	0.0179	0.0219	0.0299	0.0321	0.1126	0.0224

The standard deviation values suggest that the temporal wing has the most variation in its asymmetry values while the basioccipital-basisphenoid has the least amount of variation as indicated by the low SD value. This means that the left and right landmark sets of the temporal wing have a larger Procrustes distance, indicating that this region of the skull could potentially have asymmetry. Therefore, the birds that are outliers within this category (i.e., have the largest Procrustes distance values) exhibit the greatest potential asymmetry of the cranial skeleton.

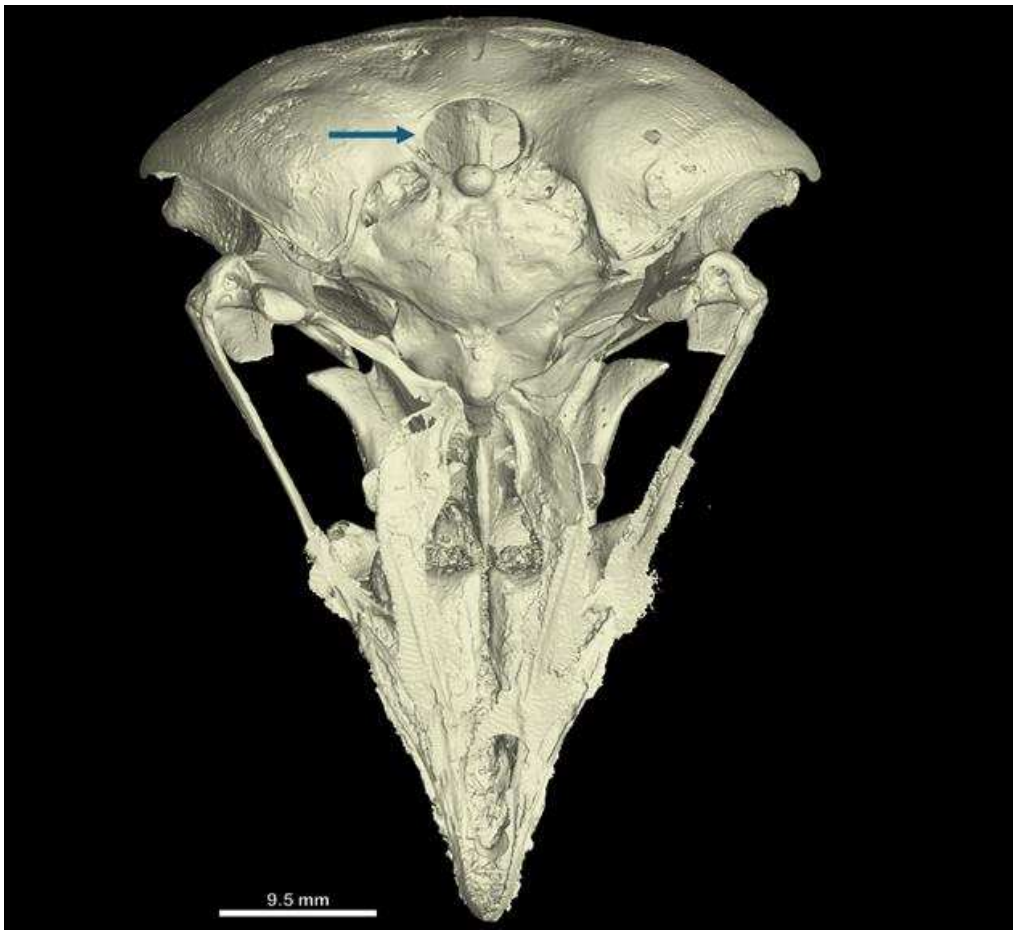


Figure 23: Ventral view of *Asio otus* (AMNH 3632) skull showing the asymmetry of the foramen magnum as indicated by the blue arrow.

6.2 Labyrinth shape asymmetry

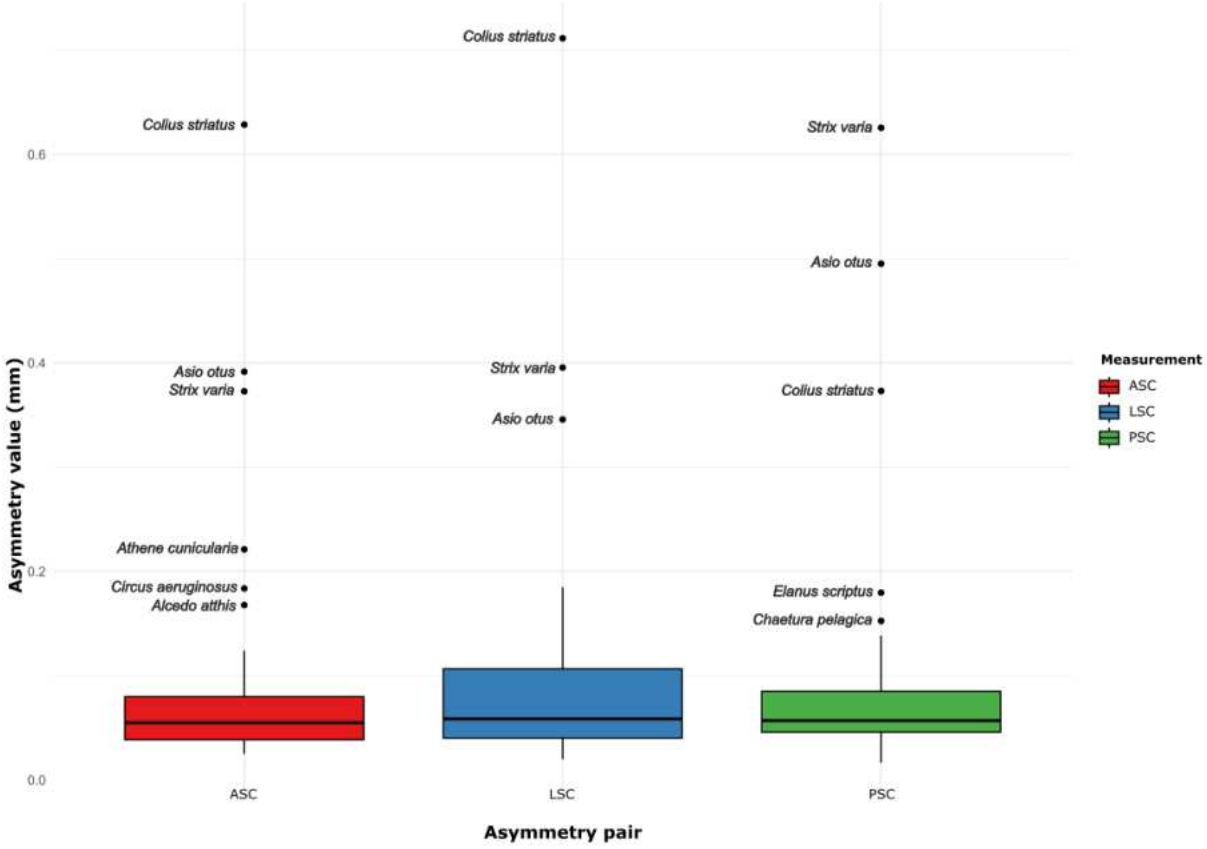


Figure 24:Box plot depicting the levels of shape asymmetry across various landmark pairs in the labyrinth. The distribution of asymmetry measurements is represented for each landmark pair, highlighting differences in positional variation among them. The x-axis represents the different semicircular pairs landmark pairs while the y-axis represents the asymmetry values (mm). The numbered points represent the outliers, and the numbers correspond to the species names in Table 2. Abbreviations: (LSC) Lateral semicircular canal; (ASC) Anterior semicircular canal; (PSC) Posterior semicircular canal

Table 16:Summary statistics of labyrinth shape asymmetry as illustrated in Figure 23. Abbreviations: (LSC) Lateral semicircular canal; (ASC) Anterior semicircular canal; (PSC) Posterior semicircular canal

Measurement	Min	Q1	Median	Mean	Q3	Max	SD
ASC asymmetry	0.0249	0.0386	0.0548	0.0907	0.0798	0.6285	0.1123
LSC asymmetry	0.0198	0.0402	0.0587	0.0970	0.1066	0.7114	0.1195

PSC asymmetry	0.0166	0.0459	0.0569	0.0924	0.085	0.6255	0.1165

The median asymmetry values and standard deviation values in Table 17 is nearly identical, with only slight differences. The standard deviation values are also almost the same in all three semi-circular canals. This suggests that the semicircular canals of birds have little to no asymmetry with the outlier taxa possibly being exceptions.

6. Phylogenetic mapping of residuals

The phylogenetic distribution of previously reported asymmetry shows that that cranial asymmetry (both skeletal and soft anatomy) has evolved at least four different times in owls and once in Accipitformes. Among the types of asymmetries, soft tissue asymmetry has evolved more times than head skeleton asymmetry amongst birds.

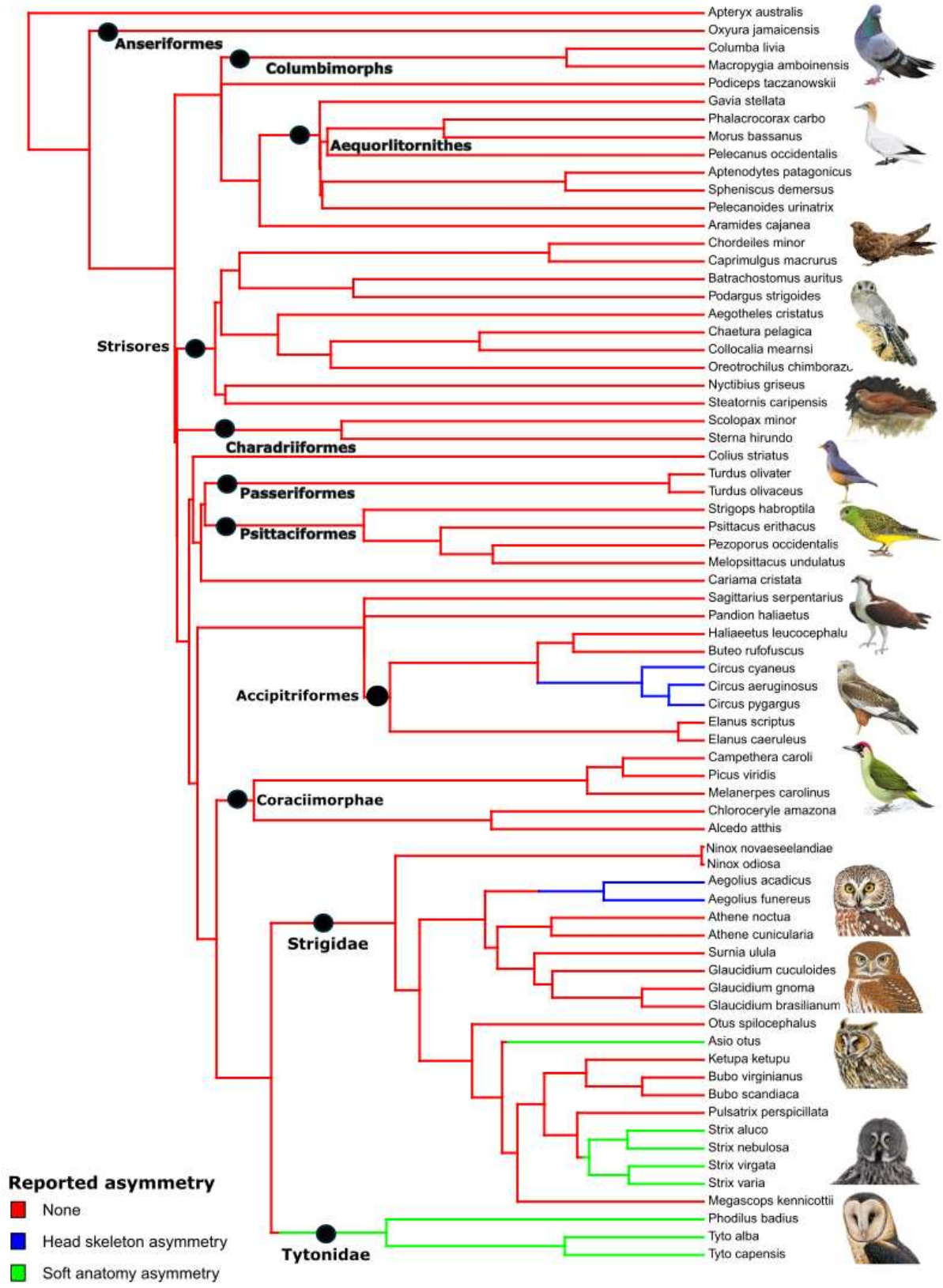


Figure 25: Phylogenetic tree of taxon sample set in this study with reported asymmetry from Norberg (2002) and Pecsis et al. (2021) mapped on. Ancestral state reconstruction

was done using maximum parsimony and was implemented in Mesquite. Head skeleton asymmetry is represented by blue. Soft anatomy asymmetry is represented by green, and no reported asymmetry is represented by red.

The mapping of the residuals reveals four independent origins of proportionally long cochlear ducts relative to braincase height in birds. Two of the origins occur in owls (*Bubo* and *Tyto*) while the other two origins have evolved in two non-owl clades. The proportionally shortest cochlear ducts relative to braincase height have four independent origins all of which have evolved in non-owl clades.

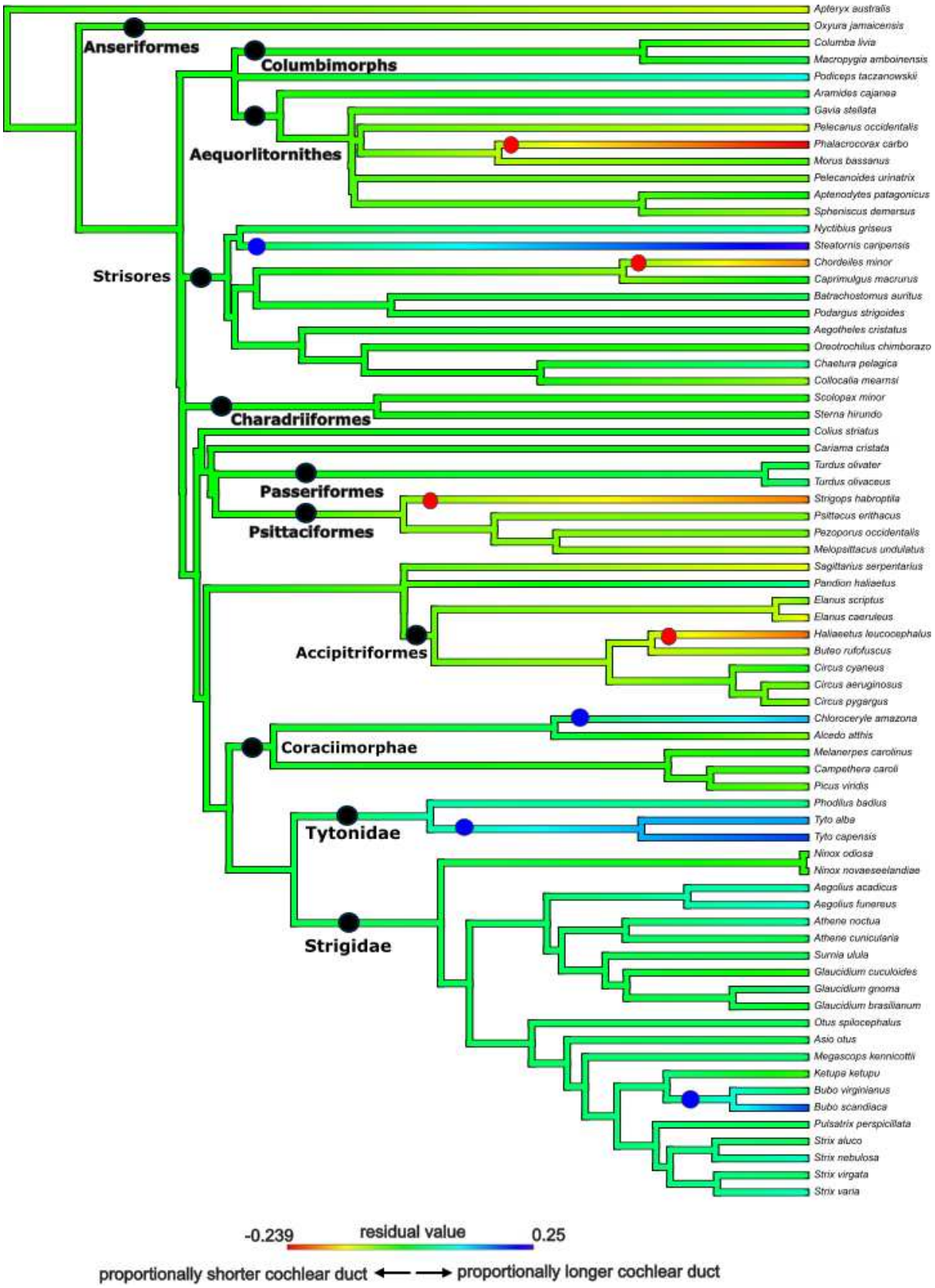


Figure 26: Phylogenetic tree showing the distribution of the cochlear duct and braincase height model residuals. The phylogenetic tree represents the evolutionary relationship between the species included in the dataset. Residuals, which are calculated as the

deviations from the predicted values of the ECD ~ BCH model in Table 13, are mapped onto the tree to visualize the direction and extent of the relationship between cochlear duct length and braincase height. Residuals are colour coded, with the positive residuals shown in shades of blue and negative residuals shown in shades of red. These colours indicate the deviations above and below the predicted values. Neutral residuals or taxa without residuals are indicated by green. The intensity of the colour gradient corresponds with the magnitude of the residuals. The black dots represent named clades of interest. The blue dots represent the inferred origins of a proportionally longer cochlear duct and the red dots represent the inferred origins of a proportionally shorter cochlear duct.

The distribution of the residuals reveals that a proportionally longer braincase height relative to body mass has three independent origins in birds. In owls, it has evolved at the beginning of their divergence. However, it was lost in *Ninox odiosa* as that taxon has among the proportionally shortest braincase heights. A proportionally shorter braincase height relative to body mass has evolved more times than a longer braincase height with Fig. 27 suggesting that it has six independent origins in birds.

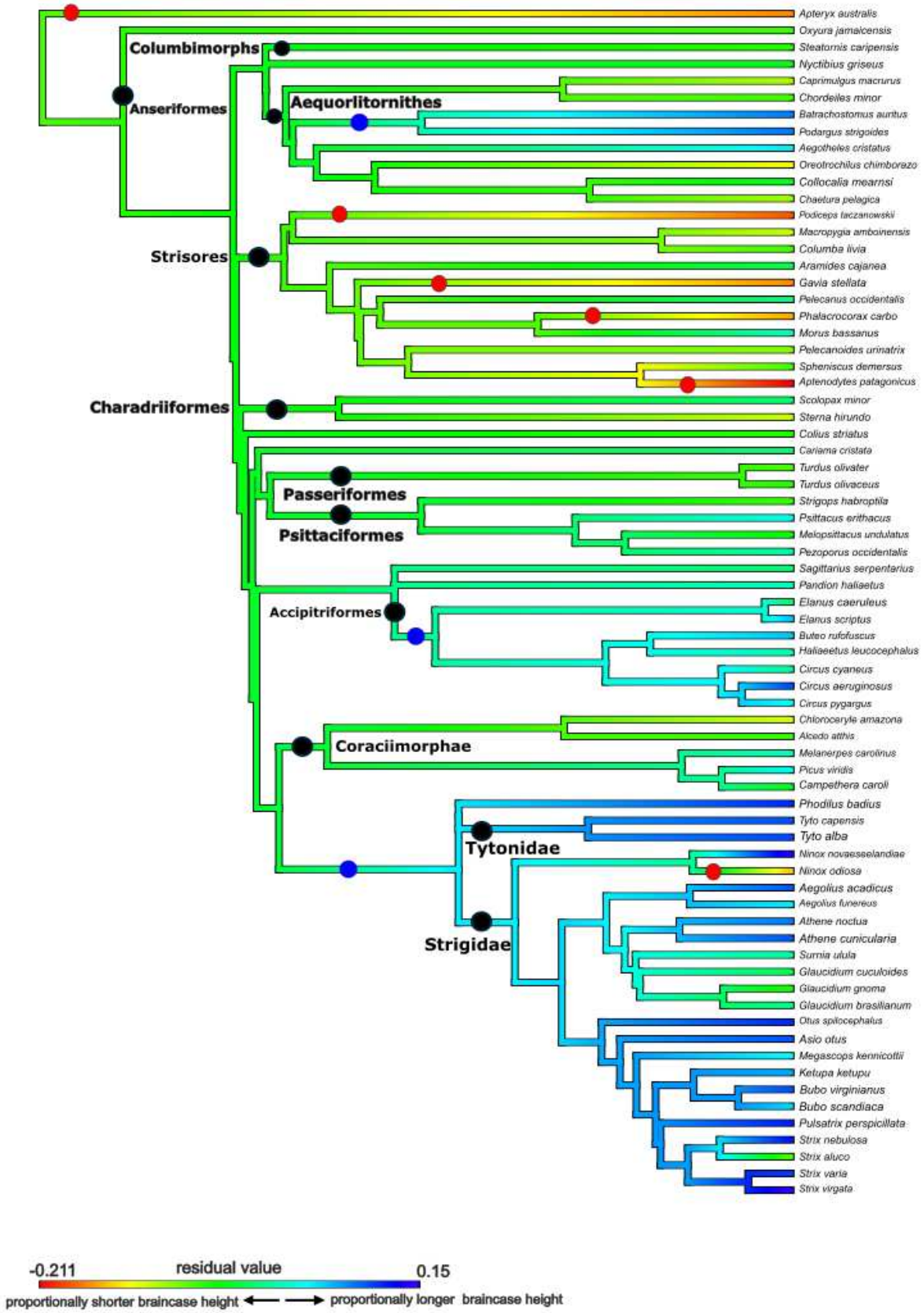

Apteryx australis
Oxyura jamaicensis
Columbimorphs
Stealornis caripensis
Nyctibius griseus
Caprimulgus macrurus
Anseriformes
Chordeiles minor
Aequorlitornithes
Batrachostomus auritus
Podargus strigoides
Aegotheles cristatus
Oreotrochilus chimborazo
Collocalia mearnsi
Chaetura pelagica
Podiceps taczanowskii
Macropygia amboinensis
Strisores
Columba livia
Aramides cajanea
Gavia stellata
Pelecanus occidentalis
Phalacrocorax carbo
Morus bassanus
Pelecanoides urinatrix
Spheniscus demersus
Aptenodytes patagonicus
Charadriiformes
Scolopax minor
Sterna hirundo
Colius striatus
Cariama cristata
Turdus olivater
Turdus olivaceus
Passeriformes
Strigops habroptila
Psittacus erithacus
Psittaciformes
Melopsittacus undulatus
Pezoporus occidentalis
Sagittarius serpentarius
Pandion haliaetus
Accipitriformes
Elanus caeruleus
Elanus scriptus
Buteo rufofuscus
Haliaeetus leucocephalus
Circus cyaneus
Circus aeruginosus
Circus pygargus
Chloroceryle amazona
Alcedo atthis
Coraciimorphae
Melanerpes carolinus
Picus viridis
Campethera caroli
Phodilus badius
Tyto capensis
Tyto alba
Tytonidae
Ninox novaeseelandiae
Ninox odiosa
Aegolius acadicus
Aegolius funereus
Athene noctua
Athene cunicularia
Strigidae
Surnia ulula
Glaucidium cuculoides
Glaucidium gnoma
Glaucidium brasilianum
Otus spilocephalus
Asio otus
Megascops kennicottii
Ketupa ketupa
Bubo virginianus
Bubo scandiaca
Pulsatrix perspicillata
Strix nebulosa
Strix aluco
Strix varia
Strix virgata
-0.211
residual value
0.15
proportionally shorter braincase height
proportionally longer braincase height

Figure 27: Phylogenetic tree showing the distribution of the braincase height and body mass model residuals. The phylogenetic tree represents the evolutionary relationship between the species included in the dataset. Residuals, which are calculated as the deviations from the predicted values of the BCH ~ BM model in Table 12, are mapped onto the tree to visualize the direction and extent of the relationship between body mass and braincase height. Residuals are colour coded, with the positive residuals shown in shades of blue and negative residuals shown in shades of red. These colours indicate the deviations above and below the predicted values. Neutral residuals or taxa without residuals are indicated by green. The intensity of the colour gradient corresponds with the magnitude of the residuals. The black dots represent named clades of interest. The blue dots represent the inferred origins of a proportionally longer braincase height and the red dots represent the inferred origins of a proportionally shorter braincase height.

The mapping of the residuals reveals two independent origins of proportionally long cochlear ducts relative to semicircular size in birds. The origins occur in in early diverging owls and *Steatornis caripensis*. The proportionally shortest cochlear ducts relative to semicircular size in birds also has four independent origins both occur in non-owl birds.

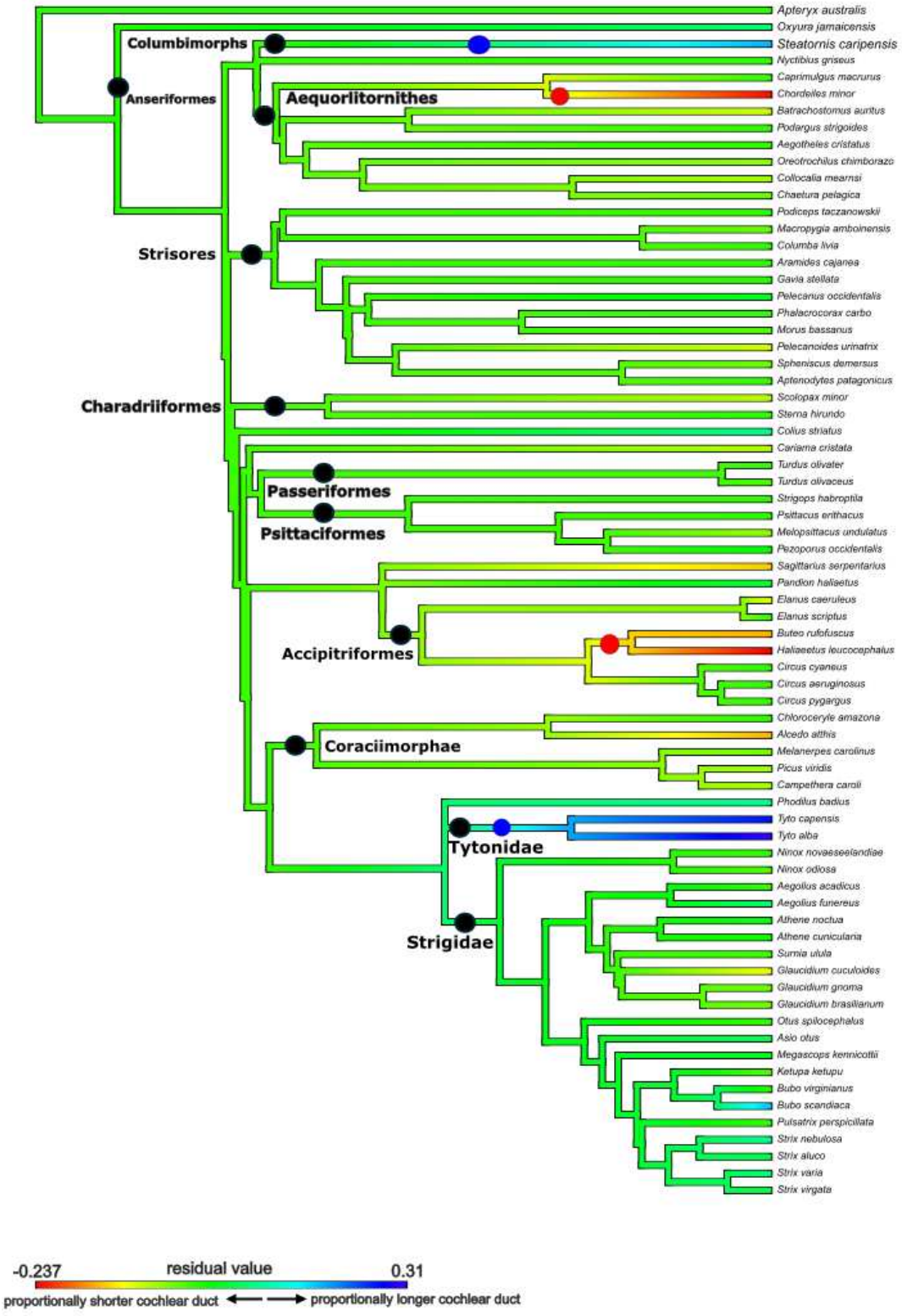


Figure 28: Phylogenetic tree showing the distribution of the sum of the semicircular canal length and cochlear duct length model residuals. The phylogenetic tree represents

the evolutionary relationship between the species included in the dataset. Residuals, which are calculated as the deviations from the predicted values of the AvSumSCC ~ AvCD model in Table 12, are mapped onto the tree to visualize the direction and extent of the relationship between the sum of the semicircular canal length and cochlear duct length. Residuals are colour coded, with the positive residuals shown in shades of blue and negative residuals shown in shades of red. These colours indicate the deviations above and below the predicted values. Neutral residuals or taxa without residuals are indicated by green. The intensity of the colour gradient corresponds with the magnitude of the residuals. The black dots represent named clades of interest. The blue dots represent the inferred origins of a proportionally longer cochlear duct length and the red dots represent the inferred origins of a proportionally shorter cochlear duct length.

Discussion

Remarkable hearing adaptations among owls have multiple origins throughout the history of the clade. One of these hearing adaptations is the shape asymmetry of the of the temporal wing region of the skull (Table 15, Fig. 21, Fig.22). The temporal wing displays a large range of asymmetry values with four of the five outliers being owls. Notably, these include *Aegolius funereus, Aegolius acadicus, Strix aluco* and *Bubo virginianus.* The placement of these taxa on the phylogenetic tree indicates multiple independent origins of temporal asymmetry in owls as these taxa are widely distributed. Among these outliers, *Aegolius* has the most asymmetrical temporal wings. This asymmetry result is also supported by my comparative anatomical observations of positional ear asymmetry, particularly in *Aegolius* species (e.g., Fig. 1C) where the right ear is positioned higher than the left, confirming the studies of Norberg who first reported on this (1978). Therefore, the morphological observations and temporal wing asymmetry value confirm that the genus *Aegolius* does indeed have cranial asymmetry of the temporal wing. Cranial asymmetry has not been described in the literature for *Bubo virginianu*s, however the temporal wing asymmetry values are nearly as asymmetrical as those of *Aegolius* (Table 5).

Natural history observations indicate that *Bubo virginianus* is a nocturnal hunter that detects prey with vision and hearing (Marti, 1974), and its hunting strategy is similar to *Aegolius* species which are known nocturnal auditory hunters (Koning et al., 2020; Sonerud et al., 1986). The similarities in their diel activity patterns and hunting strategy could explain why temporal wing cranial asymmetry evolved independently in both lineages. The last owl that independently evolved temporal wing asymmetry is *Strix nebulosa.* In the literature, *Strix nebulosa* has been reported to be seen hunting at all times of the day. Furthermore, they are generally nocturnal but crepuscular when incubating their eggs (Sibley, 2014). They have also been observed habitually occupying dense conifer forests with low light and short

sightlines (Bull and Duncan, 1993; Lutmerding and Love, 2020). They use vision and hearing to capture their prey (Bull et al., 1989) which consists predominately of voles and shrews (Kropacheva, 2018). This taxon is particularly interesting because it is the only one, out of the birds with a large temporal asymmetry value, that has been reported to have soft tissue asymmetry as well (Norberg, 2002). This suggests that this could be a species with both soft tissue asymmetry and cranial asymmetry, a characteristic which has not yet been described in any other bird so far.

The owl genera *Tyto*, *Asio*, and *Phodilus* have soft tissue asymmetry of the otic region, manifesting as differences in the left-right vertical positions of the ear openings in the skin (Norberg, 2002). My analyses showed that these genera have low temporal wing asymmetry values (Table 15), placing them among the more typical asymmetry values of most birds. This result highlights two important things. Firstly, this result shows that for these owl taxa, asymmetry is limited to only their soft tissues. Secondly, that analysing only the skull might lead to missing other forms of asymmetry which could be functionally significant. Consideration of these points is particularly important in the context of fossils as it would be difficult to determine whether fossil taxa, challenging the broad generalisations regarding hearing and asymmetry and making functional inferences difficult for extinct species. However, it is important to consider that the above results are based on shape asymmetry, and owls may also have positional asymmetry (where the structures are located rather than how the structures formed).

Outside of owls, there is little temporal wing asymmetry among birds, except for *Picus viridis*. Temporal wing asymmetry has not been described in the literature before for this woodpecker taxon. However, there might be potential for cranial asymmetry due to the way the retracted tongue wraps around the external braincase (Jung, 2015). Another possible contributor to the high asymmetry value could be due to the quality of the skull digital

reconstruction. The skull mesh for *P. viridis* that was obtained from Morphosource was poorly segmented therefore making the landmarking of the right temporal wing difficult. This could have contributed to the large temporal wing asymmetry value. Therefore, the high asymmetry value reported here may reflect methodological limitations and not biological asymmetry. Furthermore, *P. viridis* has hunting behaviours and diel activity patterns that differ significantly from birds typically associated with cranial asymmetry. It is a diurnal forager that relies mostly on vision to prey on ants (Winkler and Christie, 2020). These behavioural and ecological differences further suggest that the high temporal wing asymmetry value may not be biologically meaningful when considering its natural history.

The floor and back of the braincase (basioccipital-basisphenoid and foramen magnum, respectively) have very little asymmetry, and this is important for supporting the structural integrity of the cranium and ensuring the efficient functioning of critical systems. The bird taxon with the highest foramen magnum asymmetry value is the Long-eared Owl (*Asio otus*). This finding is particularly interesting as it appears to arise from slight variation in morphology rather than damage to the skull. Particularly, the left side of the foreman magnum is slightly less rounded than the right (Fig. 23). Importantly, this feature does not seem to be due to any segmentation issues and seems to represent a genuine part of the morphology of the skull. *Asio otus* has very low temporal asymmetry values (Table 15), but its foramen magnum asymmetry values could suggest that asymmetry is manifesting differently within this taxon. To investigate this, it would be important to analyse another *Asio otus* skulls and determine if this is a constant feature across other individuals of *Asio otus.* A comparative analysis like that could help provide more insights to whether asymmetry of the foreman magnum has any evolutionary or functional significance.

Although owls are the most-cited instance of cranial asymmetry in birds, harriers in the genus *Circus* have also been reported as having asymmetrical skulls. Studies cite the similarity

between harrier and owl hunting styles, the morphology and placement of their facial features and their reported good hearing (Rice, 1980; Nishikawa 2002). Despite these previous reports, the results from the temporal wing asymmetry in my research shows harriers particularly, the western marsh harrier (*Circus aeruginosus*), have the lowest asymmetry values amongst all the bird taxa tested. This surprising result contradicts the findings of Pecsics et al. (2021), who used landmarking to test whether harriers have cranial asymmetry and their results suggest that harriers do have temporal wing cranial asymmetry. However, *Circus aeruginosus* also exhibited the lowest asymmetry in their analysis, which could explain its similarly low value in my own findings. Therefore, future analysis should include landmarking the harrier skulls that had the highest asymmetry value in their study.

Although skull shape asymmetry has evolved in some bird linages, such as owls, the semicircular canals and cochlear ducts are symmetrical in terms of size (Fig. 9) and shape (Fig. 24). The high degree of size and shape symmetry between opposing sides strongly suggests that hearing adaptations of birds do not include variations in the left-right length of the labyrinth, suggesting that these structures are constrained for symmetry on both sides of the skull. Interestingly, owls with large temporal wing asymmetry values have very low labyrinth asymmetry values. This observation suggests that while the external ear openings are asymmetrical, and one ear is placed higher than the other, internal structures of the inner ear remain very symmetrical.

My results show that shape symmetry between the left and the right semicircular canals and cochlear ducts is a characteristic of all bird labyrinths (Fig. 24), highlighting a fundamental aspect of inner ear morphology across birds. This result greatly extends the results found in Cerio and Witmer (2019). That study found, by comparing the semicircular canals and cochlear ducts of a turkey population, that no individuals right and left sides were evidently different from each other. This result is particularly important for instances where only one

labyrinth is available for a bird species because we may be able to infer the size and morphology of the missing labyrinth based of the available labyrinth.

As size is a key functional parameter for semicircular canals, the semicircular canals are probably symmetrical in function. Having symmetrical semicircular canals is critical as each semicircular canal works together with its left or right counterpart. Any abnormalities can lead to the disruption of important function, such as disrupted balance and changes in muscle activity needed for posture. For example, the development of adolescent idiopathic scoliosis, a type of spinal deformity, has been linked to abnormal semicircular canals in adolescent children (Hawasli, 2015). Furthermore, Hitier (2015) shows that asymmetry in the semicircular canals must precede the scoliosis as semicircular canals ossify early and have a genetic pathway that inhibits remodelling. Asymmetries of the semicircular canals could be disastrous for birds as it could result in deformities such as a bent spine or asymmetrical hip region. Therefore, this could perhaps serve as the main constraint on symmetry of the inner ear and explain why asymmetry is relegated to other bones of the cranium or soft tissues around the skull.

Despite the high levels of labyrinth symmetry, several challenges were experienced during the landmarking process, which could have influenced the accuracy of the data. First, identifying the precise start and end points of the different labyrinth elements proved difficult because as these landmarks couldn't be replicated consistently in some of the of the right and left cochlear ducts. This variability could have introduced slight asymmetries that do not reflect true biological variation. Second, the quality of the meshes affected the result of the auto-skeletonization process. High-quality meshes usually produced singular, smooth auto-skeletons, making the midline landmarking more accurate. In contrast, jagged auto-skeletons were caused by lower quality meshes, making the landmarking process more complicated.

However, this issue occurred in only a few of the meshes downloaded from Morphosource, where inconsistent scanning parameters across specimens further worsened these challenges.

These limitations highlight the need for standardized scanning protocols and emphasize the potential propagation of errors in research that relies on digital reconstructions. Notably, outliers in the semicircular canal asymmetry measurements are probably artifacts caused by the auto-skeleton function in AVIZO rather than true anatomical asymmetry as well.

Many casual observers might consider nocturnality to be linked with hearing adaptations seen in owls, simply because of the lack of photons to image prey with the eyes. However, my analysis suggests that foraging mode is much more important than diel activity mode (Table 11; Fig. 15-16). There is significant variation in the proportional lengths of the cochlear duct and semicircular canals across different bird species. Even though braincase height is highly correlated with cochlear duct length (Fig. 13) notable variation in the cochlear duct length is left unexplained by this correlation, manifesting as high positive and negative residuals in my models. The highest residuals, i.e., the birds with the proportionally longest cochlear duct length, include the African grass Owl (*Tyto capensis)*, Snowy Owl (*Bubo scandiaca)*, Barn Owl (*Tyto capensis)* and the Oilbird (*Steatornis caripensis).* Even though *Tyto alba, Tyto capensis* and *Bubo scandiaca* are all owls, they have different diel activity patterns. *Tyto alba* and *Tyto capensis* are nocturnal and *Bubo scandiaca* is diurnal. Despite the different diel activity patterns, all three of these birds have a diet that consists mostly of small rodents such as mice (Boxall and Lein, 1982; Riegert et al., 2008). Their hunting technique involves listening to rodents move underneath the leaves, in the case of the *Tyto alb*a and *Tyto capensis*, or underneath the snow for the *Bubo scandiaca*. The length of the cochlear duct in birds and mammals has often been associated with hearing acuity (Lay, 1972). This has been tested recently by Peacock et al. (2024) who used Doppler vibrometry to show that the pressure gain between the inner ear vestibule and the ear canal in the barn owl is comparable

to what's seen in mammals. When combined these studies suggest, by extension that birds with a longer cochlear duct have better hearing. Therefore, these results do suggest that the proportionally long cochlear duct that these three birds have, could be an adaptation to auditory foraging and not diel activity patterns. This is supported by the regression between cochlear duct length and auditory foraging residuals having significant p-values and the insignificant p-values for all the other foraging techniques categories (Table 11).

Integrating the cochlear duct length data and the symmetry data in this study shows that owls have evolved exceptional hearing with multiple adaptive strategies. Many owls have evolved only one of these strategies, but some owls have evolved multiple of these strategies. For example, the barn owl (*Tyto alba*) has evolved the combination of soft tissue asymmetry and an elongated cochlear duct and the genus *Strix* has evolved soft tissue asymmetry and cranial asymmetry. These findings suggest that owls have evolved a wide range of solutions to the challenge of enhancing hearing to make capturing their prey more precise during different diel activity patterns, however according to my data no owl species appears to have all three.

Proportionally elongated cochlear ducts are exceedingly rare outside of owls. The oilbird (*Steatornis caripensis*) is shown to have a cochlear duct that is as proportionally long as *Tyto alba* and *Bubo scandiaca* relative to its braincase height (Fig.13). This is particularly interesting as the oilbird has been documented as a nocturnal bird that eat fruits (Snow, 1962; Stevenson, 2017). Foraging of the oilbird is assisted by their large and intensely innervated olfactory organs – perhaps obviously fruit isn't pursued using auditory clues. This suggests that the oilbird's long cochlear duct may have evolved due to factors unrelated to diet or foraging techniques, with echolocation, a trait it shares as one of only two non-mammalian echolocators, being a possible driver. Oilbirds depend mostly on vision where possible. For example, in the presence of moonlight or event artificial light sources, they will reduce the amount of sonar click emissions (Griffin, 1953; Konishi and Knudsen, 1979). The ear of

oilbirds has not been extensively described in the literature. Its cochlea has been described as simple (Martin, 1990) thus it has been thought that to have the same sensitivity levels as other birds (Dooling et al., 2000). The findings from my research suggest that the oilbird, despite having a simple cochlear duct, does have a duct much longer than what is expected for its braincase height. This suggests that it could possibly have sensitivity level that is different to other bird groups. A few species of swiftlets are also echolocators (Brinkløv et al., 2013) and it is critical for future analysis to include these species.

Relative cochlear duct length provides information on the upper frequency limit of hearing but does not provide information on best sensitivity and the lower frequency limit of hearing. Birds with an elongated cochlear duct are relatively well correlated with having a high frequency limit. For example, *Tyto alba*, a bird with one of the longest proportional cochlear ducts has the highest frequency limit at a 60dB when compared to other birds (Fig. 20). My findings are different to those of Walsh et al. (2009) who reported correlations with other measures of hearing performance. But it is important to note that they used a different normalisation procedure. Other studies like Gleich et al. (2005) show that the best frequency of hearing (kHz) is significantly correlated with basilar papilla length of birds (Gleich et al., 2005). The basilar papilla is located within the cochlear duct and length of the cochlear duct is directly related to the length of the basilar papilla because the basilar papilla extends along the floor of the cochlear duct. Therefore, when combined, these findings show the importance of gathering hearing performance data for birds as the results tend to be quite conflicting.

While birds with proportionally long cochlear ducts are rare in the dataset and have a strong association with known behavioural modifications for foraging, this is not the case for birds with proportionally shorter cochlear ducts. Birds with the shortest cochlear ducts are more abundant, with a wide range of diel activities and foraging techniques. They include the great cormorant (*Phalacrocorax carbo*), Atitlán grebe (*Podilymbus gigas*), kakapo (*Strigops*

habroptila) and the bald eagle (*Haliaeetus leucocephalus*). The diet of *Phalacrocorax carbo* and *Podilymbus gigas* consists mainly of fish (Veldkamp, 1995) and their subaqueous foraging techniques include pursuit diving or in some instances, catching fish from the surface of the water (White et al., 2008; Llimona et al., 2020). These two birds are considered to be subaqueous foragers and therefore must be able to function in both terrestrial and aquatic environments. Studies of visual adaptations in diving birds show that when birds adapted to terrestrial life enter the water, their eyes lose the refractive power of the corner (e.g., Katzir and Howland, 2003) but hearing in subaqueous foraging birds is only poorly known.

The hearing abilities of subaqueous foragers has only been studied extensively in two bird species one of which being *Phalacrocorax carbo*. Research by Johansen et al. (2016) and Hansen et al. (2017) suggested that *Phalacrocorax carbo* can perceive underwater sounds. Furthermore, Larsen et al. (2020) studied the adaptations of the outer and middle ear of the *Phalacrocorax carbo.* Their findings indicate that cormorants have in-air hearing abilities similar to other subaqueous birds of the same size, and their sensitivity to sounds underwater is at least as strong as it is in the air. However, no research has been done on their inner ears, particularly their cochlear ducts. My findings suggest that despite the adaptations observed in the outer and middle ear, subaqueous foragers such as the cormorants do have poor hearing in air, especially when compared to other non-subaqueous birds. A shorter cochlear duct may represent a functional trade-off that improves underwater hearing but sacrifices air-based hearing.

Interestingly, several subaqueous foragers have relatively long cochlear ducts, superficially falsifying the hypothesis that subaqueous foraging is associated with cochlear duct shortening. These include the amazon kingfisher (*Chloroceryle amazona*) and the osprey (*Pandion haliaetus*). Therefore, being a subaqueous forager is not necessarily what restricts

the length of the cochlear duct. Instead, a driving force could be having to dive for fish, or the length of time they spend submerged under water during foraging. For example, the osprey dives feet first into the water, therefore limiting the amount of time the head stays under water (Swenson, 1978). As opposed to *Phalacrocorax carbo* whose foraging technique includes pursuit diving (White et al., 2008) that results in the head being submerged under water for longer. Therefore, subaqueous foraging is not a reliable indicator for cochlear duct length in birds as subaqueous foragers have variable cochlear duct lengths.

Along with subaqueous foragers, a substantial number of visual foragers have proportionally shorter cochlear ducts. For example, the bald eagle (*Haliaeetus leucocephalus*) is well known for its spectacular eyesight that it uses to hunt from flight. It has also been observed hunting from perches, wading in water and participating in cooperative hunting (Salmaster, 1987). On top of subaqueous and visual foragers, olfactory foragers can also exhibit a short cochlear duct. The kakapo (*Strigops habroptilus*) is a nocturnal herbaceous bird which has been thought to use olfaction to forage and has evolved in an environment with no predators (Stephens, 1980). Therefore, while a long cochlear duct is rare amongst birds and is strongly associated with auditory foraging, short cochlear ducts are more common and have no discernible pattern of correlation with any specific type of foraging strategy.

Semicircular canal length and cochlear duct lengths covary strongly with overall body size and establishing an allometric covariate is critical for understanding variation in labyrinth length that is size-independent. The results of my research clearly show that braincase height has much stronger predictive power for the cochlear duct lengths and semicircular canal length. Previous studies such as Sipla (2007) used body mass to compare the average semicircular canal circumference to body mass across bird species. Therefore, my finding is significant as many studies have used body mass to make inferences on various aspects of bird hearing, therefore using braincase height instead will yield more accurate results.

Regressing the residual components of both the semicircular canals and cochlear duct lengths allows for the assessment of trade-offs in the proportional sizes of these structures. The model indicated that there is no association between the two residuals (Fig. 19). This result is contradictory to Benson et al. (2017) who determined that the semicircular canal size is determined by spatial constraints of the braincase with a negative allometry in birds. Pochat-Cottilloux et al. (2024) found similar results when studying the shape of extant crocodilian labyrinths. They found that shape is mainly related to braincase constraints with a negative allometry.

This result raises an intriguing question: how does exceptional hearing evolve in owls? Owls generally have proportionally bigger heads than expected for their body mass (Fig. 11) and this has evolved in all the owl lineages (Fig. 27). Owls could have evolved a bigger head to break the allometric relationship between braincase height and body mass. Therefore, the (Residuals of AvSumSCC ~ BCH) ~ (Residuals of AvCD ~ BCH) model could instead be correcting for that exact adaptation. Maybe owls just evolved proportionally bigger heads, and the ear adaptations are a byproduct of this. To test this question, more hearing performance data would need to be included.

In general, owls have a long cochlear duct related to auditory foraging and not directly to nocturnal foraging. This is important for extending what we know about theropod hearing performance. The long cochlear ducts of some theropods (e.g., *Shuvuuia*) specifically imply a high upper frequency perception (Fig. 20) – advancing on Choiniere et al. 2021 who used cochlear duct length to describe a more nebulous idea of better hearing performance.

Conclusion

This study investigated skeletal adaptations associated with specialized auditory abilities in birds, with a focus on owls. By using geometric morphometric analysis of digitally constructed bird labyrinth and skulls as well as phylogenetic comparative methods, the research offered new insights about the evolutionary pathways of traits related to hearing.

The findings revealed that a long cochlear duct, an important adaptation for enhanced auditory sensitivity, evolved independently three times in birds, highlighting its convergent evolution driven by different ecological demands. Interestingly, cochlear duct elongation and cranial asymmetry showed very little overlap and were identified as separate strategies for specialized auditory abilities in owls, demonstrating multiple pathways to evolving exceptional hearing. Additionally, relative cochlear duct length proved to be a good indicator of maximum hearing frequency in birds. However, it was not a reliable predictor of diel activity patterns. Instead, an elongated cochlear duct appears to be more closely associated with an auditory foraging strategy in birds.

This research contributes to our understanding of the evolutionary and functional diversity of the auditory systems of birds. It offers a more nuanced perspective on the evolutionary history of these hearing related traits within the owl lineage. Moreover, these results provide broader implications for sensory biology, showing the interplay between morphological innovation and ecological pressures in the evolution of intricate sensory systems.

Future research should aim to include a wider range of bird taxa and incorporate more behavioural and ecological data to further refine our understanding of these evolutionary patterns. Furthermore, scanning techniques with higher resolution and more complete audiogram datasets would increase our ability to link auditory performance with

morphological traits. This research creates a foundation for such endeavours and contributes important knowledge to evolutionary sensory biology.

References

Adams, D., Collyer, M., Kaliontzopoulou, A. & Baken, E. 2024. Geomorph: Software for geometric morphometric analyses. R package version 4.0.7. https://cran.r-project.org/package=geomorph

Baken, E., Collyer, M., Kaliontzopoulou, A. & Adams D .2021. geomorph v4.0 and gmShiny: enhanced analytics and a new graphical interface for a comprehensive morphometric experience. Methods in Ecology and Evolution, 12, 2355-2363.

Bang, B. G. 1971. Functional anatomy of t h e olfactory system in 23 orders of bird s.

Acta Anatomica 58, 1 -76.

Beatini, J. R., Proudfoot, G. A. & Gall, M. D. 2017. Frequency sensitivity in Northern saw-whet owls (*Aegolius acadicus*). Journal of Comparative Physiology A, 204(2), 145–154.

Benson, R. B. J., Starmer-Jones, E., Close, R. A., & Walsh, S. A. 2017. Comparative analysis of vestibular ecomorphology in birds. Journal of Anatomy, 231(6), 990–1018.

Berkhoudt, H. 1985. Structure and function of avian taste receptors. Form and Function in Birds, (eds A. S. King & J. McLelland). Academic Press, 3, 463-496

Bronzati, M., Vieceli, F. M., Botezelli, V. S., Godoy, P. L., Montefeltro, F. C., Nassif, J. P. M., Luzete, J., Ribeiro, D., Yan, C. Y. I., Werneburg, I., & Kohlsdorf, T. 2024. Deep-time origin of tympanic hearing in crown reptiles. Current Biology, 34(22), 5334-5340.e5.

Bull, E. L., Henjum, M. G. & Rohweder, R. S. 1989. Diet and optimal foraging of great gray owls. Journal of Wildlife Management, 53(1), 47.

Bull, E. L. & James R. D. 1993. Great Gray Owl (*Strix nebulosa*), version 2.0. In The Birds of North America (P. G. Rodewald, editor). Cornell Lab of Ornithology, Ithaca, New York, USA.

Calford, M. B. 1988. Constraints on the coding of sound frequency imposed by the avian interaural canal. Journal of Comparative Physiology A, 162(4), 491–502.

Catchpole, C. K. & Slater, P. J. 2003. Bird song: biological themes and variations. Cambridge university press.

Clark, R. 1975. A field study of the Short-eared Owl, *Asio flammeus* (Pontoppidan) in North America. Wildlife Monographs 47, 1-67.Cowles, G. S. 1967. The palate of the red-necked nightjar *Caprimulgus ruficollis* with a description of a new feature. Ibis 109, 260-265.

Cramp, S. (ed.) 1985. The Birds of the Western Palearctic, vol. IV. Oxford University Press.

Cunningham, S.J., Corfield, J.R., Iwaniuk, A.N., Castro, I., Alley, M.R., Birkhead, T.R. & Parsons, S. 2013. The Anatomy of the bill Tip of Kiwi and Associated Somatosensory Regions of the Brain: Comparisons with Shorebirds. PLOS ONE 8, e80036.

Dooling, R.J. 1992. Hearing in birds. In: Webster DB, Fay RR, Popper AN (eds) The evolutionary biology of hearing. Springer, Berlin Heidelberg New York, 545-559

Dooling, R. J. 1992. Hearing in birds. In The evolutionary biology of hearing (pp. 545-559). New York, NY: Springer New York.

Dyson, M. L., Klump, G. M., & Gauger, B. 1998. Absolute hearing thresholds and critical masking ratios in the European barn owl: a comparison with other owls. Journal of Comparative Physiology A, 182(5), 695–702.

Felsenstein, J.1985. Phylogenies and the comparative Method. The American Naturalist, 125(1), 1–15.

Fleischer, G. 1976. Hearing in extinct cetaceans as determined by cochlear structure. J Paleontol 50, 133–152.

Geisler, J. H. & Luo, Z. 1996. The petrosal and inner ear of Herpetocetus sp.(Mammalia: Cetacea) and their implications for the phylogeny and hearing of archaic mysticetes. Journal of Paleontology, 70(6), 1045-1066.

Gleich, O. & Manley, G. A. 1988. Quantitative morphological analysis of the sensory epithelium of the starling and pigeon basilar papilla. Hearing Research, 34, 69–85.

Gleich, O., Dooling, R. J., & Manley, G. A. 2005. Audiogram, body mass, and basilar papilla length: Correlations in birds and predictions for extinct archosaurs. Naturwissenschaften, 92(12), 595–598.

Godfrey, W. E. 1967. Some winter aspects of the Great Gray Owl. Can. Field Nat. 81, 99-101.

Gottschaldt, K. M. 1985. Structure and function of avian somatosensory receptors. Form and Function in Birds, vol. 3 (eds A. S. King & J. McLelland). Academic Press, 375-461.

Grafen, A. 1989. The phylogenetic regression. Philosophical Transactions of the Royal Society of London. Series B, Biological Sciences, 326(1233), 119–157.

Gray, O. 1951. An introduction to the study of the comparative anatomy of the labyrinth. The Journal of Laryngology & Otology, 65(10), 681-703.

Gunz, P., Ramsier, M., Kuhrig, M., Hublin, J., & Spoor, F. 2012. The mammalian bony labyrinth reconsidered, introducing a comprehensive geometric morphometric approach. Journal of Anatomy, 220(6), 529–543.

Hackett, S. J., Kimball, R. T., Reddy, S., Bowie, R. C. K., Braun, E. L., Braun, M. J., Chojnowski, J. L., Cox, W. A., Han, K., Harshman, J., Huddleston, C. J., Marks, B. D., Miglia, K. J., Moore, W. S., Sheldon, F. H., Steadman, D. W., Witt, C. C. & Yuri, T. 2008. A

phylogenomic study of birds reveals their evolutionary history. Science, 320(5884), 1763–1768.

Hansen, K. A., Maxwell, A., Siebert, U., Larsen, O. N. & Wahlberg, M. 2017. Great cormorants (*Phalacrocorax carbo*) can detect auditory cues while diving. Sci. Nat. 104, 45.

Hawasli, A.H., Hullar, T.E. & Dorward, I.G. 2015. Idiopathic scoliosis and the vestibular system. European spine journal: official publication of the European Spine Society, the European Spinal Deformity Society, and the European Section of the Cervical Spine Research Society. 24(2),227–33.

Heffner, H. E., Koay, G. & Heffner, R. S. 2016. Budgerigars (*Melopsittacus undulatus*) do not hear infrasound: the audiogram from 8 Hz to 10 kHz. Journal of Comparative Physiology A, 202(12), 853–857.

Hilden, O. & Helo, P. 1981. The Great Grey Owl *Strix nebulosa* - a bird of the northern taiga. Ornis Fennica 58, 159-166.

Hitier, M., Hamon, M., Denise, P., Lacoudre, J., Thenint, M., Mallet, J., Moreau, S., & Quarck, G. 2015. Lateral Semicircular Canal Asymmetry in Idiopathic Scoliosis: An Early Link between Biomechanical, Hormonal and Neurosensory Theories? PLoS ONE, 10(7), e0131120.

Hudspeth, A. J. 1983. The Hair Cells of the Inner Ear. Scientific American, 248(1), 54–65.

Iljitschew, W. D. 1974. Adaptionsokologische Parallelismenmosaikartige Evolution. Das Horsystem des Vogel als Objeckt der funktionellen Morphologic. Biol. Zbl. 93, 165-180.

Jetz, W., Thomas, G. H., Joy, J. B., Hartmann, K. & Mooers, A. O. 2012. The global diversity of birds in space and time. Nature, 491(7424), 444–448.

Johansen, S., Larsen, O. N., Christensen-Dalsgaard, J., Seidelin, L., Bostrom, M., Lunneryd, S.-G. & Wahlberg, M. 2016. In-air and underwater hearing in the great cormorant (*Phalacrocorax carbo*). In The Effects of Noise on Aquatic Life II (ed. A. N. Popper and A. Hawkins), 505-512. New York, NY: Springer New York.

Jung, J., Naleway, S. E., Yaraghi, N. A., Herrera, S., Sherman, V. R., Bushong, E. A., Ellisman, M. H., Kisailus, D., & McKittrick, J. 2016. Structural analysis of the tongue and hyoid apparatus in a woodpecker. Acta Biomaterialia, 37, 1–13.

Katzir, G. & Howland, H. C. 2003. Corneal power and underwater accommodation in great cormorants (*Phalacrocorax carbo sinensis*). J. Exp. Biol. 206, 833-841.

Ketten, D. R. 1992. The marine mammal ear: Specializations for aquatic audition and echolocation. In The Evolutionary Biology of Hearing (D. Webster, R. R. Fay, and A. N. Popper, eds). Springer-Verlag; New York, 717-754.

Kilner, R. & Johnstone, R. A. 1997. Begging the question: are offspring solicitation behaviours signals of need?. Trends in Ecology & Evolution, 12(1), 11-15.

Knudsen, E. I. 1981. The Hearing of the Barn Owl. Scientific American 245(6): 113–25.

Knudsen, E. I. & Konishi, M. 1979. Mechanisms of sound localisation in the barn owl (*Tyto alba*). J. Comp. Physiol. 133, 13-21.

Konishi, M. 1973. How the owl tracks its prey. Am Sci, 61,414-424.

Köppl, C. 1997. Phase locking to high frequencies in the auditory nerve and cochlear nucleus magnocellularis of the barn owl, Tyto alba. The Journal of Neuroscience 17(9), 3312–3321.

Kreithen, M. L. & Quine, D. B. 1979. Infrasound detection by the homing pigeon: a behavioral audiogram. Journal of Comparative Physiology, 129(1), 1-4.

Kropacheva, Y. E., Smirnov, N. G., Zykov, S. V., Cheprakov, M. I., Sadykova, N. O. & Bachurin, G. N. 2019. The Diet of the Great Gray Owl, Strix nebulosa, at Different Levels of Prey Abundance during the Nesting Season. Russian Journal of Ecology, 50(1), 43–49.

Lay, D. M. 1972. The anatomy, physiology, functional significance, and evolution of specialized hearing organs of Gerbilline rodents. Journal of Morphology, 138(1), 41–120.

Llimona, F., del Hoyo, J., Christie, D. A., Jutglar, F. & Kirwan, G. M. 2020. Atitlan Grebe (*Podilymbus gigas*), version 1.0. In Birds of the World (J. del Hoyo, A. Elliott, J. Sargatal, D. A. Christie, and E. de Juana, Editors. Cornell Lab of Ornithology, Ithaca, NY, USA.

Lutmerding, J. A. & Love, A. S. 2020. Longevity records of North American birds. Version 2020. Patuxent Wildlife Research Center, Bird Banding Laboratory 2020.

Sibley, D. A. 2014. The Sibley Guide to Birds, second edition. Alfred A. Knopf, New York, NY, USA.

Lohr, B., Brittan-Powell, E. F. & Dooling, R. J. 2013. Auditory brainstem responses and auditory thresholds in woodpeckers. The Journal of the Acoustical Society of America, 133(1), 337–342.

Lüdecke, D., Mattan, S., Patil, B., Waggoner, P. & Makowski, D. 2021. performance: An R Package for Assessment, Comparison and Testing of Statistical Models. Journal of Open Source Software, 6(60), 3139.

Maclean, G. L. 1985. Roberts' birds of southern Africa. Cape Town: John Voelcker Bird Book Fund.

Marti, C. D. 1974. Feeding ecology of four sympatric owls. Condor. 76, 45-61.

Martin, G. (2010) Birds by night. London: T & AD Poyser.

Maxwell, A., Hansen, K. A., Ortiz, S. T., Larsen, O. N., Siebert, U. & Wahlberg, M. 2017. In-air hearing of the great cormorant (*Phalacrocorax carbo*). Biology Open.

McGee, J., Nelson, P. B., Ponder, J. B., Marr, J., Redig, P. & Walsh, E. J. 2019. Auditory performance in bald eagles and red-tailed hawks: a comparative study of hearing in diurnal raptors. Journal of Comparative Physiology A, 205(6), 793–811.

Nieboer, E., Van der Paardt, M.1977. Hearing of the african wood owl, *Strix woodfordii*. Neth J Zool 27, 227-229.

Nishikawa, K. C. 2002. Evolutionary convergence in nervous systems: insights from comparative phylogenetic studies. – Brain, Behavior and Evolution 59(5–6), 240–249.

Norberg, R. Å. 1968. Physical factors in directional hearing in *Aegolius funereus* (Stringiformes), with special reference to the significance of the asymmetry of the external ears. Ark. Zoo. 20, 181-204.

Norberg, R. Å. 1977. Occurrence and independent evolution of bilateral ear asymmetry in owls and implications on owl taxonomy. Phil. Trans. R. Soc. 280, 376-408.

Norberg, R. Å. 2002. Independent evolution of outer ear asymmetry among five owl lineages; morphology, function, and selection. In: Newton, I., Kavanagh, R., Olsen, J. and Taylor, I. 2002. Ecology and Conservation of Owls. 329-342.

Orme, D., Freckleton, R., Thomas, G., Petzoldt, T., Fritz, S., Isaac, N. and Pearse, W. 2023. caper: Comparative Analyses of Phylogenetics and Evolution in R. R package version 1.0.3,

https://CRAN.R-project.org/package=caper.

Payne, R. S. 1962. How the Barn Owl locates prey by hearing. Living Bird 1,151-159.

Payne, R. S. 1971. Acoustic location of prey by Barn Owls (*Tyto alba*). J. Exp. Biol. 54, 535-573.

Pecsics, T., Marx, A., & Csörgő, T. 2021. The possible occurrence of cranial asymmetry in three harrier (Accipitridae: Circus) species. Ornis Hungarica, 29(1), 139–148.

Paradis, E. & Schliep, K. 2019. ape 5.0: an environment for modern phylogenetics and evolutionary analyses in R. Bioinformatics. 35, 526-528. doi:10.1093/bioinformatics/bty633

Payne, R. S. & Drury, W. H. 1958. Marksman of the darkness. Nat. Hist. (N.Y.) 67, 316-323.

Pennell, M., Eastman, J., Slater, G., Brown, J., Uyeda, J., Fitzjohn, R., Alfaro, M. & Harmon, L. 2014. geiger v2.0: an expanded suite of methods for fitting macroevolutionary models to phylogenetic trees. Bioinformatics, 30, 2216-2218.

Pochat-Cottilloux, Y., Perrichon, G., Hautier, L., Rinder, N., Amiot, R., Raselli, I., Adrien, J., Lachambre, J., Fernandez, V., & Martin, J. E. 2024. Size, not phylogeny, explains the morphology of the endosseous labyrinth in the crown clade Crocodylia. Journal of Anatomy.

R Core Team. 2023. R: A language and environment for statistical computing. R Foundation for Statistical Computing. https://www.R-project.org/

Rainey, H., Zuberbühler, K. & Slater, P. 2004. The responses of black-casqued hornbills to predator vocalisations and primate alarm calls. Behaviour, 141(10), 1263-1277.

Reid, B. & Williams, G. R. 1975. Biogeography and Ecology in New Zealand (ed. G. Kuschel). Junk, The Hague. The Kiwi. 301-330.

Revell, L. J. 2024. phytools 2.0: an updated R ecosystem for phylogenetic comparative methods (and other things). PeerJ, 12, e16505.

Rice, W. R. 1980. Acoustical localization of concealed prey by the diurnal harrier (Circus cyaneus). – PhD Dissertation, Corvallis, Oregon, Oregon State University

Ritchison, G. 1983. The function of singing in female black-headed grosbeaks (*Pheucticus melanocephalus*): family-group maintenance. The Auk, 100(1), 105-116.

Stephens, G. 1980. New Zealand adrift. A.H. & A.W. Reed, Wellington.

Thermo Fisher Scientific. Avizo Software (Version 2021.1). Waltham, MA, USA: Thermo Fisher Scientific; 2024. Available at: https://www.thermofisher.com

Swaddle, J. P. & Page, L. C. 2007. High levels of environmental noise erode pair preferences in zebra finches: implications for noise pollution. Animal behaviour, 74(3), 363-368.

Swenson, J. E. 1978. Prey and foraging behavior of ospreys on Yellowstone Lake, Wyoming. Journal of Wildlife Management, 42(1), 87.

Van Dijk, T. 1972. A comparative study of hearing in owls of the family strigidae. Netherlands Journal of Zoology, 23(2), 131–167.

Van Dijk, T. 1973. A comparative study of hearing in owls of the family Strigidae. Neth J Zool, 23, 131-167.

Vee, S., Barclay, G. & Lents, N. H. 2022. The glow of the night: The tapetum lucidum as a co-adaptation for the inverted retina. BioEssays, 44(10), 2200003.

Volume Graphics. 2020. *VGStudio MAX* (Version 3.2.2). Volume Graphics GmbH. https://www.volumegraphics.com

White, C. R., Butler, P. J., Grémillet, D., & Martin, G. R. 2008. Behavioural strategies of cormorants (Phalacrocoracidae) foraging under challenging light conditions. Ibis, 150(s1), 231–239.

Wenzel, B. M. 1968. Olfactory prowess of the Kiwi. Nature (Lond.), 220, 1133-1134.

Wickham, H. ggplot2: Elegant Graphics for Data Analysis. Springer-Verlag New York, 2016.

Wilman, H., Belmaker, J., Simpson, J., de la Rosa, C., Rivadeneira, M. M. & Jetz, W. 2014. EltonTraits 1.0: Species-level foraging attributes of the world's birds and mammals: Ecological Archives E095-178. Ecology, 95(7), 2027-2027.

Winkler, H. & Christie, D. A. 2020. Eurasian Green Woodpecker (*Picus viridis*), version 1.0. In Birds of the World (J. del Hoyo, A. Elliott, J. Sargatal, D. A. Christie, and E. de Juana, Editors). Cornell Lab of Ornithology, Ithaca, NY,USA.

Wood, J. M., Mitchell, K. J., Scofield, R. P., De Pietri, V., Rawlence, N.J. & Cooper, A. 2016. Phylogenetic relationships and terrestrial adaptations of the extinct laughing owl, *Sceloglaux albifacies* (Aves: Strigidae). Zoological Journal of the Linnean Society. 10.1111/zoj.12483.

Appendix 1

Species name	Media type	Specimen number	Morphosource media number
Alcedo atthis	Skull mesh	NHMUK S1994	00018987
Alcedo atthis	CT scan	NHMUK S/1994.7.1	000108986
Aptenodytes patagonicus	Skull mesh	UMZC 184D	000523314
Apteryx australis	Skull mesh	FMNH 391011	000108120
Apteryx australis	Labyrinth mesh	FMNH 391011	000362465
Aramides cajanea	Skull mesh	UMZC Vertebrates 300.A	000523358
Aramides cajanea	CT scan	UMZC Vertebrates 300.A	000523328
Athene cunicularia	CT scan	AMNH 7448	000514881
Batrachostomus auritus	CT scan	NHMUK 1968.74.20	000522305
Bubo virginianus	CT scan	OUVC 10220	000115487
Campethera caroli	CT scan	NHMUK 191.5.31.453	000522338
Caprimulgus macrurus manillensis	Skull mesh	FMNH 392245	000108215
Caprimulgus macrurus manillensis	Labyrinth mesh	FMNH 39224	000362479
Cariama cristata	CT scan	UMZC 724	000375527
Chaetura pelagica	CT scan	FMNH 439071	000521397
Chordeiles minor	Labyrinth mesh	UMMZ 233923	000362484
Chordeiles minor	Skull mesh	NHMUK S1998	000523830
Circus cyaneus	CT scan	AMNH 24085	00032717
Circus cyaneus	Labyrinth	AMNH 24085	000032718
Colius striatus	CT scan	FMNH 384817	000109734
Collocalia mearnsi	CT scan	FMNH 441729	000481573
Columba livia	Labyrinth mesh	NHMUK pal:001	0000334444

Columba livia	Cranium mesh	NHMUK pal:001	000370151
Elanus caeruleus	CT scan	NHMUK 1850.8.15.159	000092040
Elanus caeruleus	Skull mesh	NHMUK 1850.8.15.159	000092041
Elanus scriptus	CT scan	NMV B 8617	000164353
Gavia stellata	CT scan	NHMUK 1891.7.20.132	000092076
Gavia stellata	Cranium mesh	NHMUK 1891.7.20.132	000092077
Glaucidium brasilium	CT scan	AMNH FLUID 7407	000514882
Glaucidium gnoma	CT scan	AMNH FLUID 7407	000514884
Haliaeetus leucocephalus	CT scan	TMMM 7260	N/A
Macropygia amboinensis	CT scan	KU B 93202	000086023
Megscopes kennicottii	CT scan	AMNH FLUID 9732	000157592
Melanerpes carolinus	CT scan	NHMUK S/1988.103.7	000522474
Melopsittacus undulatus	CT scan	OUVC 10569	000115505
Morus bassanus	CT scan	NHMUK 1896	000522593
Ninox odiosda	CT scan	AMNH FLUID 7424	000514883
Nyctea scandiaca	Labyrinth mesh	NHMUK S/1998.59.1	000157591
Nyctea scandiaca	Cranium mesh	NMHUK S/1998.59.1	000158342
Nyctibius griseus	Cranium mesh	UMMZ 136351	000083605
Nyctibius griseus	Labyrinth mesh	UMMZ 136351	000362505
Oreotrochilus estella	CT scan	AMNH FLUID 4692	000541735
Otus spilocephalus	Labyrinth mesh	NHMUK S/1974.25.42	000157595
Otus spilocephalus	Cranium mesh	NHMUK S/1974.25.42	000158348
Oxyura jamacensis	CT scan	NHMUK 1985.70.4	000126060
Oxyura jamacensis	Cranium mesh	NHMUK 1985.70.4	000126061
Pandion haliaetus	CT scan	FMNH 437336	000093616

Pandion haliaetus carolinensis	Cranium mesh	FMNH 437336	000093618
Pelecanoides urinatrix	CT scan	NHMUK S/2006.1.14	000092459
Pelecanus occidentalis	Skull mesh	NHMUK S/1973.66.16	000092473
Pezoporus occidentalis	CT scan	QM O 29055	000040639
Phalacrorax carbo	Skull mesh	NMS Z2000	000032747
Phalacrorax carbo	Labyrinth mesh	NMS Z2000	000032768
Picus virdis	CT scan	NHMUK S/1982.5.1	00092596
Podargus strigoides	CT scan	FMNH 345114	000083618
Podargus strigoides	Cranium mesh	FMNH 345114	000083619
Podargus strigoides	Labyrinth	FMNH 345114	000362511
Podiceps taczanowskii	Cranium mesh	UMMZ 150794	000158380
Podiceps taczanowskii	Labyrinth mesh	UMMZ 156784	000158396
Podilymbus gigas	Cranium mesh	UMMZ 150794	000158382
Podilymbus gigas	Labyrinth mesh	UMMZ 150794	000158398
Psittacus erithacus	Labyrinth mesh	NMHUK S/1992.41.60	000032598
Psittacus erithacus	Cranium mesh	NMHUK S/1992.41.60	000093679
Pulsatrix perspicillata	Labyrinth mesh	NHMUK 1871.10.25.6	000157597
Pulsatrix perspicillata	Cranium mesh	NHMUK 1871.10.25.6	000158361
Sagittarius serpentatarius	CT scan	NHMUK 1898.5.7.1	000093036
Sceloglaux albifacies	CT scan	UMZC 497d	000522124
Scolopax minor	CT scan	FMNH 432410	000521457
Spheniscus demersus	CT scan	L JZ 60	000166695
Steatornis caripensis	Labyrinth mesh	FMNH 318679	000032648

Steatornis caripensis	Cranium mesh	FMNH 318679	000125569
Sterna hirundo	Cranium mesh	NMUK S/1975.65.4	000109909
Strigops habroptilus	Cranium mesh	NHMUK 1881.1.1	000158358
Strigops habrootilus	Labyrinth	NHMUK 1881.1.1	000362517
Strix aluco	CT scan	NHMUK S/2001.81.1	000093947
Strix aluco	Cranium mesh	NHMUK S/2001.81.1	000093048
Strix aluco	Labyrinth mesh	NHMUK S/2001.81.1	000362520
Turdus olivaceous	CT scan	L JZ 94	000167415
Turdus olivater kemptoni	CT scan	FMNH 319675	000107976
Turdus olivater kemptoni	Skull mesh	FMNH 319675	000107978
Tyto alba insularis	CT scan	AMNH FLUID 7473	000514902